Implementation, Development and Assessment of Local Hybrid Density Functionals

Dissertation

zur Erlangung des naturwissenschaftlichen Doktorgrades der

Julius-Maximilians-Universität Würzburg

vorgelegt von

Hilke Bahmann

aus Duisburg, Deutschland

Oktober, 2010

Eingereicht bei der Fakultät für Chemie und Pharmazie am:

_____

Gutachter der schriftlichen Arbeit

1. Gutachter: _____

2. Gutachter: _____

Prüfer des öffentlichen Promotionskolloquiums

1. Prüfer: _____

2. Prüfer: _____

3. Prüfer: _____

CONTENTS

LIST OF ABBREVIATIONS

AC	Adiabatic Connection
AO	Atomic Orbital
BH	Barrier Height
DFT	Densitiy Functional Theory
FDO	Functional Derivative with respect to the Orbitals
GGA	Generalized Gradient Approximation
HFCC	Hyperfine Coupling Constant
HK	Hohenberg-Kohn
HT	Hydrogen Transfer
I/O	input/output
LDA	Local Density Approximation
LMF	Local Mixing Function
LSDA	Local Spin Density Approximation
KS	Kohn-Sham
MAE	Mean Absolute Error
MSE	Mean Signed Error
MO	Molecular Orbital
NHT	Non-Hydrogen Transfer
OEP	Optimized Effective Potential
RI	Resolution of the Identity
SCF	Self-Consistent Field
TM	Transition Metal
ZPE	Zero Point Energy

CHAPTER 1

INTRODUCTION

Electronic structure calculations represent potentially the most important tool at hand for chemists to explain and predict experimental observations of quantum phenomena in molecules. The methods that are routinely used in chemistry can be divided in two main categories: wave function methods and Density Functional Theory (DFT). The former offer the advantage that they can systematically converge to more accurate results, at the expense of a dramatic increase in the computational cost associated with the methods. The latter, based on an approximate representation of the electron density, provides an efficient alternative and has so far offered the best compromise between accuracy and efficiency. Finding its roots in theoretical physics, where it is typically used to represent extended systems, DFT has become very popular amongst chemists in the last twenty years. The importance of the method was recognized in 1998, when the Nobel Prize for chemistry was awarded to Walter Kohn [1] and John A. Pople for the development of density-functional theory and computational methods in quantum chemistry, respectively. Although a formally exact method, DFT as specified by Kohn and Sham in their seminal paper [2] is approximate in practice. In this theory, all non-classical electron-electron interactions and parts of the correlated kinetic energy are gathered in the so-called exchange-correlation energy functional. While the exact form of the exchange-correlation functional is unknown, several exact physical and mathematical constraints have been found to guide the development of increasingly sophisticated and accurate approximations.

A wide choice of density functionals allows thus for the efficient calculation of molecular properties, such as enthalpies of formation, molecular structures, kinetics etc. Some properties remain more challenging, e.g., the $s-d$ transfer energies in atoms, the dissociation behavior of small radical cations or charge-transfer excitations, and a general functional that performs equally well for all the aforementioned problems has yet to be found. Functionals based in the generalized-gradient approximation (GGA) such as BLYP, [3, 4] BPW91, [5] PBE, [6] or or the more elaborate meta-GGA TPSS [7] are usually outperformed by global hybrid functionals. The latter contain a constant fraction of the exact-exchange energy from Hartree-Fock theory and are still the most widely used functionals in present-day chemical applications of DFT. There is considerable flexibility in the definition of the optimal amount of exact exchange to be included in the hybrid functional and there is evidence that it depends strongly on the property under investigation. [8–12] It thus became common practice to fit the global mixing coefficient, as well as other parameters, to empirical data so as to achieve better agreement with the desired experimental properties. The most popular global hybrid functional, B3LYP, [13] was optimized to reproduce thermochemical data and contains 20% exact exchange. Based on a systematic prodecure for refining gradient corrections proposed by Becke [14] several extensively parameterized hybrid functionals have been introduced in the last years: Some representatives are the HCTC (Hamprecht-Cohen-Tozer-Handy) family, the MO6 suite by Truhlar and coworkers, [15] the BMK (Boese-Martin for Kinetics) [15] and the Becke98 [16] functional. The exact exchange admixtures in the correponding functionals ranges between 20 and 54%. Additional inclusion of second order perturbation corrections as in the double hybrid functional B2PLYP improves properties that require a more accurate description of dynamical

correlation effects. [17]

Some failures of pure density functionals, e.g., in the calculation of charge-transfer excitation energies [18] and dissociation of 3-electron bonds have been attributed to missing long-range exchange and correlation effects. This observation lead among others to the introduction of range-separated hybrid functionals where the exchange component is separated into a short-range and a long-range part. Using exact exchange at large interelectronic distances, as in the LC-PBE [19] and CAM-B3LYP [20] functional, has been shown to improve the above-mentioned properties at the expense of poorer results for atomization energies and vibrational frequencies as compared to global hybrid functionals. [21–23]

Local hybrid functionals [24] represent another avenue towards the design of more flexible, and thus potentially more universal density functionals. The concept consists in including more or less exact exchange in the functional as a function of the position in the molecule. The level of admixture is controlled by a position-dependent local mixing function (LMF) in real-space, thus yielding molecule-specific amounts of exact exchange.

Previous studies demonstrated how such local mixing functions could be derived from physical considerations, employing for example an adiabatic connection approach [25] or the one-particle density matrix. [26] At the same time, other authors have introduced the PSTS local hybrid functional using TPSS meta-GGA exchange and correlation. The corresponding LMF is derived from considerations on the exchange-correlation hole associated with the chosen meta-GGA ingredients, but it includes nonetheless several empirical parameters. [27]

Pursuing a clearly semi-empirical approach, physically justified parameterized LMFs are employed im this work. The corresponding parameters are

subsequently fitted to atomization energies and barrier heights. The resulting local hybrid functionals are assessed for thermochemistry and kinetics of main group test sets. Further, the performance for dissociation energies, equilibrium bond lengths and $s-d$ transfer energies of $3d$ transition metal compounds is studied. In the self-consistent implementation of the new functionals, the local hybrid potential is computed as the functional derivative of the exchange-correlation energy with respect to the orbitals. To reduce the computational cost of the local hybrid functionals, the calculation of the exact-exchange energy-density and all terms with the LMF-weighted exact-exchange potential are commonly simplified using a resolution of identity approximation. Deviations from the numerically exact potential will be discussed for isotropic hyperfine coupling constants as well as the total and the orbital energies.

CHAPTER 2

THEORETICAL BACKGROUND

In the non-relativistic limit, the ground state of many-particle systems such as atoms, molecules or solids is represented by the time-independent Schrödinger equation

$$\hat{H}\Psi = E\Psi \ , \tag{2.1}$$

where the Hamilton operator $\hat{H}$ includes quantum-mechanical operators for all interactions that occur in the system. They are more specifically the kinetic energy of the electrons and the nuclei as well as the nuclear repulsion, electron-electron repulsion and Coulomb attraction between electrons and nuclei. The wave function Ψ contains all information about the system.

The Born-Oppenheimer approximation allows for separating the movement of the electrons from those of the nuclei and thus in electronic structure calculations just the electronic Hamiltonian is used while the nuclei are fixed. For a system with N electrons and A nuclei, the electronic Hamilton operator in atomic units (a.u.) is given as

$$\hat{H}_{el.} = \hat{T} + \hat{V}_{ne} + \hat{V}_{ee} = \sum_{i=1}^{N} \left(-\frac{1}{2}\nabla_i^2 \right) - \sum_{i=1,\alpha=1}^{N,A} \frac{Z_\alpha}{r_{i\alpha}} + \sum_{i<j}^{N} \frac{1}{r_{ij}} \ . \tag{2.2}$$

Even after separating the movement of the electrons from the movement of the nuclei, an analytically exact solution to the Schrödinger equation with the electronic Hamilton operator is possible only for one-electron systems such as the hydrogen atom. Consequently several approaches to find an approximate solution to the Schrödinger equation are available and even numerically

almost exact solutions are possible but restricted to very small systems. For larger N-electron systems, the wave function depending on $3N$ coordinates becomes increasingly complicated and its calculation is a rather extensive task. In the framework of Kohn-Sham density functional theory (DFT) this problem is circumvented by considering the electron density that depends only on 3 coordinates instead of the whole wave function. In this work improved approximations in the framework of DFT are sought. Therefore the basic ideas of the theory will be summarized before turning towards a detailed description of the density functionals under investigation.

The first Hohenberg-Kohn [28] (HK) theorem constitutes a one-to-one mapping between the ground-state electron density ρ_0 and a given external potential v_{ext} as e.g. that of the nuclei. Since the ground-state density is directly related to the corresponding wave function, the later is also mapped to the external potential. The theorem states that a universal functional of the density exists that describes electronic interactions in any system. Following from the second HK theorem

$$E_0[\rho_0] \leq E[\rho] = F_{HK}[\rho] + \int v_{ext}(\mathbf{r})\rho(\mathbf{r}) \, , \tag{2.3}$$

with

$$F_{HK}[\rho] = T[\rho] + V_{ee}[\rho] = \left\langle \Psi | \hat{T} + \hat{V}_{ee} | \Psi \right\rangle \, , \tag{2.4}$$

defining the universal HK functional, also the variational principle holds. That is, the electronic energy from a trial density will always be greater than the true ground state energy obtained from the true ground state density

Applying the Levy constraint-search method, the energy can be minimized by searching over a restricted space of wave functions. [29] Although

this approach proves that technically the total energy is a functional of the ground state density, in principal, a wave function has to be constructed, and there is no gain in efficiency. In order to bypass the construction of wave functions, a mathematical expression for the HK energy functional has to be derived. Considering the two respective contributions in equation 2.4, the major challenge represents the kinetic energy functional $T[\rho]$. This is a rather large part of the total energy as compared to, e.g., the non-classical electron-electron interaction, and first approximations to the kinetic energy functional have shown poor performance in atoms and molecules. [29] Only with the introduction of Kohn-Sham theory DFT became a viable tool in quantum chemistry and physics.

In this chapter, Hartree-Fock and Kohn-Sham theory are introduced, compared to each other, and similarities in the corresponding pseudo-eigenvalue equations are discussed. As the local hybrid functionals investigated in this work employ existing approximations to pure density functionals some of the well-known underlying assumptions and physical constraints will be summarized. Note that spin variables are dropped for most of the equations assuming closed shell systems. Also spatial variables are suppressed if not essential for understanding.

2.1 Kohn-Sham and Hartree-Fock theory

In Kohn-Sham (KS) theory the largest part of the kinetic energy problem is circumvented by shifting a small positive kinetic energy contribution into the exchange-correlation functional and calculating the largest part exactly. This is done by introducing a non-interacting reference system of N electrons

as described by a Slater determinant [2, 28]

$$\Psi_S\left(\mathbf{r}_1, \mathbf{r}_2, \ldots \mathbf{r}_N\right) = \begin{vmatrix} \varphi_1\left(\mathbf{r}_1\right) & \varphi_1\left(\mathbf{r}_2\right) & \cdots & \varphi_1\left(\mathbf{r}_N\right) \\ \varphi_2\left(\mathbf{r}_1\right) & \varphi_2\left(\mathbf{r}_2\right) & \cdots & \varphi_2\left(\mathbf{r}_N\right) \\ \vdots & \vdots & \ddots & \vdots \\ \varphi_N\left(\mathbf{r}_1\right) & \varphi_n\left(\mathbf{r}_2\right) & \cdots & \varphi_n\left(\mathbf{r}_N\right) \end{vmatrix}, \tag{2.5}$$

that yields by definition the correct ground state density of the interacting system. The kinetic energy of a Slater determinant can be calculated straightforwardly

$$T_S\left[\{\varphi_i\}\right] = \left\langle \Psi_S \left| \sum_i^N \nabla_i^2 \right| \Psi_S \right\rangle = -\frac{1}{2} \sum_i^N \int \varphi_i(\mathbf{r}) \nabla^2 \varphi_i(\mathbf{r}) d\mathbf{r} \,, \tag{2.6}$$

and it covers a large part of the total kinetic energy.

Then the total electronic KS energy can be assembled in the following way, including the above defined kinetic energy of our non-interacting reference system

$$E_{KS} = T_S\left[\varphi_i^{KS}\right] + V_{ne}\left[\rho\right] + J\left[\rho\right] + E_{XC}\left[\rho\right] \,, \tag{2.7}$$

the nuclear-electron attraction term

$$V_{ne}\left[\rho\right] = \int v_{ne}(\mathbf{r}) \rho(\mathbf{r}) d\mathbf{r} \,, \tag{2.8}$$

where v_{ne} represents an external potential arising from the nuclei, and the Coulomb repulsion between electrons

$$J\left[\rho\right] = \frac{1}{2} \int \int \frac{\rho(\mathbf{r}_1)\rho(\mathbf{r}_2)}{r_{12}} d\mathbf{r} \,. \tag{2.9}$$

The remaining non-classical electronic contributions are gathered in the exchange-correlation functional E_{XC}, that constitutes the workhouse of KS DFT. This term also includes the difference between the kinetic energy of the fully interacting and the non-interacting reference system arising from electron correlation effects that are not described by a Slater determinant.

Assuming orthonormalized one-electron wave functions $\{\varphi_i\}$ (usually denoted molecular orbitals), the electron density is obtained by taking the sum over the square of all occupied orbitals

$$\rho(\mathbf{r}) = \sum_{i}^{N_{occ.}} |\varphi_i(\mathbf{r})|^2 \ . \tag{2.10}$$

Although this would be an exact theory in principle, the exchange-correlation functional is not known exactly, and there is no route for systematic improvement available. Also, the variational principle does not hold fully for an approximate exchange-correlation functional in the sense that lower energies than the exact ground state energy may be obtained with a given ground-state density. However, many physical constraints have been revealed about the functional itself and even more about the associated exchange-correlation hole which will be briefly introduced in section 2.3. The exchange-correlation energy E_{XC} is commonly expressed in terms of an exchange-correlation energy density $\varepsilon_{XC}(\rho(\mathbf{r}))$ weighted by the electron density

$$E_{XC}\left[\rho\right] = \int d\mathbf{r}\, \rho(\mathbf{r})\, \varepsilon_{XC}\left(\rho\left(\mathbf{r}\right)\right) \ . \tag{2.11}$$

A similar energy expression to Eq. 2.7 is obtained in HF theory, where the Slater determinant is used as an approximation to the correct wave function. Assuming it is normalized, the total electronic Hartree-Fock energy is given

as

$$E_{HF}\left[\{\varphi_i\}\right] = T_S\left[\{\varphi_i\}\right] + V_N\left[\{\varphi_i\}\right] + J\left[\{\varphi_i\}\right] + E_X\left[\{\varphi_i\}\right] \ . \tag{2.12}$$

Here, the only non-classical electron-electron interaction term arises in the last term

$$E_X^{HF}\left[\{\varphi_i\}\right] = -\frac{1}{2}\sum_{ij}\int \frac{\varphi_i(\mathbf{r}_1)\varphi_j(\mathbf{r}_1)\varphi_i(\mathbf{r}_2)\varphi_j(\mathbf{r}_2)}{r_{12}} d\mathbf{r}_1 d\mathbf{r}_2 \ . \tag{2.13}$$

It is related to the Pauli principle that requires anti-symmery of the electronic wave function and seems to describe an interchange of electrons from one orbital to another. Therefore this part of the HF energy is called the exchange energy.

The kinetic energy is denoted T_S indicating that it related to a Slater determinant that does not describe sufficiently a system of interacting electrons. Although both kinetic energy expressions in Eqs. 2.7 and 2.12 coincide mathematically, different orbitals enter the expression in 2.6, thus yielding different values for the kinetic energy in KS as compared to HF. Just the same holds for the two Coulomb terms. Both are genuine functionals of the electron density in contrast to the kinetic energy functional and the HF exchange energy. If KS orbitals are used to evaluate expression 2.13, the result is usually termed *exact-exchange energy* rather than HF exchange energy, emphasizing the difference in the resulting energy value.

Based on historical rather than physical reasons, the exchange-correlation functional is conveniently divided into an exchange and a correlation part

$$E_{XC}\left[\rho(\mathbf{r})\right] = E_X\left[\rho(\mathbf{r})\right] + E_C\left[\rho(\mathbf{r})\right] \ . \tag{2.14}$$

With wave function methods, the correlation energy E_C^{WF} is defined as the difference between the exact ground state energy and HF

$$E_C^{WF} = E_{exact} - E_{HF} \tag{2.15}$$

. But this definition is not entirely transferable to density functionals, since the known (approximate) exchange functionals include usually also part of the electron correlation and, consequently, the DFT correlation functional does not correspond to the above defined correlation energy.

2.1.1 Kohn-Sham equations and the exchange-correlation potential

According to the variational principle, for a given external potential the ground state density minimzes the total energy. Besides, the density is an expansion of molecular orbitals. Thus, the total energy expression may be subjected to a variation with respect to the orbitals in order to obtain the ground state density. Simultaneously imposing orthonormality of the corresponding KS orbitals

$$\int \varphi_i(\mathbf{r})\varphi_j(\mathbf{r})d\mathbf{r} = \delta_{ij} \ , \tag{2.16}$$

and applying a unitary transformation to the molecular orbitals yields the KS equations in their canonical form

$$\hat{f}_{KS}\varphi_i = \varepsilon_i\varphi_i \ , \tag{2.17}$$

where the KS operator is given through

$$\hat{f}_{KS}(\mathbf{r}_1) = \hat{h}_i + \int \frac{\rho(\mathbf{r}_2)}{r_{12}} d\mathbf{r}_2 + v_{XC}(\mathbf{r}_1) \ , \tag{2.18}$$

and the eigenvalues ε_i correspond to orbital energies. Note that the orthonormality condition 2.16 also implies that the electron density (cf. Eq. (2.10)) is normalized to the number of electrons

$$\int \rho(\mathbf{r}) d\mathbf{r} = N \ . \tag{2.19}$$

The KS operator $\hat{f}_{KS}$ in Eq. (2.17) contains the one-electron operator $\hat{h}_i$ (including the kinetic energy operator and the nuclear Coulomb potential), a repulsive electronic Coulomb potential and the exchange-correlation potential defined as the functional derivative of the exchange-correlation energy with respect to the density

$$v_{XC} = \frac{\delta E_{XC}}{\delta \rho} \ . \tag{2.20}$$

If the exchange-correlation energy E_{XC} depends only on the density and its gradient, the corresponding potential is fully local and multiplicative. A non-local operator is, e.g., the exchange operator from HF theory.

$$\hat{v}_X^{exact} \varphi_i(\mathbf{r}_1) = \sum_j \int \frac{\varphi_j(\mathbf{r}_2)\varphi_i(\mathbf{r}_2)}{r_{12}} d\mathbf{r}_2 \varphi_j(\mathbf{r}_1) \ . \tag{2.21}$$

The HF equations differ from Eq. (2.17) only in the last term of the one-electron operator and are obtained accordingly by variation of the HF energy (Eq. (2.12) with respect to the orbitals. If the exchange-correlation energy in KS becomes orbital dependent (as in hybrid functionals through the exact

exchange), the corresponding potential is obtained through the functional derivative of E_{XC} with respect to the orbitals (FDO). The latter is related to the derivative with respect to the density via

$$v_X^{KS}\varphi_i = \frac{\delta E_{XC}}{\delta \rho}\varphi_i = \frac{1}{2}\frac{\delta E_{XC}}{\delta \varphi_i} \, . \tag{2.22}$$

So far, we have only considered closed-shell systems with an equal number of α and β electrons. For open-shell systems, unrestricted KS is performed, that is the α and β electron of the same shell may occupy different spatial wave functions and the orbital coefficients are obtained from two coupled KS matrices. They are coupled because information about β electrons enters the Coulomb as well as the correlation potential acting on the α electrons and vice versa. Exchange interactions arise by definition between same-spin electrons only and in DFT a spin-scaling relationship can be used to derive the exchange energy for open-shell systems from the corresponding closed-shell case.

2.1.1.1 The Kohn-Sham matrix - introduction of an atomic orbital basis

In principle, the KS equations (Eq. (2.17)) could be solved numerically, but mostly the KS orbitals are expanded in a finite atomic orbital (AO) basis of N_{BF} basis functions

$$\varphi_i(\mathbf{r}) = \sum_{\nu}^{N_{BF}} C_{i\nu}\chi_\nu(\mathbf{r}) \tag{2.23}$$

and only the coefficients $C_{i\nu}$ are varied to minimize the total energy.

This done by first calculating the KS operator in a given AO atomic

orbital basis set yielding the KS matrix with elements

$$F_{\mu\nu}^{XC} = \int \chi_\mu(\mathbf{r}) \hat{f}_{KS} \chi_\nu(\mathbf{r}) d\mathbf{r} \; . \tag{2.24}$$

The corresponding matrix equation has to be solved iteratively, because the KS matrix itself depends through the Coulomb and exchange-correlation potential on the density which in turn is calculated from the orbitals (cf. Eq. (2.18)). In each iteration the (transformed) KS matrix is diagonalized yielding a new set of orbitals and thus a new density. This procedure is repeated until self-consistency is reached, i.e. when from one cycle to another the change in energy and density lies below a given threshold. Therefore, this approach is also referred to as self-consistent field (SCF) method. It has been introduced in connection with HF where all the elements of the corresponding Fock matrix can be computed analytically. This does not hold for the exchange-correlation part of the KS matrix in DFT and the corresponding integrals

$$\int \chi_\mu(\mathbf{r}) v_{XC} \chi_\nu(\mathbf{r}) d\mathbf{r} \tag{2.25}$$

as well as the exchange-correlation energy (cf. Eq. (2.11)) itself have to be evaluated numerically on a grid.

2.1.2 Self-interaction error

In the expression for the Coulomb repulsion (Eq. (2.9)) between electrons, the interaction of an electron with itself emerges. This can be seen easily by

replacing the density by the orbital expansion from Eq. (2.10)

$$J = \frac{1}{2}\sum_{ij}\int \frac{\varphi_i(\mathbf{r}_1)\varphi_i(\mathbf{r}_1)\varphi_j(\mathbf{r}_2)\varphi_j(\mathbf{r}_2)}{r_{12}} d\mathbf{r}_1 d\mathbf{r}_2 \ . \tag{2.26}$$

Due to the double summation, terms with $i = j$ arise. Comparison with the expression for the exact exchange (Eq. (2.13)) shows that this so-called self-interaction is cancelled by exact exchange and HF is thus self-interaction free. Most of the density functionals, however, do not accomplish this, and many failures such as dissociation of one-electron systems and radicals, treatment of fractional numbers of electrons, charge transfer processes, underestimation of reaction barriers, and overestimation of polarizabilities have been attributed to the self-interaction error. Based on the adiabatic connection one-electron self-interaction free functionals have been proposed [30] but it has been shown that such a functional is not necessarily many-electron self-interaction free. [31] An explicit treatment has been proposed by Perdew and Zunger (PZ) in 1981 [32] but the corresponding energy functional is not invariant under orbital transformation rendering a self-consistent implementation complicated. This correction provides little or no improvement for reaction energies and results in too short bond lenghts in molecules. It was observed that many-electron systems are overcorrected by using the PZ approach. [33, 34]

2.2 Adiabatic connection

The concept of the non-interacting reference system that yields the correct ground state density constitutes a basis for the KS approach. It is possible to connect such a non-interacting system to the physical and thus interacting system via a coupling strength parameter λ. This parameter scales the

electron-electron interaction V_{ee} in the corresponding Hamilton operator

$$\hat{H}_\lambda = \hat{T} + \lambda \hat{V}_{ee} + \hat{V}_\lambda \ , \tag{2.27}$$

where λ goes smoothly from zero to one. In order to keep the density constant upon variation of λ, the potential

$$\hat{V}_\lambda = \int d\mathbf{r} v_\lambda(\mathbf{r}) \rho(\mathbf{r}) \ , \tag{2.28}$$

becomes coupling-strength dependent while the electron-electron repulsion operator $\hat{V}_{ee}$ is not, per definition

$$\hat{V}_{ee} = \sum_{i<j} \frac{1}{|r_i - r_j|} \ . \tag{2.29}$$

Note that for $\lambda = 1$, the potential v_λ becomes the external potential only whereas for the uncoupled system ($\lambda = 0$) it includes as well the classical Coulomb and the non-classical exchange operator leading to the non-interacting reference system, i.e. a Slater determinant. [35]

Therefrom follows an Adiabatic Connection (AC) formalism [36] for the exchange-correlation energy

$$E_{XC} = \int E_{XC,\lambda} d\lambda \ , \tag{2.30}$$

where the coupling-strength dependent interaction energy is defined as the difference between the expectation value of the electron-electron repulsion operator and the Coulomb energy.

$$E_{XC,\lambda} = V_{ee,\lambda} - J \ . \tag{2.31}$$

In the non-interacting limit ($\lambda = 0$), only exchange contributes to the non-classical electron-electron interaction, i.e. $E_{XC}^{\lambda=0} = E_X$. Additionally, in the non-interacting limit, the gradient of the exact AC with respect to λ is known as a functional of the KS orbitals (the Görling-Levy second-order perturbation theory correlation energy). [37, 38] The AC provides a general justification for hybrid functionals that mix the exact-exchange energy with DFT exchange and correlation. [35, 39] Approximate functionals for the systems H_2 and He were derived using parametrized functions of λ and fitting to the exact full CI energies of the corresponding molecules. [40] Similarly local mixing functions for local hybrids were deduced from the AC [25] but will not be further addressed in this work.

2.3 Exchange-correlation hole

In the KS total energy expressions of Eq. (2.7) the exchange-correlation energy is a purely quantum mechanical feature. It stems from the fact that electrons are correlated and, as compared to a purely classical interaction between charged particles, they avoid each other in order to lower repulsion. Thus the exchange-correlation energy as well as exchange in HF (Eq. (2.12)) constitute a negative contribution to the total electronic energy. Having this in mind, the entire electron-electron interaction (Coulomb and exchange-correlation energy) can be written as a repulsion between the charge density $\rho(\mathbf{r}_1)$ and another charge density $\rho(\mathbf{r}_2)$ reduced by the so-called exchange-correlation hole ρ_{XC}

$$J + E_{XC} = \frac{1}{2} \int \frac{\rho(\mathbf{r}_1) \left[\rho(\mathbf{r}_2) + \rho_{XC}(\mathbf{r}_1, \mathbf{r}_2)\right]}{r_{12}} d\mathbf{r}_1 d\mathbf{r}_2 \, . \tag{2.32}$$

This hole function depends on both coordinates and reduces the charge density $\rho(\mathbf{r}_2)$ around the reference electron at $\mathbf{r}_1$. The hole function is directly related to the diagonal element of the second order density matrix $\rho_2(\mathbf{r}_1, \mathbf{r}_2)$ which describes the probability of finding an electron at position $\mathbf{r}_1$ if the other is located at $\mathbf{r}_2$

$$\rho_2(\mathbf{r}_1, \mathbf{r}_2) = \rho(\mathbf{r}_1)\rho(\mathbf{r}_2) + \rho(\mathbf{r}_1)\rho_{XC}(\mathbf{r}_1, \mathbf{r}_2) \; . \tag{2.33}$$

In the quest for improved approximations to the exchange-correlation functional, considerable attention has been paid to the exchange-correlation hole ρ_{XC}, [41,42] and consequently, many of its properties are known. Hence, many density functionals are derived from models [43–45] for the exchange-correlation hole or at least based on considerations about the underlying hole function.

Since the angular dependence is irrelevant for the calculation of exchange-correlation energies (cf. Eq. (2.32)) usually only the angle-average of the hole function is considered. Hence, the exchange-correlation energy density (Eq. (2.11)) can be represented in terms of the angle-averaged exchange-correlation hole

$$\varepsilon_{XC}\left(\rho(\mathbf{r})\right) = \int du \, 2\,\pi\, u \, \rho_{XC}(\rho(\mathbf{r}), u) \; , \tag{2.34}$$

where u is the interelectronic distance

$$u = |\mathbf{r} - \mathbf{r}'|. \tag{2.35}$$

According to the the exchange-correlation functional, the hole function

can be divided into an exchange and a correlation part

$$\rho_{XC}(\rho(\mathbf{r}), u) = \rho_X(\rho(\mathbf{r}), u) + \rho_C(\rho(\mathbf{r}), u) \ , \tag{2.36}$$

and the focus will henceforth lie on the exchange hole and the exchange functional.

In open-shell systems spin polarization

$$\zeta = \frac{\rho_\alpha - \rho_\beta}{\rho} \tag{2.37}$$

has to be considered, where the total electron density is the sum over the respective spin-densities ($\rho = \rho_\alpha + \rho_\beta$) . Since by definition exchange interaction only occurs between same-spin electrons, the exchange hole for open-shell systems is obtained from two separate α and β exchange holes. For the exchange hole an exact spin-scaling relationship is available. [46–49] Thus, only the spin-unpolarized case ($\zeta = 0$) needs to be considered for exchange hole models and spin polarization can be introduced later on.

As pointed out before, several properties of the exchange and correlation holes are well stablished. Three of them have been shown to be crucial for the success of approximate densitiy functionals. [41, 50] First, the exchange hole is normalized to a unit charge

$$4\pi \int u^2 \rho_X(\rho(\mathbf{r}), u) du = -1 \ . \tag{2.38}$$

Second, it is bound to be negative for any interelectronic distance u, and thirdly it possesses a finite on-top value [41]

$$\rho_X(\rho(\mathbf{r}), u = 0) = \frac{1}{2}\rho(\mathbf{r}) \tag{2.39}$$

for vanishing interelectronic distances u. The curvature of the exchange hole at small u is zero

$$\frac{d\rho_X}{du}|_{u\to 0} = 0 \,, \tag{2.40}$$

while the correlation hole exhibits a cusp. [51] In the high-density limit, the exact exchange-correlation hole reduces to exchange only .

The exact exchange-hole (from HF theory) can be calculated from the one-particle density-matrix. It may be strongly delocalized, e.g. in stretched systems, and just in combination with the exact correlation hole a rather localized hole is obtained. [52] By contrast, approximations to the exchange and correlation functionals are based on localized holes around the reference electron. Due to the missing non-locality of the underlying exchange hole in common density functionals, the electrons are sometimes described as short-sighted. A localized exchange hole in DFT also corresponds to the finding that the exchange functional includes some static correlation. It should be noted that, starting from the exchange hole for the homogeneous electron gas, gradient corrections usually make the hole deeper and thus more localized around the reference electron.

A few models [43, 45, 53–55] for the exchange and correlation hole exist and progress in this area is expected to be quite useful for the developement of new density functionals or at least for replacing empirical parameters in existing approaches.

2.4 Approximations to the exchange and correlation functional

The earliest approximation to the exchange correlation energy density is based on the homogeneous electron gas model, [2, 28] a system with constant

density which may be described using periodic boundary conditions similar to the particle in a box. [29] The analytical form for the exchange-energy density, also called Slater exchange [56] is given through

$$\varepsilon_X^{Slater}\left(\rho(\mathbf{r})\right) = C_x \int \rho^{\frac{4}{3}}(\mathbf{r}) d\mathbf{r} \ , \tag{2.41}$$

with the coefficient $C_x = \frac{3}{4}\left(\frac{3}{\pi}\right)^{\frac{1}{3}}$. For the correlation energy, which has to be evaluated numerically, several fits exist, [47, 57] the most popular ones being those by Vosko, Wilk and Nusair [57] (VWN). Another fit frequently used is the one by Perdew and Wang. [47] Since in the homogeneous electron gas exchange and correlation depend on the density only and no gradients appear, it is also called the local density approximation (LDA) or for open-shell systems, the local spin density approximation (LSDA). Slater exchange and VWN correlation are the corresponding functionals, if the LSDA is employed. Although LSDA yields reasonable results for solid metals that are naturally closer to the homogeneous electron gas due to their band structure, it is not satisfying for atoms and molecules: Binding energies are, e.g., systematically overestimated and total atomic energies usually too high (magnitude too low). [58]

A straightforward way of improvement over such a local functional would be a Taylor expansion in the density. Indeed, a gradient expansion of the exact exchange hole exists and has been used as a basis to introduce a gradient correction to the LDA exchange energy density. However, if higher gradients of the density are neglected, the exchange hole is not normalized to a unit charge any more and furthermore the negativity condition is violated. Among others, these constraints have been shown to be the major reason for the former success of LSDA. [36, 59] Actually, simply adding a gradient

correction according to the gradient expansion in some cases even detoriated results. [29] In order to restore the important properties of the exchange hole, a so called generalized-gradient approximation (GGA) has been introduced independently by Perdew [60, 61] and Becke [62]. Their approaches differ in the underlying gradient expansion: while Perdew has used the expansion in the density, Becke employed the exact behavior of the sphercially averaged exchange hole at small interelectronic distances u

$$\rho_X(u) = \frac{1}{2}\rho + \frac{1}{12}\left(\nabla^2\rho + 2\tau + \frac{1}{2}\left[\frac{(\nabla\rho)^2}{\rho}\right]\right)u^2 \,. \tag{2.42}$$

Obviously this expression reduces to the correct on-top value for vanishing values of u.

In the GGA real-space cut-offs applied to the exchange hole guarantee that it is negative everywhere and restores normalization. Via integration of the interelectronic distance (cf. Eq. (2.34)) the exchange energy density is obtained from the modified hole. The latter is related to the exchange energy through integration over space (cf. Eq. (2.11)). That is why the Laplacian of the density that emerges in the exact gradient expansion of the exchange hole can be suppressed by partial integration over $\mathbf{r}$. As will be discussed later, this procedure gives rise to part of the gauge problem of the exchange-energy density in local hybrid functionals. [63] Note that the correlation functional by Lee, Yang and Parr (LYP) [4, 13] which is typically called a GGA, has been derived from the Colle-Salvetti correlation energy formula that employs the HF second-order density matrix rather than the gradient expansion of the correlation hole. The correlation functional by Perdew and Wang (PW91) [5] and its simplified follow-up,the PBE functional, [6] on the other hand are based on a similar procedure as described above for exchange, but for the

correlation hole instead.

Quite often such GGA functionals contain one or more empirical parameters, such as three fitted to the helium atom in the LYP correlation functional or one in the B88 exchange functional [3] obtained from a least-squares fit to the HF exchange energies of noble gas atoms. In the PW91 and PBE exchange and correlation functionals, parameters are fitted to constraints such as the slow and rapidly varying density limits or the high density limit. [5, 6, 53, 64]

In the Jacob's ladder hierarchy of density functionals introduced by Perdew [46] the LSDA constitutes the first step, GGAs the second and on the third functionals such as meta-GGAs that depend not only on the density and its gradient but additionally on explicitly orbital-dependent quantities as the kinetic energy density or the Laplacian of the density

$$\tau = \frac{1}{2}\sum_i |\nabla\varphi_i|^2 \ . \tag{2.43}$$

Hybrid functionals incorporate a constant fraction of exact exchange as defined in Eq. (2.13), which is an orbital dependent and non-local quantity. These functionals are therefore assigned to the fourth rung of Jacob's ladder, also termed hyper-GGAs: The first hybrid functional introduced by Becke includes 50% exact-exchange energy mixed with 50% Slater exchange and this mixing scheme is therefore referred to as Becke's half and half functional SH&HSVWN. Its GGA based descendent, BH&HLYP, employs the same scheme. One of the most popular and commonly used density functinals, B3LYP, [13, 65] is based on a semi-empirical parametrization scheme (with 3 parameters fitted to the atomization energies of the small G2-1 set), incorporating 20% exact exchange. Despite such a semi-empricial procedure, its

universal applicability has been questionned only in the last years after effectively being the default density functional in quantum chemistry for more than 10 years. Since the exact-exchange admixture is constant throughout the whole system, the above described functionals are often called *global hybrids* and in a general form may be given through

$$E_{XC} = a_0 E_X^{exact} + (1-a_0) E_X^{LSDA} + b\Delta E_X^{(meta-)GGA} + E_C^{LSDA} + c\Delta E_C^{(meta-)GGA} \,. \tag{2.44}$$

Here $\Delta E_X^{(meta-)GGA}$ and $\Delta E_X^{(meta-)GGA}$ denote either meta- or simpler GGA corrections to the LSDA exchange and correlation respectively. In the B3-scheme [65] the parameters have been optimized to $a = 0.2$, $b = 0.72$ and $c = 0.81$. After their inital success, several limitations of global hybrid functionals have been revealed. In particular varying amounts of exact-exchange admixture were suggested depending on physical considerations or simple fits to molecular properties.

Functionals that are located on the fifth and final rung of Jacob's ladder towards *density functional heaven* include additional information on the virtual orbital space. According to the Jacob's ladder terminology, this rung is called generalized random phase approximation. Representatives are, e.g., double local hybrid functionals, such as the B2-PLYP functional [17] that includes some MP2 correlation energy additionally to exact exchange, Becke exchange and LYP correlation.

Another classification of functionals proposed by Kaupp and Arbuznikov [66] consists of only three categories and reflects a more implementational viewpoint. The lowest category includes only the density and its derivatives and gives rise to a local and multiplicative potential. Functionals belonging

to the second class contain ingredients that depend on occupied orbitals such as the kinetic-energy density and the exchange-energy density. The corresponding potentials are non-multiplicative and usually non-local. In the third class, functionals contain information about the virtual orbital space as well. Meta-GGAs may belong to either the first if they include the Laplacian of the density or the second category if the kinetic-energy density is involved.

A systematic procedure for refining gradient corrections to the LSDA exchange and correlation energy densities introduced by Becke [14] has paved the way for a whole series of extensively parametrized GGA, meta-GGA and global hybrid functionals. In this approach GGA exchange and correlation correction factors are expanded in a power series in a mapping of the the reduced density gradient squared s^2, where

$$s\left(\mathbf{r}\right) = \frac{\left|\nabla\rho\left(\mathbf{r}\right)\right|}{2\left(3\pi^2\right)^{1/3}\rho\left(\mathbf{r}\right)^{4/3}}\,. \tag{2.45}$$

The corresponding GGA global-hybrid functional [14] (B98) contains 10 empirical parameters fitted to thermochemical data. Since the parameters have been fitted in basis set free calculations, its performance can be exceeded by other functionals when atomic basis sets are employed. Using the same ansatz, the HCTC functional [67] has been obtained and by including information about the exchange-correlation potential it was possible to increase the number of parameters up to 15 without problems of overparameterization. By including the kinetic energy density and the exact-exchange energy, the related meta-GGA τ-HCTC and the τ-HCTC hybrid [68] have been developed by Handy et al. The meta-GGA global hybrid M05 [69, 70] by Truhlar and coworkers includes 25 parameters, their follow-up functionals that constitute the M06 suite [15] even more. Another meta-GGA hybrid, the BMK func-

tional, [71] based on the form of the τ-dependent HCTC hybrid functional includes 42% exact exchange and in total 17 parameters. Obviously, most of these functionals yield impressive results for their underlying training sets and related properties. For other test sets, however, performance may detoriate and as a consequence different functionals have been recommended for different properties and molecule classes. [72, 73] Also, the constant amount of exact exchange in global hybrids of this series of functionals varies between 19 and 54%. Since the global mixing parameter appears to be non-unique the concept of mixing exact exchange with density functional exchange was generalized pursuing two different routes.

One route leads to range-separated hybrid functionals that are based on a partitioning of the r_{12} operator in the exchange interaction into different ranges, using DFT at one and exact exchange at the other range. An error function is generally employed to go smoothly from DFT to exact exchange and at least one parameter is required that determines the slope of this function.

In the Coulomb-attenuated method, exact exchange is used at long range, improving properties that suffer from the incorrect potential. These include the polarizability of long chains, excitations for Rydberg states and charge transfer excitations using time-dependent DFT. One representative of this class would be CAM-B3LYP [20] which improves the above-mentioned properties as well as classical reaction barriers. [23] By appropriately fitting the parameter inside the error function, $s - d$-transfer energies have been improved considerably with a long-range corrected GGA functional. [74] Studies on long-range corrected hybrids with PBE exchange and correlation have revealed that an improvement over the PBE global hybrid with 25% exact exchange is attained for barrier heights and for dissociation of two-center

three-electron systems. Atomization energies for the small G2-1 set are still more acurate with the global hybrid. For the full G2 and G3 set the range-separated hybrid, however, performs better. [19, 22]

A hybrid functional based on a screened Coulomb potential by Heyd, Scuseria and Ernzerhof (HSE) on the other hand uses a fraction of exact exchange at short range only. It has been developed explicitly for metallic systems that require periodic boundary calculations. The latter become quite expensive if hybrid functionals are employed due to the long-range exchange interaction. The HSE functional has therefore the advantage over the corresponding global hybrid of being more efficient for extended systems while maintaining a given accuracy. Both functionals, CAM-B3LYP and HSE yield worse enthalpies of formation than B3LYP.

In addition to the long- and short-range corrected functionals, a PBE based functional with exact exchange in the middle range of the interelectronic distance has been investigated; the results are very similar to those obtained from the long-range corrected PBE. [75]

2.5 Local hybrid functionals

Another natural generalization of global hybrid functionals are local hybrids where the constant mixing parameter a_0 (cf. Eq. (2.44)) is replaced by a real-space function yielding thus a position dependent admixture

$$E_{XC}^{Lh} = \int g\left(\mathbf{r}\right) \varepsilon_X^{exact}\left(\mathbf{r}\right) d\mathbf{r} + \int \left(1 - g\left(\mathbf{r}\right)\right) \varepsilon_X^{DFT}\left(\mathbf{r}\right) d\mathbf{r} + E_C \; . \qquad (2.46)$$

The local mixing function (LMF) $g\left(\mathbf{r}\right)$ should be bound between zero and one. (If not a physically unjustified negative exchange hole may, for example, occur.) Possible choices for $g(\mathbf{r})$ will be addressed in section 4. Since the

correlation part of a global or local hybrid functional is just a pure density functional, the corresponding potential remains unaffected by the LMF. In the following, basic equations will thus be derived with focus on the exchange part only.

2.5.1 The local hybrid potential

Hybrid functionals are explicitly orbital-dependent, and the associated potential is clearly non-local due to the exact-exchange part. It has been argued that this represents a step outside the original KS scheme where the potential is assumed to be purely local and multiplicative. [2, 76] Actually, an optimized effective potential [77–80] (OEP) could be derived from the non-local and non-multiplicative one but the procedure often suffers from numerical instabilities and is computationally more expensive. In this work, the potential has thus been evaluated as a functional derivative with respect to the orbitals (FDO) (cf. Eq. (2.22)) without further localization of the potential. For the exchange part of local hybrid functionals, the FDO is given by

$$\begin{aligned}\frac{\delta E_X}{\delta\varphi_i(\mathbf{r})} =& \, g(\mathbf{r})\,\hat{v}_X^{exact}\varphi_i(\mathbf{r}) + \hat{v}_X^{exact}\left(g(\mathbf{r})\,\varphi_i(\mathbf{r})\right) \\ &+ \left[1-g(\mathbf{r})\right]\frac{\partial\varepsilon_X^{DFT}}{\partial\varphi_i} - \nabla\left(\left[1-g(\mathbf{r})\right]\frac{\partial\varepsilon_X^{DFT}}{\partial\nabla\varphi_i}\right) \\ &+ \frac{\partial g(\mathbf{r})}{\partial\varphi_i}\Delta\varepsilon_X - \nabla\left(\frac{\partial g(\mathbf{r})}{\partial\nabla\varphi_i}\Delta\varepsilon_X\right) \,, \end{aligned} \tag{2.47}$$

where

$$\Delta\varepsilon_X = \varepsilon_X^{exact} - \varepsilon_X^{DFT} \,. \tag{2.48}$$

The first two terms in Eq. (2.47) are a result of the variation in the exact-

exchange energy density weighted by the local mixing function $\int g(\mathbf{r})\,\delta\varepsilon_X^{exact}(\mathbf{r})\,d\mathbf{r}$. They have to be evalutated numerically on the grid or analytically using an auxiliary basis set and the resolution of the identity. The next two terms in the potential are essentially identical to the well-known DFT potential weighted by the local mixing function. In the last two terms derivatives of the local mixing functions are needed, and in this implementation they are evaluated employing partial derivatives with respect to the density, the absolute square of the density gradient $|\nabla\rho|^2$, and the kinetic energy density τ.

$$\frac{\partial g}{\partial \varphi_i} = \frac{\partial g}{\partial \rho}\frac{\partial \rho}{\partial \varphi_i} + \frac{\partial g}{\partial |\nabla\rho|^2}\frac{\partial |\nabla\rho|^2}{\partial \varphi_i} = 2\frac{\partial g}{\partial \rho}\varphi_i + 4\frac{\partial g}{\partial |\nabla\rho|^2}\nabla\rho\cdot\nabla\varphi_i \quad (2.49)$$

$$\frac{\partial g}{\partial \nabla\varphi_i} = \frac{\partial g}{\partial |\nabla\rho|^2}\frac{\partial |\nabla\rho|^2}{\partial \nabla\varphi_i} + \frac{\partial g}{\partial \tau}\frac{\partial \tau}{\partial \nabla\varphi_i} = 4\frac{\partial g}{\partial |\nabla\rho|^2}(\nabla\rho)\,\varphi_i + \frac{\partial g}{\partial \tau}\nabla\varphi_i \quad (2.50)$$

Applying several times partial integrations in order to avoid second-order derivatives of the basis functions and gradients of the LMF or the DFT exchange-energy density, the following integrals are obtained

$$\begin{aligned} F_{\mu\nu}^X =& \frac{1}{2}\left(\int \chi_\mu g \hat{v}_X^{exact}\chi_\nu + \int \chi_\mu \hat{v}_X^{exact}(g\chi_\nu)\right) \\ &+ \int \chi_\mu [1-g]\frac{\partial \varepsilon_X^{DFT}}{\partial \rho}\chi_\nu + 2\int [1-g]\frac{\partial \varepsilon_X^{DFT}}{\partial |\nabla\rho|^2}\nabla\rho\cdot\nabla(\chi_\mu\chi_\nu) \\ &+ \int \chi_\mu \Delta\varepsilon_X\frac{\partial g}{\partial \rho}\chi_\nu + 2\int \Delta\varepsilon_X\frac{\partial g}{\partial |\nabla\rho|^2}\nabla\rho\cdot\nabla(\chi_\mu\chi_\nu) \\ &+ \frac{1}{2}\int \Delta\varepsilon_X\frac{\partial g}{\partial \tau}\nabla\chi_\mu\cdot\nabla\chi_\nu\,. \end{aligned} \quad (2.51)$$

They constitute the exchange part of the Kohn-Sham matrix.

2.6 Exact-exchange energy-density and potential

In local hybrid functionals due to the real-space weighting one has to deal with exchange-energy densities derived from different approximations. In contrast to the integrated exchange energy, the exchange energy per particle is not well-defined and any function integrating to zero could be added. This fact has been addressed in the literature as the gauge-problem. Furthermore, for the potential in self-consistent calculations, non-standard exchange integrals have to be evaluated, where the exact exchange potential is additionally weighted by the local mixing function. Just as any exact-exchange energy density these would have to be calculated by numerical integration which is rather costly. A more efficient, yet approximate solution is found by applying a resolution of the identity which is a common procedure to speed up electronic structure calculations with HF, DFT or relativistic approaches. After briefly outlining the gauge problem, more details on the resolution of the identity will be given below.

2.6.1 The gauge problem

The relation between the exchange energy and its energy density per particle shows that any function $F(\mathbf{r})$ integrating to zero can be added to the latter without changing the energy

$$E_X = \int d\mathbf{r} \varepsilon_X \left(\rho(\mathbf{r})\right) + F(\mathbf{r}) \,, \tag{2.52}$$

where $\int F(\mathbf{r}) d\mathbf{r} = 0$.

In global hybrids this problem does not arise as integrated exchange energies are combined by a factor outside the integrated quantities. Local hybrids, however, yield an unrecoverable error if two energy densities with

different gauges are mixed. Since the expression for the exchange energy in the LSDA (Slater exchange) can be derived from the HF approximation of a unifrom electron gas, the exact-exchange energy density and the Slater counterpart appear to share by definition the same gauge. [81] This could explain partly the success of local hybrid functionals without gradient correction in the DFT part.

But GGA functionals loose this gauge due to the integration by parts as outlined above. Since they yield the homogeneous limit in regions of constant density, a larger error occurs most likely in inhomogeneous regions with GGAs as compared to the LSDA. [66] Or, as has been pointed out by Mattson and Armiento [82], there is no analytic gradient expansion for the exchange energy per particle but only for the total exchange energy or the exchange hole. Nevertheless, it is possible to calculate an unambiguous energy density or so-called virial energy densities. But, in the case of exact exchange, both require calculation of the corresponding optimized effective potential [63] which is computationally more demanding and also often numerically unstable. [80] Moreover, additional errors can be introduced in such a gauge correction through an approximation to the OEP.

For a recently proposed local hybrid functional with TPSS meta-GGA exchange and correlation, [27] a gauge has been constructed from the divergence of a vector field. This gauge function includes three adjustable parameters found by making the TPSS exchange-energy density as close as possible to the exact exchange in appropriately chosen systems. In the homogeneous limit, the gauge function tends to zero. It has been discussed that the gauge has a larger influence on atomization energies than on barrier heights.

The gauge presented in Ref. [83] contains additionally second-order derivatives of the density, and a self-consistent implementation using the corrected

gauge is thus rather elaborate. Consequently, in a recent assessment, only self-consistent results for the conventional gauge have been presented. [84] Other suggestions to convert the exact-exchange energy density to the gauge of a semi-local functional (GGA or meta-GGA) employ a coordinate transformation of the exact-exchange hole, [83] which is costly to calculate.

2.6.2 Resolution of the identity approximation

It is possible to reduce computational cost of HF and DFT calculations by approximating the two-electron integrals $(\mu\nu|\eta\lambda)$ which constitute a significant bottleneck in many types of electronic structure calculations. The corresponding procedure is sometimes referred to as density fitting although mostly only basis function pairs are fitted. The same result can be obtained by inserting a complete basis leading to the term resolution of the identity (RI) approximation. Note that the underlying algorithm to both methods are identical. For Coulomb integrals the formal scaling can be reduced by applying the RI approximation while just a smaller prefactor is obtained for the calculation of exchange integrals. The fundamental idea is to expand a product of basis functions in a new auxiliary basis

$$\chi_\mu(\mathbf{r})\chi_\nu(\mathbf{r}) \approx \sum_u^{N_{aux}} d_u^{\mu\nu}\alpha_u(\mathbf{r}) \;, \tag{2.53}$$

which is approximate if the new basis is finite (with N_{aux} basis functions). Such an expansion can be employed in principle for any function and it is also the underlying principle of the AO expansion of MOs (Eq. (2.23)). A residual function measures the difference between the exact quantity and the

basis set expansion

$$R_{\mu\nu}(\mathbf{r}) = \chi_\mu(\mathbf{r})\chi_\nu(\mathbf{r}) - \sum_u d_u^{\mu\nu}\alpha_u(\mathbf{r}) \; . \tag{2.54}$$

The coefficients $d_u^{\mu\nu}$ in Eq. (2.53) are obtained by minimizing either the overlap integral also called the norm

$$\int R_{\mu\nu}(\mathbf{r})R_{\mu\nu}(\mathbf{r})d\mathbf{r} \; , \tag{2.55}$$

or the self-repulsion

$$\int\int R_{\mu\nu}(\mathbf{r}_1)r_{12}^{-1}R_{\mu\nu}(\mathbf{r}_2)d\mathbf{r}_1 d\mathbf{r}_2 \tag{2.56}$$

of the residual function. From minimization of the overlap integral follows an expressionfor the coefficients

$$d_u^{\mu\nu} = \sum_t \int \chi_\mu(\mathbf{r})\chi_\nu(\mathbf{r})\alpha_t(\mathbf{r})d\mathbf{r} \; (\mathbf{S}^{-1})_{tu} \tag{2.57}$$

that involves the overlap integral $S_{tu} = \int \alpha_t(\mathbf{r})\alpha_u(\mathbf{r})d\mathbf{r}$. Minimizing the self-repulsion yields

$$d_u^{\mu\nu} = \sum_t \int \chi_\mu(\mathbf{r}_1)\chi_\nu(\mathbf{r}_1)r_{12}^{-1}\alpha_t(\mathbf{r}_2)d\mathbf{r}_1 d\mathbf{r}_2 \; (\mathbf{V}^{-1})_{tu} \; , \tag{2.58}$$

where $V_{tu} = \int\int \alpha_t(\mathbf{r}_1)r_{12}^{-1}\alpha_u(\mathbf{r}_2)d\mathbf{r}_1 d\mathbf{r}_2$ denotes a two-electron repulsion integral.

Formally, evaluation of Coulomb and exchange matrices scales with the fourth power of the number of basis functions N_{BF}. When using the RI-approximation, scaling for the evaluation of the Coulomb matrix reduces to

$O(N_{BF}^2 N_{aux})$. The formal scaling behavior for the exchange matrix remains unchanged but the cost is reduced due to a smaller prefactor. [85]

2.6.2.1 Approximated quantities in local hybrid calculations

The goal of the RI-approximation to the Coulomb and exchange part of the electronic-interaction part of the KS matrix is reduction of computational cost. In case of the local hybrid functionals the RI is applied to avoid even more expensive numerical integration as some integrals or quantities can simply not be calculated analytically. Numerical integration of the LMF-weighted exchange integrals would have to be done on every grid point and the impact of the RI is thus even larger for local hybrid functionals. Considering e.g. the first integral in Eq. (2.51)

$$\tilde{K}_{\mu\nu} = \int \chi_\mu(\mathbf{r})\, g(\mathbf{r})\, \hat{v}_X^{exact} \chi_\nu(\mathbf{r})\, d\mathbf{r} \ , \tag{2.59}$$

which includes additionally to the exact-exchange potential the LMF and therefore would have to evaluated numerically. Similar to fitting the basis function pairs, the exact-exchange potential acting on a basis function may be expanded in an auxiliary basis $\{f_a\}$

$$\hat{v}_X^{exact} \chi_\nu(\mathbf{r}) = \sum_a^{n_{aux}} d_a^\nu f_a(\mathbf{r}) \ . \tag{2.60}$$

Minimizing the overlap of the residue function

$$R_\nu = \hat{v}_X^{exact} \chi_\nu(\mathbf{r}) - \sum_a d_a^\nu f_a(\mathbf{r})(\mathbf{r}) \ , \tag{2.61}$$

the expansion coefficients are found to be

$$d_a^{\nu} = \sum_b \mathbf{S^{-1}}_{ab} \int f_b(\mathbf{r})\, \hat{v}_X^{exact} \chi_\nu(\mathbf{r})\, d\mathbf{r}\ , \tag{2.62}$$

where $\mathbf{S}$ denotes the (rectangular) overlap matrix between auxiliary basis functions $\{f_a\}$ and the atomic basis set $\{\chi_\nu\}$. Inserting the expression for the expansion coefficients (eq. 2.62) into expansion 2.60 yields the RI-approximation to the exchange potential

$$\hat{v}_X^{exact} \chi_\nu(\mathbf{r}) = \sum_{a,b} \mathbf{S^{-1}})_{ab} \int f_b(\mathbf{r}')\, \hat{v}_X^{exact} \chi_\nu(\mathbf{r}')\, d\mathbf{r}'\, f_a(\mathbf{r})\ . \tag{2.63}$$

There are two caveats: (i) the basis set expansion does not yield the correct asymptotic behavior for the potential and (ii) rather large and weakly contracted basis sets of high quality are needed. [79]

Suppose an AO basis with n_{bas} contracted and n_{aux} auxiliary basis functions. The formal scaling for the calculation of the exact-exchange energy-density would be $(n_{bas})^2 (n_{aux})^2$. Hence, the cost is increased as compared to global hybrid functionals due to the larger number of auxiliary basis functions. Furthermore the exact-exchange energy-density and the corresponding potential would have to be calculated numerically further away from the molecule in order to obtain the correct asymptotics.

As compared to the overlap norm, the error is reduced by one order of magnitude if the Coulomb norm is employed. In the context of OEP approximations, Hesselmann and Manby therefore proposed the use of the Coulomb norm together with Poisson functions as an auxiliary basis in Eq. (2.60). This would yield correct asymptotics and increase the accuracy with a normal-sized basis. Poison functions are, however, not readily available in any quan-

tum chemical programs, and the corresponding integrals are more expensive. By choosing the more feasible overlap norm, even for energy calculations large uncontracted basis sets should be used in order to minimize errors due to the RI approximation. Based on studies with OEP approximations a thorough validation with different basis sets and under consideration of the numerically exact potential is strongly recommended.

If instead of the overlap norm, the Coulomb norm was employed for the expansion coefficients, the error in the potential would be one order of magnitue smaller. Indeed, Hesselmann and Manby [86] proposed the use of the Coulomb norm together with Poisson functions as a basis. This would yield correct asymptotics and reasonable accuracy with a normal sized basis. But again higher accuracy is bought by increasing computational cost and while the effects in property calculations with local hybrids remain to be analyzed, total energies are likely to be less sensitive.

If the atomic orbital basis is used as an auxiliary basis, the above expression for the potential simplifies to

$$\hat{v}_X^{exact}\chi_\nu(\mathbf{r}) = \sum_{\gamma,\sigma}\chi_\gamma(\mathbf{r})\,\mathbf{S^{-1}}_{\gamma\sigma}K_{\sigma\nu}\ , \tag{2.64}$$

where $\mathbf{K}$ is the matrix representation of the exchange operator in the AO basis

$$K_{\mu\nu} = \int \chi_\mu(\mathbf{r})\,\hat{v}_X^{exact}\chi_\nu(\mathbf{r})\,d\mathbf{r} \tag{2.65}$$

and $\mathbf{S^{-1}}$ the inverse of the overlap matrix in the orbital basis with elements

$$S_{\mu\nu} = \int \chi_\mu(\mathbf{r})\,\chi_\nu(\mathbf{r})\,d\mathbf{r}\ . \tag{2.66}$$

Inserting the resulting expression for the exact-exchange potential from Eq. (2.64) into Eq. (2.59), yields an analytical expression for the LMF weighted exact-exchange integral

$$\tilde{K}_{\mu\nu} = \sum_{\gamma,\sigma} G_{\mu\gamma} \mathbf{S^{-1}}_{\gamma\sigma} K_{\sigma\nu} \ , \tag{2.67}$$

where the LMF weighted overlap matrix

$$G_{\mu\nu} = \int \chi_\mu (\mathbf{r})\, g(\mathbf{r})\, \chi_\nu (\mathbf{r})\, d\mathbf{r} \tag{2.68}$$

is calculated on a grid together with the other DFT integrals without further increasing the costs.

Finally, the integral related to the second term in Eq. (2.47) is just the transpose of the first, and both terms together are simply two times the symmetric part of the $\tilde{K}$ matrix.

$$\int \chi_\mu (\mathbf{r})\, g(\mathbf{r})\, \hat{v}_X^{exact} \chi_\nu (\mathbf{r})\, d\mathbf{r} + \int \chi_\mu (\mathbf{r})\, \hat{v}_X^{exact} \left(g(\mathbf{r})\, \chi_\nu (\mathbf{r}) \right) d\mathbf{r} = \tilde{K}_{\mu\nu} + \tilde{K}_{\nu\mu} \ . \tag{2.69}$$

In a similar way to the above-discussed potential terms, the exact-exchange energy-density

$$\varepsilon_X^{exact} (\mathbf{r}_1) = -\frac{1}{2} \sum_{ij} \varphi_i (\mathbf{r}_1)\, \varphi_j (\mathbf{r}_1) \int r_{12}^{-1} \varphi_i (\mathbf{r}_2)\, \varphi_j (\mathbf{r}_2)\, d\mathbf{r}_2 \tag{2.70}$$

can be calculated analytically based on the relation in Eq. (2.64) as follows [78]

$$\varepsilon_X^{exact} (\mathbf{r}) = Tr \left(\mathbf{X}(\mathbf{r})\, \mathbf{S^{-1}KP} \right) \ , \tag{2.71}$$

where the matrix $\mathbf{X}$ contains products of basis functions

$$X_{\mu\nu} = \chi_\mu(\mathbf{r})\chi_\nu(\mathbf{r}) \; . \tag{2.72}$$

Since this matrix is clearly symmetric and the product of an antisymmetric matrix with a symmetric matrix has zero trace, only the symmetric part of the product matrix $\mathbf{S^{-1}KP}$ is needed.

For both of these RI approximations, the assumption has been made that the atomic orbital basis constitutes a complete set for the exchange potential Eq. (2.64). But even a decontraction of the AO basis does not provide a reliable solution in all cases. The employment and development of an auxiliary basis for future use of local hybrid functionals is mandatory.

Another solution might be an RI approximation to the product between the local mixing function and a basis function in Eq. (2.59) instead. Especially if it $g(\mathbf{r})$ includes empirical parameters, possible inaccuracies in the basis set expansion would be absorbed. As a result, however, the parameters would be only valid for a given auxiliary basis set and thus not transferable.

CHAPTER 3

TRAINING AND ASSESSMENT SETS

Despite the continuous success of density functional methods for the calculation of various properties, such as molecular geometries, magnetic properties, excitation energies etc. most studies are preceded by a thorough calibration. In this way, for almost any quantum chemical problem an appropriate density functional can be found, but the result is far from being universal. It is therefore desirable that new functionals that may be constructed for a given purpose are also applicable to properties that are known to be well described by established and popular functionals. The B3LYP functional is, e.g., commonly used as a reference, although an increasing number of examples for its limitations has been revealed in the last years. This chapter provides an overview over several relevant and established test sets. They include thermochemical properties such as atomization energies or dissociation energies as well as kinetics and structural parameters. For each of them merely general trends in the performance of density functionals will be outlined leaving a detailed discussion on the performance of local hybrid functionals, including their limitations, to section 7.

3.1 Atomization energies

The atomization energy is defined as the energy required to break a molecule into its component atoms. It is a quite sensitive test for any quantum chemical method as a balanced description of atoms and molecules is imperative. Furthermore, quantum chemical calculations often benefit from error cancellation, especially if as many bonds are broken as formed. In the case of

atomization energies, no such compensation occurs, as all bonds are broken. Atomization energies are directly related to enthalpies of formation $\Delta_f H^0$ which can be measured experimentally. Here, atomization energies from the so-called G3/99 [10] set are used. Historically it is divided into the G2-1, G2 and G3 subsets. For a given molecule $A_x B_y H_z$ the atomization energy D_e, excluding the zero point energy (ZPE), is calculated via

$$D_e = x\,E(A) + y\,E(B) + z\,E(H) - E_e(A_x B_y H_z)\ . \tag{3.1}$$

The corresponding zero-point corrected atomization energy D_0 is obtained by adding the ZPE to the molecular energy

$$D_0 = D_e - ZPE(A_x B_y H_z)\ . \tag{3.2}$$

Experimental enthalpies of formation at $0K$ can be converted into atomization energies under consideration of experimental enthalpies of formation at $0K$ for gaseous atoms as in Ref. [87]

$$D_0 = x\Delta_f H^0(A) + y\Delta_f H^0(B) + z\Delta_f H^0(H) - \Delta_f H^0(A_x B_y H_z)\ . \tag{3.3}$$

Here rather large uncertainties occur for the atoms Be, B and Si (2.0, 1.2 and 1.0 kcal/mol respectively).

Theoretical enthalpies of formation at 298 K are calculated by thermal correction to $\Delta_f H^0$ at 0 K. For simpler comparison with calculated atomization energies, instead of correcting the latter to 298 K, experimental $\Delta_f H^0(298K)$ for the G3 subsets have been converted to D_e values. For this purpose scaled HF ZPEs and thermal corrections based on HF frequencies have been taken from the literature [88]. The accordingly converted and ZPE

exclusive atomization energies for the G2 and G2-1 subset have been taken from Ref. [89].

While the LSDA strongly overbinds such molecules, GGAs already improve atomization energies. Hybrid functionals with 20 to 25% exact exchange as in B3LYP or PBE hybrid have been shown to be best for these thermochemical properties. However, mean errors increase especially for B3LYP when going from the G2-1 over G2 to the G3 test set, which is most probably due to the increasing number of larger hydrocarbons that give rise to cumulative errors in the atomization energy.

3.2 Barriers heights

Standard GGA and meta-GGA functionals tend to underestimate reaction barriers due to an overstabilization of the transition state. [90] Incorporation of exact exchange as in global hybrid functional improves this tendency but as compared to thermochemical properties, it has been shown that a higher exact-exchange admixture around 50 % is required for barrier heights (BH). This fact usually points towards a more pronounced self interaction error which is cancelled only by exact exchange (or computationally more demanding self-interaction corrected KS theory). Expecting a higher flexibility for local hybrid functionals, they are thus tested for reaction barriers as well. In this work, a test set introduced by Truhlar and coworkers [9, 91] that comprises 19 non-hydrogen transfer (NHT) and 19 hydrogen-transfer (HT) forward and backward barrier heights will be employed. It is part of the larger set used for optimization of density functionals known as the M05 and M06 suite. Their benchmark values are mostly so-called best estimates based on a combination of experimental rate constants and dynamical simulations. [9] Some quantities from the hydrogen-transfer set and most of the

non-hydrogen transfer barriers are based on CCSD(T) calculations extrapolated to the complete basis set limit. Reverse barriers were calculated from the forward barrier and either experimental or computed ZPE-exclusive atomization energies. More details on how the best estimates were obtained, and explicit explanations on each reaction can be found in Refs. [9, 91–94]. Density functionals such as BMK, [71] M05-2X or M06-2X that have been shown to perform well for these reaction barriers incorporate at least 40% of exact exchange and yield mean absolute errors below 2 kcal/mol. Pure GGA functionals on the other hand were clearly inferior with MAEs up to more than 8 kcal/mol and could not be recommended. [15]

3.3 AE6/BH6 set

Especially for parameter optimization, a smaller fit or training set is to be preferred over large ones that contain probably a large number of molecules. The AE6/BH6 set [95] consisting of 6 atomization energies and 6 barrier heights (forward and backward) has been assembled by Truhlar et al. as a small representative subset of the much larger database 3. [96] It has been obtained by minimizing the root-mean-square deviation between standard error measures (mean signed, mean absolute and root mean square error) calculated using the full database and the subset only. For a better transferability to other methods, the errors have been averaged over 80 quantum chemical methods beforehand. As benchmark values for the atomization energies, experimental enthalpies of formation $\Delta_f H^0(298K)$ have been converted to electronic atomization energies using MP2/cc-pVDZ geometries and the corresponding frequencies scaled by 0.9790 . [97] Only hydrogen-transfer barrier heights enter this smaller set and are marked in table 3.1

Reaction	Forward	Reverse Barrier
$Cl + H_2 \rightarrow HCl + H$	8.7	5.7
$OH + H_2 \rightarrow H + H_2O$	5.1	21.2
$CH_3 + H_2 \rightarrow H + CH_4$	12.1	15.3
$OH + CH_4 \rightarrow CH_3 + H_2O$[b]	6.7	19.6
$H + H_2 \rightarrow H_2 + H$	9.6	9.6
$OH + NH_3 \rightarrow H_2O + NH_2$	3.2	12.7
$HCl + CH_3 \rightarrow Cl + CH_4$	1.7	7.9
$OH + C_2H_6 \rightarrow H_2O + C_2H_5$	3.4	19.9
$F + H_2 \rightarrow H + HF$	1.8	33.4
$OH + CH3_3 \rightarrow O + CH_4$	8.1	13.7
$H + PH_3 \rightarrow PH_2 + H_2$	3.1	23.2
$OH + H \rightarrow H_2 + O$[b]	10.7	13.1
$H + H_2S \rightarrow H_2 + HS$[b]	3.5	17.3
$O + HCl \rightarrow OH + Cl$	9.8	10.4
$CH_4 + NH \rightarrow NH_2 + CH_3$	22.4	8.0
$C_2H_6 + NH \rightarrow NH_2 + C_2H_5$	18.3	7.5
$C_2H_6 + NH_2 \rightarrow NH_3 + C_2H_5$	10.4	17.4
$NH_2 + CH_4 \rightarrow CH_3 + NH_3$	14.5	17.8
cis-$C_5H_8 \rightarrow$ cis-C_5H_8	38.4	38.4

Table 3.1: Benchmark values in kcal/mol for 19 forward and reverse hydrogen-transfer barrier heights mostly based on experimental values if not stated otherwise. [a] From CCSD(T) calculations. [b]These reactions are also included in the smaller AE6/BH6 fit set.

Reaction	Forward	Reverse Barrier
6 Heavy atom transfer		
$H + N_2O \rightarrow OH + N_2$	18.14	83.22
$H + FH \rightarrow HF + H$	42.18	42.18
$H + ClH \rightarrow HCl + H$	18.00	18.00
$H + FCH_3 \rightarrow HF + CH_3$	30.38	57.02
$H + F_2 \rightarrow HF + F$	2.27	106.18
$CH_3 + FCl \rightarrow CH_3F + Cl$	7.43	60.17
8 Nucleophilic Substitution		
$F^- + CH_3F \rightarrow FCH_3 + F^-$	-0.34	-0.34
$F^-...CH_3F \rightarrow FCH_3...F^-$	13.38	13.38
$Cl^- + CH_3Cl \rightarrow ClCH_3 + Cl^-$	3.10	3.10
$Cl^-...CH_3Cl \rightarrow ClCH_3...Cl^-$	13.61	13.61
$F^- + CH_3Cl \rightarrow FCH_3 + Cl^-$	-12.54	20.11
$F^-...CH_3Cl \rightarrow FCH_3...Cl^-$	2.89	29.62
$OH^- + CH_3F \rightarrow HOCH_3 + F^-$	-2.78	17.33
$OH^-...CH_3F \rightarrow HOCH_3...F^-$	10.96	47.20
5 Unimolecular and Association Reactions		
$H + N_2 \rightarrow HN_2$	14.69	10.72
$H + CO \rightarrow HCO$	3.17	22.68
$H + C_2H_4 \rightarrow CH_3CH_2$	1.72	41.75
$CH_3 + C_2H_4 \rightarrow CH_3CH_2CH_2$	6.85	32.97
$HCN \rightarrow HNC$	48.16	33.11

Table 3.2: Benchmark values in kcal/mol of 19 forward and reverse non-hydrogen transfer barrier heights based on to the basis set limit extrapolated CCSD(T) calculations.

Molecule	D_e
SiH_4	322.4
SiO	192.08
S_2	101.67
C_3H_4 (propyne)	704.79
$C_2H_2O_2$ (glyoxal)	633.345
C_4H_8 (cyclobutane)	1149.01

Table 3.3: Molecules in the small AE6 test set and corresponding benchmark values for atomization energies in kcal/mol based on experimental enthalpies of formation taken from Ref. [95].

3.4 Dissociation of symmetric radical cations

Several studies have shown a failure of GGA or even meta-GGA density functionals in the description of small radical dimer cations. [98–102] Considering, e.g., the He_2^+ molecule, they reproduce total energies of the He atom and of the He^+ ion rather accurately while they consistently underestimate (too negative) the total energy of the radical cation dimer. [98, 101] A comparison between pure density functionals and HF reveals that the former usually strongly overbind such systems while HF tends to underbind. Thus not too surprisingly the BH&HLYP functional which includes 50% exact exchange has been shown to be superior with respect to the pure density functionals. It performs also better than B3LYP or other hybrids based on the B3 scheme. Equilibrium bond lengths are usually found too long with the common density functionals which seems to be contradicting the overbinding. As a reason for this shortcoming an overestimation of nondynamical correlation directly related to the too localized exchange hole in pure density functionals has

been argued. [98, 101] Another interpretation mostly preferred by chemists corresponds to the self-interaction error present in all approximate density functionals. Indeed a self-interaction error corrected approach where the KS operator explicitly depends on the orbitals yields the correct dissociation behavior. [102] Introduction of more exact exchange in hybrid functionals or local hybrid functionals [24] provides a cure for the same reason. However, 100% exact exchange together with LYP correlation did not improve results for $He_2{}^+$, $Ne_2{}^+$ and $Ar_2{}^+$ as compared to BH& HLYP.

The overall incorrect dissociation behavior does not seem to influence the dissociation energies D_e which are calculated using separated cation and neutral fragments and the equilibrium structure

$$D_e\left(A_2^+\right) = E\left(A\right) + E\left(A^+\right) - E_{eq.}\left(A_2^+\right) \ . \tag{3.4}$$

The first local hybrid functional employing the unscaled quantity $\frac{\tau_W}{\tau}$ as LMF improves the description of such 2-center-3-electron systems to a large extent [24] and the same molecules are included as a test set in the assessment of new local hybrid functionals. The seven systems include $H_2{}^+$, $He_2{}^+$, $Ne_2{}^+$, $Ar_2{}^+$, $(HF)_2{}^+$, $(H_2O)_2{}^+$ and $(NH_3)_2{}^+$. CCSD(t) benchmark values will be given together with local hybrid results in chapter 7.

3.5 Transition metal compounds

For structural investigations of large transition metal (TM) complexes, DFT represents the only feasible tool and in particular carbonyl complexes have served in the past as calibration systems because reliable experimental data is available. [52] Most of the parameterized density functionals are however fitted to common test sets that are biased towards main group compounds

such as the G3 set. [10] Even the extensive training set for the parameterization of new density functionals developed by Truhlar contains only a few transition metal dimers. [103] The test set remains to be dominated by main group compounds. [73] For coordinatively saturated transition metal compounds, some gradient-corrected and hybrid functionals have been shown to give reliable structures and energies and the BP86 and the B3LYP functional have become the preferred ones for this purpose. [52, 104] As a more sensitive test for the performance of semilocal and hybrid density functionals, the bonding situation in coordinatively unsaturated transition-metal compunds, such as dimers and monohydrides, have been investigated by different groups. [103, 105]

3.5.1 Atomic *s*-*d* transfer energies

Upon bond formation of TM atoms *s*-*d* hybridization occurs to some extent, and excitation of an electron from one atomic orbital to another prior to bond formation is thus included in the resulting bonding energy. On account of this, *s*-*d* excitation energies are an interesting subject of investigation, and a systematic underestimation with pure density functionals has been pointed out a long time ago. [106] Introduction of hybrid functional did not provide a cure and interconfigurational energies in 3*d* metals remain rather challenging for DFT. [105] Almost all functionals predict, e.g., the wrong ground state for the Co atom. On average, B3LYP outperforms the pure density functionals while the hybrid TPSSh [107] is only marginally better than other tested functionals. Based on these results it was concluded that errors in *s*-*d* transfer energies are mainly self-interaction errors. [105] HF without any correlation yields slightly too small *s*-*d* transfer energies though close to experimental values for the 3*d* atoms Sc through Cr, but it largely overestimates

s-d transfer energies for the remaining $3d$ elements, being overall inferior to DFT. [106] This behavior has been explained by the strength of correlation depending on spin pairs in a given configuration, considering that correlation effects are entirely missing in HF: for the first half row, correlation effects are stronger in the $4s^1 3d^{n-1}$ configuration leading to an overstabilization of this state with HF. In the other half row the correlation effects due to $3d$ opposite spin pairs are predominant and the $4s^1 3d^{n-1}$ configuration is thus destabilized as compared to $4s^2 3d^{n-2}$. For our assessment set experimental benchmark values (corrected for relativistic effects) for s-d transfer energies of Sc through Cu are taken from Ref. [105] and we followed the procedure described therein for calculation of the relative energies.

3.5.2 Transition metal dimers

Going back to small sized TM compounds such as dimers, several studies [105, 106, 108, 109] showed that no functional exists that yields satisfying results for equilibrium bond lengths and dissociation energies of $3d$ TM dimers and some dimer cations. Even assigning the correct ground state to the particular dimers already poses a challenge and the result depends to a large extent on the density functional. These difficulties in the theoretical treatment of transition metal systems result partly from strong dynamical correlation that are due to the tightly packed electrons in the d-shell. Additionally, TM dimers usually exhibit several low lying excited or nearly degenerate spin-states that emerge upon formation of d bonds. Description of such near-degeneracy effects with a single-determinant method such as KS DFT is a rather tricky task. [106] A study by Schaeffer and coworkers [108] revealed slightly improved dissociation energies for the dimers Sc_2 through Cu_2 (Mn_2 is usually treated as a van-der-Waals complex and excluded here) when using

B3LYP as compared to BLYP without exact exchange while augmenting the exact exchange admixture as in BH&HLYP rather deteriorate the results. Furche and Perdew showed that the meta-GGA hybrid TPSSh performed best for dissociation energies followed by the pure meta-GGA TPSS and pure GGAs and B3LYP. Experimental bond lengths on the other hand were reproduced more accurately with pure gradient-corrected density functionals. [105, 108] Altogether $3d$ TM dimers provide a sensitive test for the accurate treatment of nondynamical correlation in density functionals.

3.5.3 Transition metal monohydrides

In Ref. [105] additionally TM monohydrides were investigated, and it has been pointed out that due to the fundamentally different bonding situation self-interaction errors play a larger role in these systems. In contrast to the metal-metal bond in TM dimers, the bonding situation here may be described either as an ordinary 2-electron bond or, depending on the s-d-transfer energies, as a 3-electron-bond. The former is based on an $4s^2$ configuration in the TM atom and the latter results from a $4s^1$ configuration. Equilibrium bond lengths were predicted reliably by most of the functionals with a mean absolute error of 1.5 pm for B3LYP. The maximum error of 4.1 pm was obtained for NiH with B3LYP. The same functional gave, not too surprisingly considering the above described bonding situation, the best results for the dissociation energies of TM monohydrides. In Table 3.4 the TM dimers and monohydrides are listed together with benchmark values taken from Ref. [105].

Molecule	D_e (kcal/mol)	r_e (pm)	Molecule	D_e (kcal/mol)	r_e (pm)
K_2	12.0	390.5	KH	42.2	224.3
Sc_2	38.4	-	CaH	$\leq$ 41.0	200.3
Ti_2	36.1	194.3	ScH	47.5	-
V_2^+	73.2	173.5	TiH	50.0	177.9
V_2	64.3	177.0	VH	51.4	-
Cr_2	33.9	167.9	CrH	46.8	165.6
Fe_2	26.9	202.0	MnH	31.1	173.1
Co_2	39.4	-	FeH	39.2	158.9
Ni_2^+	52.2	222.3	CoH	48.4	152.0
Ni_2	48.1	215.5	NiH	61.3	147.5
Cu_2	46.7	221.9	CuH	63.4	146.3

Table 3.4: Experimental benchmark values for dissociation energies D_e and equilibrium bond lengths r_e of transition metal dimers and monohydrides. All values are taken from Ref. [105], for detailed information see references therein.

3.6 Isotropic hyperfine coupling constants

So far, the thermochemical and kinetic properties associated with the above described test sets require only the unperturbed total molecular energy. Hence, evaluation of the latter without relaxation of the orbitals is sufficient for the calculation of atomization energies and barrier heights. Furthermore, the differences between self-consistent and post-SCF results are rather small, as will be shown below. In order to assess the local hybrid potential or the self-consistent implementation, respectively, the isotropic hyperfine coupling constants A_{iso} (HFCCs) of 13 small main group radicals [110] are calculated and compared to experimental data. The isotropic HFCC is chosen because, in the absence of spin-orbit corrections, it is a first order property and thus the simplest quantity that depends on the relaxed SCF orbitals without the

need of a perturbative treatment. Also in some cases, it has been shown that this magnetic property is very sensitive to the underlying potential. The isotropic HFCC is directly proportional to the electronic spin densities at a nucleus K

$$A_{iso} = \frac{4\pi}{3}\mu_B\mu_N g_e g_K \left\langle \hat{S}_z \right\rangle^{-1} \left(\rho_\alpha(\mathbf{r}_K) - \rho_\beta(\mathbf{r}_K)\right) \ , \tag{3.5}$$

where μ_B denotes the Bohr magneton, g_e and g_K the nuclear and electronic g-values respectively. $\hat{S}_z$ represents the expectation value of the z-component of the total electronic spin.

In other studies [110,111] hybrid functionals based on the B3-scheme have been shown to be an improvement over GGAs in the calculation of isotropic HFCCs. In particular the B3LYP functional was repeatedly confirmed to outperform other GGA and hybrid functionals which is why it will be used as a reference in this work. The same test set of 13 small main group radicals (listed together with benchmark data in Table 3.5) will be used in this work.

A more recently introduced test set by Hermosilla et al. [112] consists of 75 molecules providing in total 241 theoretical HFCC values which are compared to 174 experimental ones. An extensive study using hybrid functionals showed the B3LYP functional to be superior to B3P86 and B3PW91. This larger test set might be useful for future, more thorough validation of local hybrid functionals. For a first validation of the SCF implementation in this work, the smaller one is considered to be sufficient.

The HFCCs of the nitrogen and the phosphorus atom in their ^{4}S ground state represent a particular challenge not only for density functional methods. Especially for the phosphorus atom, no standard functional even reproduces the correct sign of A_{iso}. It was pointed out that special attention has to be paid when using optimized-effective potentials (OEPs) in combination with

Molecule	Nucleus	A_{iso} (MHz)	Nucleus	A_{iso} (MHz)	Nucleus	A_{iso} (MHz)
Cl_2^-	^{35}Cl	109.0				
CN	^{14}N	-12.6	^{13}C	588.5		
F_2^-	^{19}F	750.8				
FCl	^{19}F	586.6	^{35}Cl	152.2		
FCN	^{13}C	647.7	^{19}F	1363.0	^{14}N	17.9
FCO	^{13}C	803.2	^{19}F	905.8	^{17}O	-
H_2CO^+	^{13}C	-108.7	^{1}H	371.9	^{17}O	-
H_2O^+	^{1}H	-73.1	^{17}O	-83.2		
HCN^-	^{13}C	211.3	^{1}H	384.5	^{14}N	19.9
HCO	^{13}C	371.3[a]	^{1}H	367.4[a]	^{17}O	-
NO_2	^{17}O	-54.1[a]	^{14}N	153.3		
OH	^{17}O	-68.0[a]	^{1}H	-68.7[a]		
CH_3	^{13}C	106.5[a]	^{1}H	-64.5		

Table 3.5: Experimental isotropic hyperfine coupling constants of 13 small main group radicals taken from Ref. Ref. [110]. [a]average value of an experimental range

.

basis-set expansions giving rise to significant deviation from the exact OEP result. If an approximation to the exact OEP is employed it can introduce additional errors. [113]

CHAPTER 4

CHOICE OF LOCAL MIXING FUNCTION

As outlined earlier, suitable LMFs for known approximations to the exchange and correlation functional represent the key quantity in this work. While the basic concept of local hybrid functionals has been suggested earlier, [114] the first LMF to be proposed by Jaramillo et al. was based on the ratio of the von Weizsäcker kinetic-energy density

$$\tau_W(\mathbf{r}) = \frac{|\nabla\rho(\mathbf{r})|^2}{8\rho(\mathbf{r})} \tag{4.1}$$

and the kinetic-energy density τ (cf. Eq. (2.43))

$$t(\mathbf{r}) = \frac{\tau_W(\mathbf{r})}{\tau(\mathbf{r})}\,, \tag{4.2}$$

in the following denoted by t. This function is per definition restricted to the range $[0, 1]$. It was combined in the original work with either Becke exchange and LYP correlation or PBE exchange and PKZB correlation. The LMF brings in 100% exact exchange in one-electron regions (this was thought to be favorable to reduce self-interaction) but no exact exchange in homogeneous regions which are usually well described by pure density functionals. The corresponding local hybrid GGA functional with B88 exchange and LYP correlation provides an improvement over BLYP or B3LYP for the dissociation behavior of two-center, three-electron symmetric radicals and for reaction barriers in linear hydrogen abstraction, but overall very poor atomization energies. This failure can be ascribed to an overall to high amount of exact exchange. Simple powers of t reduce the average exact-exchange admixture

but provide no significant improvement. Furthermore, they deteriorate the description of hydrogen bonds. [115]

Other approaches for ab initio LMFs have been introduced parallel to this work. E.g., it has been shown that LMFs for the LSDA and GGA can be derived from the adiabatic connection. [25] In another approach the density matrix has been employed for the construction of a LMF [26] which has been subsequently parametrized. [116] And a recently proposed local hybrid functional mixes exact exchange with the meta-GGA TPPS where the local mixing function has been derived based on considerations about the underlying exchange-correlation hole. [27]

4.1 Local mixing functions

In this work a clearly semi-empirical approach is pursued, and while approximations to the local mixing function are sought, we rely on existing approximations to the density functional exchange and correlation energies. Although some physical limits can be assigned, and experience with molecular properties provides a rough guideline, in regions between these given limits the LMFs are not defined by any physical constraint. Hence, fitting to experimental data is appropriate. Thus all our LMFs contain at least one parameter which is fitted to the mean absolute error of either the small AE6/BH6 set or the larger G3 set of atomization energies. In the following we will distinguish three different families of LMFs: (i) LMFs based on the down scaled quotient of kinetic energy densities t mentioned above, referred to as t-LMF, (ii) so called s-LMFs which are functions of the reduced density gradient(iii) LMFs that depend additionally on the spin polarization ζ (cf. Eq. (2.37)). Their distinctive properties will be discussed in this section by visualization of LMFs that were optimized with local density functional ex-

change and correlation (Slater and VWN, respectively). Plots are provided for the CS, the F_2, the HF and the CN molecule at equilibrium distance. For N_2 and HFH LMFs are plotted for varying distances allowing for evaluation of the dissociation behavior.

4.1.1 Local mixing functions based on kinetic energy densities and the reduced density gradient

It will be shown [115] that, as compared to global hybrid functionals with one or more parameters, the properties investigated in this work are improved to a large extent with a simple one-parameter t-LMF of the form

$$g(\mathbf{r}) = a\, t(\mathbf{r}) \;, \tag{4.3}$$

combined with only local density functional exchange and correlation. In equation 4.3, the quantity t is simply down scaled in order to obtain lower exact-exchange admixtures. By doing so we sacrifice the correct limit of 100% exact exchange in the high-density limit and in one-electron regions. It should be noted, however, that most of our succesful local hybrid functionals are based on LSDA exchange and correlation or incorporate only partial gradient corrections, and that LSDA correlation violates both of these conditions. [46] Such a down-scaled t-LMF allows thus for error cancellation between the exchange and correlation density functional even in the high-density limit and one-electron regions that are not correctly described by 100% exact exchange together with LSDA correlation. Furthermore, the potential does not yield the correct asymptotics in the tail of the electron density far away from the molecule, which does not seem to affect the properties tested in this work.

Another possible variable that appears as well in the gradient expansion

of the exchange hole is the reduced or dimensionless density gradient, defined in Eq. (2.45). It goes from zero to infinity and has to be mapped onto the range [0,1] in order to use it as a local mixing function. Several possibilities have been proposed by Arbuznikov et al. [117], each including one parameter to determine the slope. In this work, local hybrid functionals with s-LMFs based on the error function

$$g(\mathbf{r}) = \mathrm{erf}\left(a\, s\left(\mathbf{r}\right)\right) \ , \tag{4.4}$$

and a Padé mapping

$$g(\mathbf{r}) = \left(\frac{s(\mathbf{r})}{a + s(\mathbf{r})}\right)^2 \tag{4.5}$$

will be discussed.

From fig. 4.1 can be seen that both, the t- and the s-LMF attain lower values in the bonding region and increase in the core regions. [115, 117] At the nuclei, the t-LMF yields a maximum whereas the s-LMF drops to a cusp. It should be mentioned that at some plots, t-LMFs may exhibit a negative spike; this is a numerical artifact due to the Gaussian basis functions having unphysical zero derivatives at the nuclei. As a consequence, according to the definitions for τ and τ_W in Eqs. 2.43 and 4.1 a numerical uncertainty "0/0" is produced. This effect is most pronounced for hydrogen and becomes negligible for heavier atom basis sets that include functions with sufficiently large Gaussian exponents to recover the electron-nuclear cusp. [76] This numercial uncertaintity could be taken care of inside the source code by adding thresholds.

We presume that the inner part of the core region is not important for thermochemistry and barriers since both LMF types yield similar results,

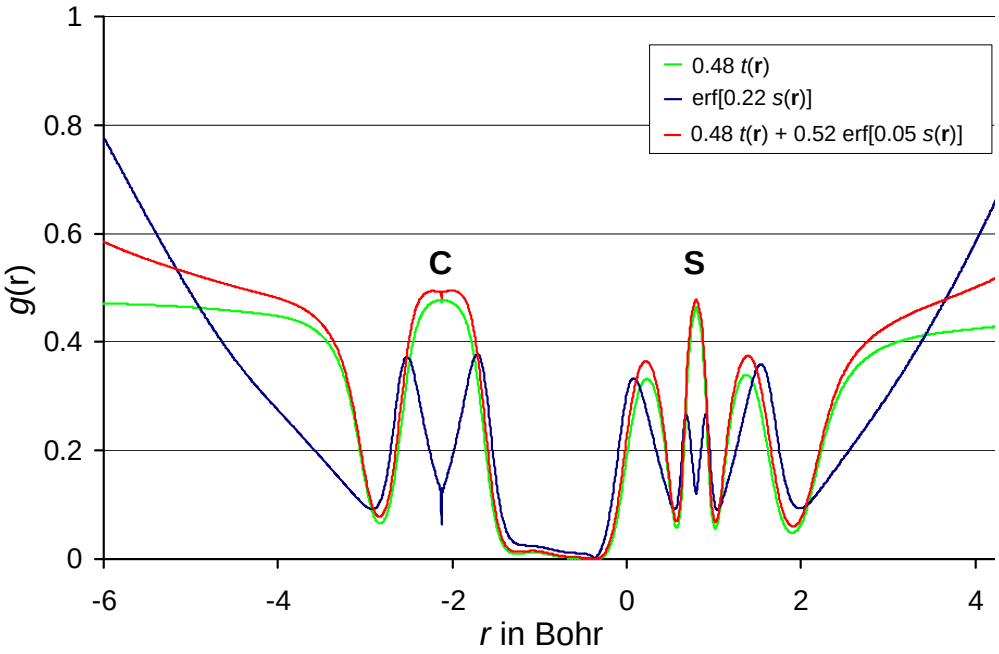

Figure 4.1: Local mixing functions based on kinetic energy densities (t) and the reduced density gradient (s), plotted along the bond axis in the CS molecule.

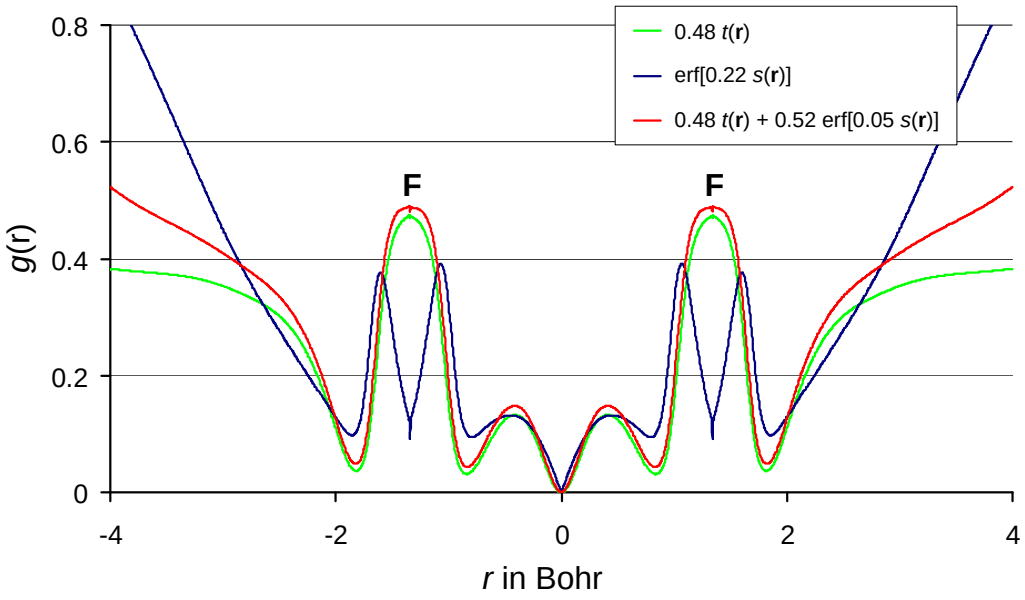

Figure 4.2: Local mixing functions based on kinetic energy densities (t) and the reduced density gradient (s), plotted along the bond axis in the F_2 molecule.

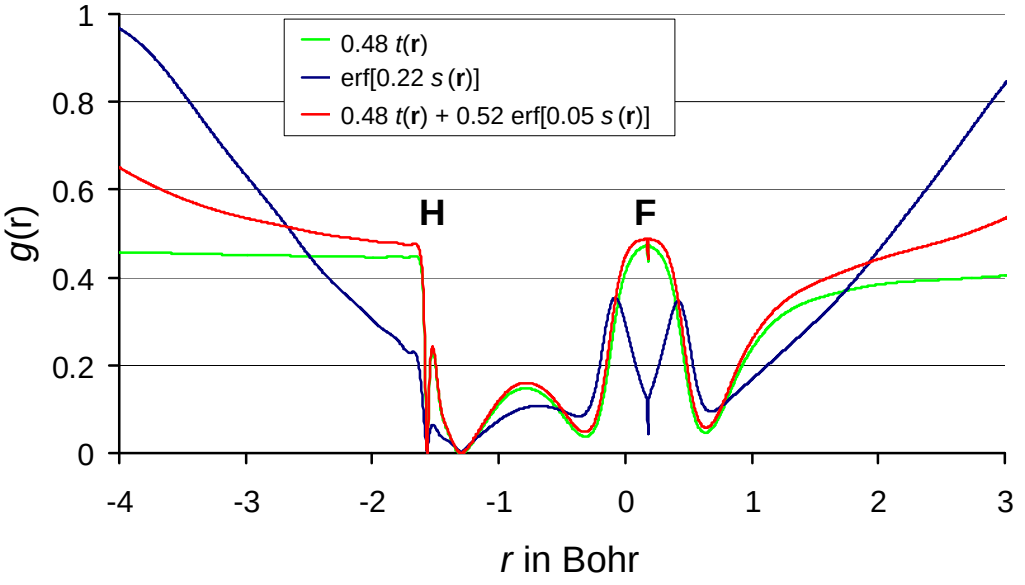

Figure 4.3: Local mixing functions based on kinetic energy densities (t) and the reduced density gradient (s), plotted along the bond axis in the HF molecule.

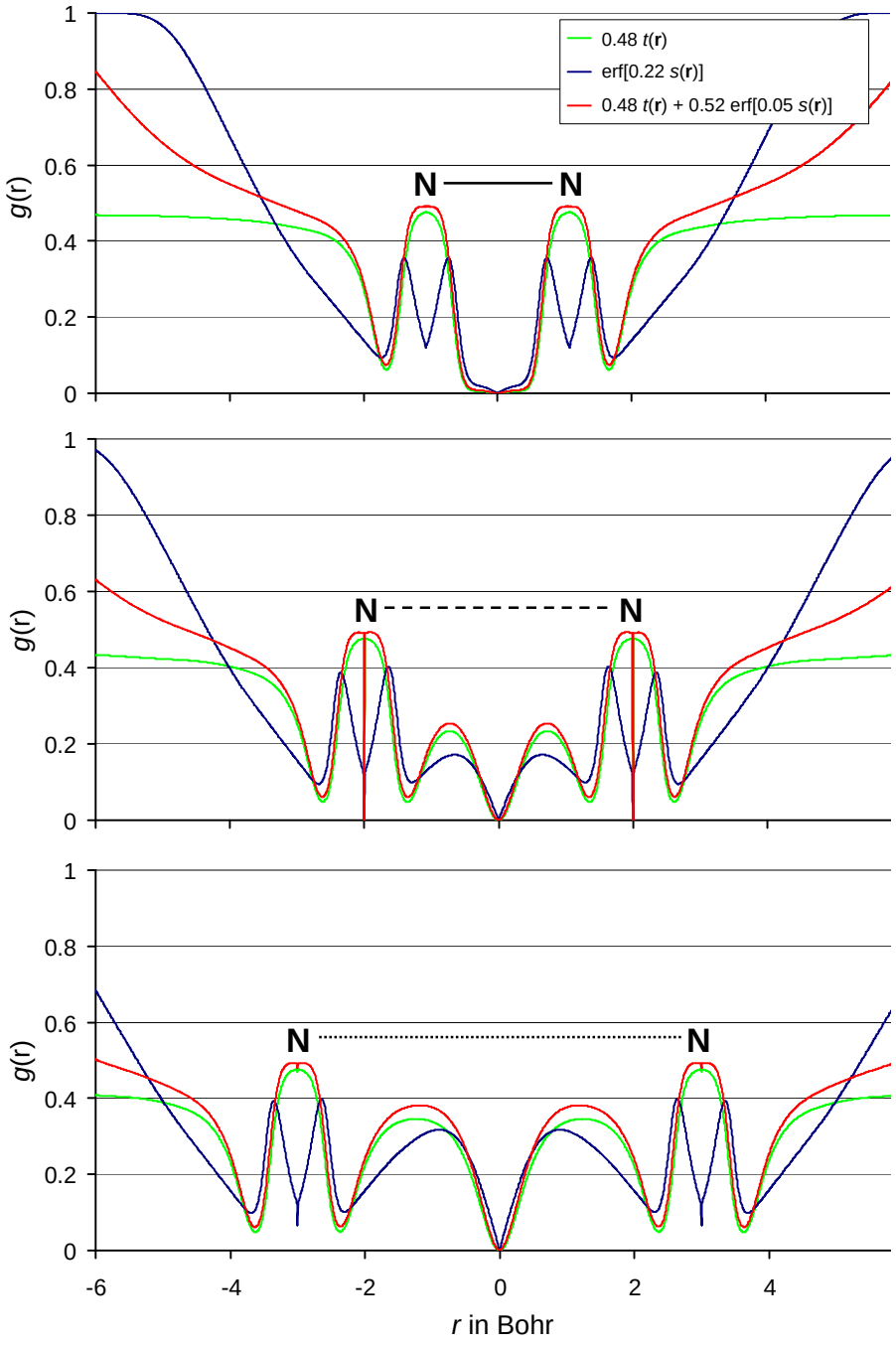

Figure 4.4: Local mixing functions based on kinetic energy densities (t) and the reduced density gradient (s), plotted along the bond axis in the N_2 molecule for three different interatomic distances.

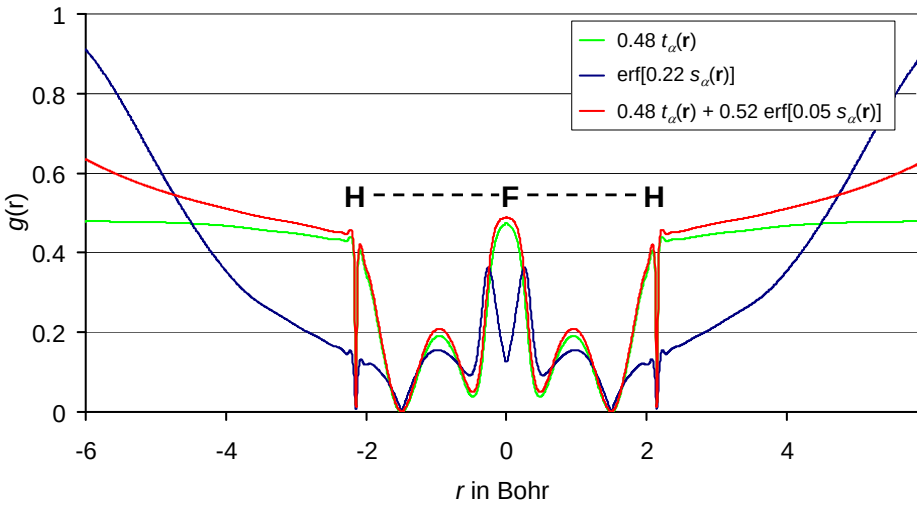

Figure 4.5: Local mixing functions based on kinetic energy densities (t) and the reduced density gradient (s), plotted along the bond axis of the HFH transition state.

whereas the outer-core region may well be. Both LMFs reflect the shell structure around each atom but the s-LMF dips a little less betweent core and valence shells. Along the C-S bond (cf. Fig. 4.1) very small local maxima are found in the t-LMF where for the s-LMF only weak shoulders appear. In contrast, the local maxima in the bond region are much more pronounced for F_2 (Fig. 4.2); again the features are less clear for the s-LMF. As has been discussed in detail by Grüning et al. [90] for the dimensionless density gradient and related quantities, these local maxima in the bond region are indicative of some occupation of antibonding orbitals.

The local maxima in the bonding region are particularly important for the following discussion of reaction barriers. Figs. 4.4 shows how both the t- and s-LMF change when the bond in N_2 is stretched from the equilibrium position to intermediate distances of 4 Bohr, to near dissociation of 6 Bohr. At equilibrium position, local maxima in the bonding region are essentially absent for this strong bond. They develop notably at 4 Bohr and increase

still further and get wider at 6 Bohr. What is most interesting is that the *t*-LMF exhibits the local maxima rather more pronouncedly at the intermediate distance of 4 Bohr than the *s*-LMF. In contrast, at the still larger distance of 6 Bohr, the two LMFs exhibit local maxima of relatively similar height and width for the dissociated atoms. The transition state in the reaction H + FH $\rightarrow$HF + H exhibits similar maxima along the stretched bond (cf. Fig. 4.5.

4.1.2 LMFs with explicit dependence on spin polarization

As pointed out above, the exchange functional in DFT somehow models parts of the nondynamical correlation. But following from its definition, exchange interaction is restricted to electrons of like spin. As a result, in most functionals, opposite-spin nondynamical correlation is only mimicked by terms involving same-spin quantities. An exception are models, such as Becke's coordinate-space model of nondynamical correlation, [118, 119] that separately treat non-classical interactions between same-spin electrons as well as opposite-spin correlation explicitly. The implementation of such a model is, however, rather challenging. In this approach spin-dependent cross-terms that implicitly account for nondynamical correlation are introduced by extending the *t*- and *s*-LMFs by the spin density ζ as an additional variable. [81] Ensuring mathematically equivalent potentials for α and β spin electrons and thus avoiding spurious spin polarization during an SCF calculation leads to the following spin polarized *t*-LMF

$$g(\mathbf{r})_\alpha = \quad (a + b\,\zeta(\mathbf{r}))\,t(\mathbf{r})_\alpha \tag{4.6}$$

$$g(\mathbf{r})_\beta = \quad (a - b\,\zeta(\mathbf{r}))\,t(\mathbf{r})_\beta\ , \tag{4.7}$$

and the respective s-LMF

$$g(\mathbf{r})_\alpha = \quad \mathrm{erf}[(a + b\,\zeta(\mathbf{r}))\, s\,(\mathbf{r})_\alpha] \tag{4.8}$$

$$g(\mathbf{r})_\beta = \quad \mathrm{erf}[(a - b\,\zeta(\mathbf{r}))\, s\,(\mathbf{r})_\beta]\ . \tag{4.9}$$

The function $\zeta(\mathbf{r})$ is restricted to the interval $[-1, 1]$ but overall is predominantly positive (as a result of the α-spin density being greater than the β-spin density) except for strongly spin-contaminated SCF solutions. Figure 4.6 illustrates t- and s-LMFs as well as their spin-polarized counterparts along the bond axis of the CN molecule. Additionally, the spin polarization itself is plotted in the upper picture together with the t-LMFs. At the nuclei, ζ goes to zero due to high densities and takes larger values only in regions with a lower total electron density such as the bonding region and outside of the molecule. With $a = 0.455$, the optimized same-spin scaling parameter a in the spin-polarized version of our t-LMF is slightly smaller than the 0.48 in the best ordinary LMF for Slater exchange and VWN correlation. The opposite-spin scaling parameter b is about one magnitude smaller than a. As a result, at the nuclei where α and β LMF coincide, the spin-polarized alpha and beta LMFs take smaller values than their simpler counterparts. Differences between the optimized spin-polarized and the simple t-LMF are rather subtle in the bonding region due to the LMF being generally small in this area. The minima of the LMFs are located at the same position. Although the same-spin parameter a is slightly smaller in the spin-polarized LMF, the α-spin LMFs overlap for high values of ζ due to the additional ζ-dependent term in the spin-polarized LMF. While outside of the molecule, for the t-LMF, the α function is larger than it's β counterpart, the contrast holds for the s-LMFs. Since the maximum in the β t-LMF at the nuclei is

broader, density averaging of the LMFs yields still larger values for the β-spin function as will be discussed later.

4.2 Optimization procedure

In order to obtain the optimal local mixing function in combination with fixed exchange and correlation energy functional for a given training or fit set, the mean absolute error of a given test set was minimized with respect to one or more parameters. Thus, in general the global minimum is requested. But if appropriate starting values are known, e.g., from a former fit, a local optimization procedure is sufficient. In this work, a Simulated Annealing algorithm [120, 121] was employed for global optimizations followed by a Nelder-Mean Simplex procedure. [122, 123] Since the local optimization involves less function calls, the Simplex algorithm was also taken if the starting values were known to be close to the optimum.

If the LMF depends linearly on the empirical parameter as, e.g., the simple or ζ-dependent t-LMF the scaling coefficients can be excluded from the integration in the energy expression. Consider, for instance, the exchange energy with the one-parameter t-LMF

$$E_X^{Lh} = a \int t(\mathbf{r}) \varepsilon_X^{exact}(\mathbf{r}) d\mathbf{r} + E_X^{Slater}\left[\rho(\mathbf{r})\right] - a \int t(\mathbf{r}) \varepsilon_X^{Slater}(\mathbf{r}) d\mathbf{r} \ , \quad (4.10)$$

as the simplest example. Then the atomization energies of all molecules in the whole fit set and subsequently the deviations from benchmark data are calculated for $a = 0$ and $a = 1$. Two error vectors are obtained: The one with $a = 0$ represents simply LSDA results and is denoted $\mathbf{\Delta E}_{LSDA}^{AE}$. The other one with $a = 1$ contains deviations with a local hybrid functional based on the unscaled t-LMF, Slater exchange and VWN correlation ($\mathbf{\Delta E}_{Lh-SVWN}^{AE}$).

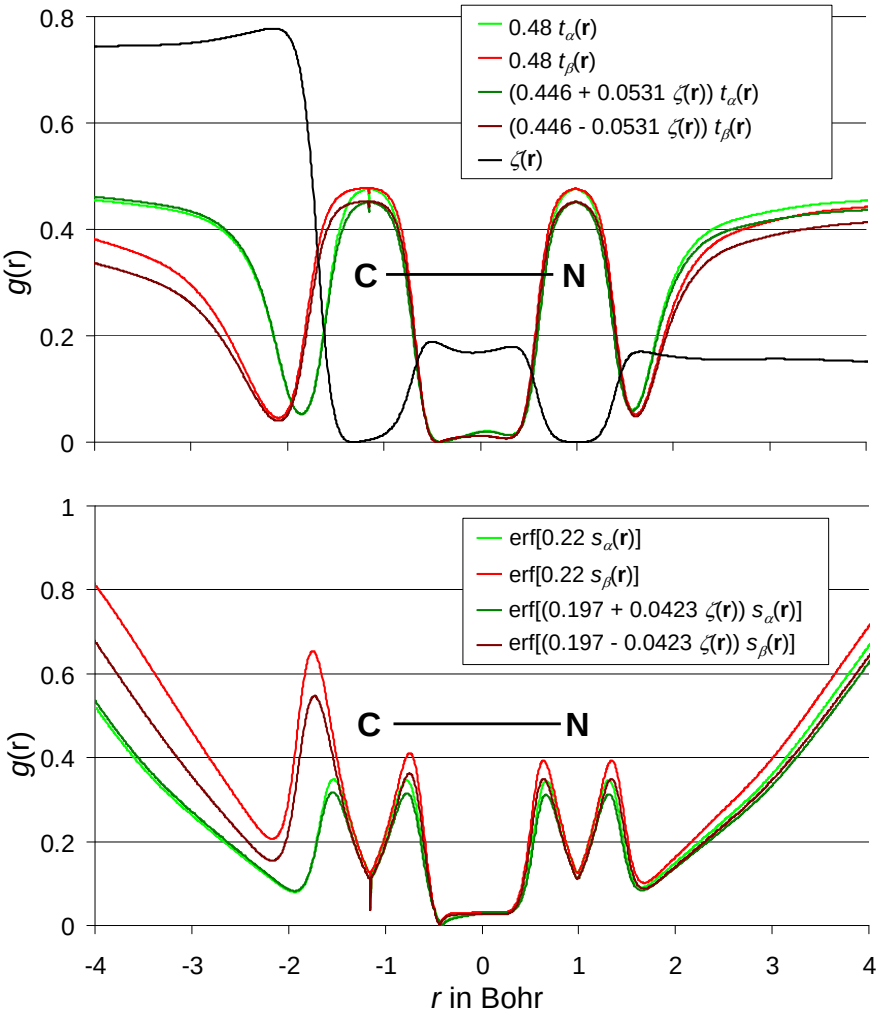

Figure 4.6: LMFs based on the kinetic energy density ratio t (a), the reduced density gradient (b) and their spin-polarized counterparts as well as spin polarization along the bond axis in the CN molecule.

Finally, an error vector depending on the empirical parameter a is computed by combining the two precalculated vectors

$$\mathbf{\Delta E}(a) = \mathbf{\Delta E}^{AE}_{LSDA} + a\left(\mathbf{\Delta E}^{AE}_{Lh-SVWN} - \mathbf{\Delta E}^{AE}_{LSDA}\right) \ , \tag{4.11}$$

such that the MAE as a functional of a is given as the sum over all absolute values divided by the number of molecules N_{mols}

$$\mathrm{MAE}(a) = \frac{1}{N_{mols}} \sum_i \left|\Delta E\left(a\right)\right|_i \ , \tag{4.12}$$

In case of a two-parameter LMF as the spin-polarized t-LMF, a total of three error vectors are needed in order to assemble the MAE as a function of the parameters. If the non-local exchange or correlation admixture are to be fitted additionally to one parameter in the LMF, at least 5 vectors are required.

For s-LMFs and their spin-polarized counterparts the parameters are inside of an error function and for them and in general local mixing functions that do not depend linearly on the empirical parameter(s), the optimization is more costly. This is due to the fact that each function call (calculation of the MAE) involves calculation of the total energy for all molecules and atoms present in the fit set. And although several systems may be calculated in parallel, this step constitutes the bottleneck in optimization procedures.

CHAPTER 5

IMPLEMENTATION

The implementation of local hybrid functionals for electronic structure calculations has been done stepwise. First, as only a few selected density functionals are available in Turbomole, [124,125] the possibility to use customized hybrid functionals has been enabled. The option *functional hybrid* allows for user-defined exchange and correlation density functionals as well as weights for non-local corrections and the amount of exact exchange. Such customized hybrids are also enabled for structure optimizations and frequency calculations as well as for TD-DFT in our local version of Turbomole 5.10. They are highly useful for comparison and debugging the subsequent local hybrid implementation. More general, such custom hybrids allow for systematic studies on the exact-exchange admixture for various molecular properties.

In the second step, local hybrid functionals were implemented in a non-self-consistent fashion. That is, for a given density and KS orbitals, only the energy expression according to Eq. (2.46) is evaluated. Finally, in the third step, the local-hybrid potential was implemented as a FDO giving rise to a non-local potential (cf. Eqs. 2.22 and 2.47). The integrals involving the LMF weighted exact-exchange potential (Eq. (2.59)) were chosen to be computed either following the RI approximation given in section 2.6 or numerically for comparison. In figure 5.1 a flow-chart gives an overview over the most important subroutines that have been modified or that are added. Merely algebraic operations such as transformation of a matrix from SAO to CAO representation or matrix multiplication and symmetrization are left out. Mostly, unmodified subroutines present in the program were employed

for these purposes.

5.1 Post-SCF local hybrid functionals

Here the major step was to obtain the exact-exchange energy-density on a grid which is evaluated according to the RI approximation in Eq. (2.71). Therefore, the overlap matrix of the AO basis, which is evaluated generally in any self-consistent DFT calculation, has to be inverted. This has to be done equally with the auxiliary basis set in a DFT calculation with the RI option and the corresponding subroutine was employed. Attention should be paid if some of the basis functions are linearly dependent, especially if decontracted basis sets are used. Small linear dependencies can be projected out but for strong linear dependencies, the inversion fails. This can be checked by comparing the numerically integrated exact-exchange energy to the exact expression obtained from the exchange and the density matrix

$$\int \varepsilon_X^{exact}(\mathbf{r}) d\mathbf{r} = E_X^{exact} = -\frac{1}{2} \sum_{\mu\nu} P_{\mu\nu} K_{\mu\nu} \; . \tag{5.1}$$

with the matrix elements $K_{\mu\nu}$ as defined in Eq. (2.65).

Usually, in the dscf module the Coulomb part and the exchange part of the KS matrix are calculated as a sum in the *shloop* module. I.e. each two-electron integral is evaluated only once and used for construction of the Coulomb and exchange matrix simultaneously. For local hybrids, only the Coulomb part to the KS matrix is calculated analytically, and the exchange part is obtained via numerical integration on a grid analogous to the DFT exchange-correlation potential. However, for the RI approximation to the exact-exchange energy density the exchange matrix $\mathbf{K}$ is needed separately. In a modified version *shloop_lhyb* of the original two-electron integral rou-

tine, where each integral is evaluated just once (or in each cycle depending on whether a direct approach is used), the Coulomb and exchange matrices are still computed simultaneously but simply stored separately. The density matrix $\mathbf{P}$ is evaluated anyway at the beginning of each SCF cycle and is handed over to the driver subroutine for numerical integration on a grid *xclhyb* together with the inverse overlap matrix $\mathbf{S^{-1}}$ and the exchange matrix $\mathbf{K}$. Thereafter the symmetric part of the product matrix $\mathbf{S^{-1}KP}$ is calculated and, finally, the RI approximation to the exact-exchange energy-density defined as

$$\varepsilon_X^{exact}(\mathbf{r}) = \frac{1}{2}\sum_{\mu\nu}\chi_\nu(\mathbf{r})\left(\mathbf{S^{-1}KP} + \mathbf{PKS^{-1}}\right)_{\nu\mu}\chi_\mu(\mathbf{r}) \ , \tag{5.2}$$

is computed by using the same subroutine that calculates the density on a grid and handing over the matrix product $\frac{1}{2}\left(\mathbf{S^{-1}KP} + \mathbf{PKS^{-1}}\right)$.

Batchwise, the density, its gradients, and the kinetic energy density are evaluated on the grid. In order to avoid recompiling for every new local mixing function, they are handed over to a python script that calculates the LMF which is specified as a string in the dscf program. As this involves a lot of input/output operations, this procedure is rather time-consuming. However, it is highly useful for quick tests of new local mixing functions and parameter fitting. Some local mixing functions such as the spin-polarized ones (that include as well simple *t*- and *s*-LMFs as a special case by setting the second parameter to zero) have been hard-coded.

5.2 Self-consistent implementation of local hybrid functionals

RI approximations to Coulomb and exchange integrals have been established [85,126] as a major speed up and the corresponding auxiliary basis sets could

be optimized using a variational procedure. [127] For the exact-exchange potential, several studies [78,86] showed that a fit based on the overlap norm requires quite large uncontracted basis sets. Although errors in the total energy are expected to be rather small, the inaccuracies in the potential could lead to larger discrepancies for orbital-dependent properties. Thus, rigorous tests on the basis set dependence and especially comparison with results obtained from the numerically exact local hybrid potential are mandatory. For this reason, the numerical local hybrid potential has been implemented additionally to the RI potential.

5.2.1 RI approximation

The bottleneck in a SCF calculation is evaluation of the two-electron integrals $(\mu\nu|\eta\lambda)$, as this step scales with the number of basis functions to the fourth. Efficiency is thus mostly achieved through a rigorous integral prescreening. Additionally, the Coulomb and exchange part of the KS matrix are constructed recursively in the dscf module, in order to reduce computational cost. [128] As for the RI approximations in the self-consistent implementation of local hybrid functionals, the full exchange matrix has to be recovered and therefore small modifications had to be introduced into the scf subroutine with respect to the post-SCF version.

In each SCF cycle n, the density matrix $\mathbf{P}^{(n)}$ is calculated from the orbital coefficients. Then the difference between the density matrix from the current and the previous cycle is obtained via

$$\Delta\mathbf{P}^{(n)} = \mathbf{P}^{(n)} - \mathbf{P}^{(n-1)} \; . \tag{5.3}$$

The Coulomb and exchange matrix elements are subsequently calculated from

the difference density matrix $\Delta\mathbf{P}^{(n)}$ and assembled from previous matrices which yields the following expression for the full exchange matrix

$$\mathbf{K}^{(n)} = \mathbf{K}^{(n-1)} + \mathbf{K}\left[\Delta\mathbf{P}^{(n)}\right] \ . \tag{5.4}$$

Evidently, the difference-density matrix-elements become successively smaller near convergence. A major speed-up is thus achieved by using the difference density matrix, instead of the total density matrix, during the integral pre-screening (in direct SCF). [128] As a consequence, for SCF calculations with local hybrid functionals, the exchange and Coulomb matrices from previous cycles have to be stored and reassembled separately as well.

In the numerical integration routine *xclhyb*, after computation of the density, its gradients and the kinetic energy density, at first, the LMF is calculated by use of the *scflmf* subroutines. Besides the function itself, its derivatives with respect to the density, the gradient of the density and the kinetic energy density is calculated as well and handed over to the lochyb subroutines.

Additionally to the usual integrals, the $\mathbf{G}$ matrix (representation of the LMF in the AO basis, cf. Eq. (2.68)) has to be evaluated. This is done numerically and in the same fashion, the exchange-correlation part of the KS matrix is computed by handing over the LMF instead of a multiplicative potential. Subsequent calculation of the symmetrized $\tilde{\mathbf{K}}$ matrix (cf. Eqs. 2.69 and 2.67) is carried out in the same manner as the symmetrized matrix product for the exact-exchange energy-density.

At the end of the numerical integration part, the LMF weighted exact-exchange matrix (Eq. 2.69) is assembled. Note that the corresponding matrix manipulations are done in the SAO basis, thus fully exploiting symmetry, while numerical integration is generally performed in the CAO basis.

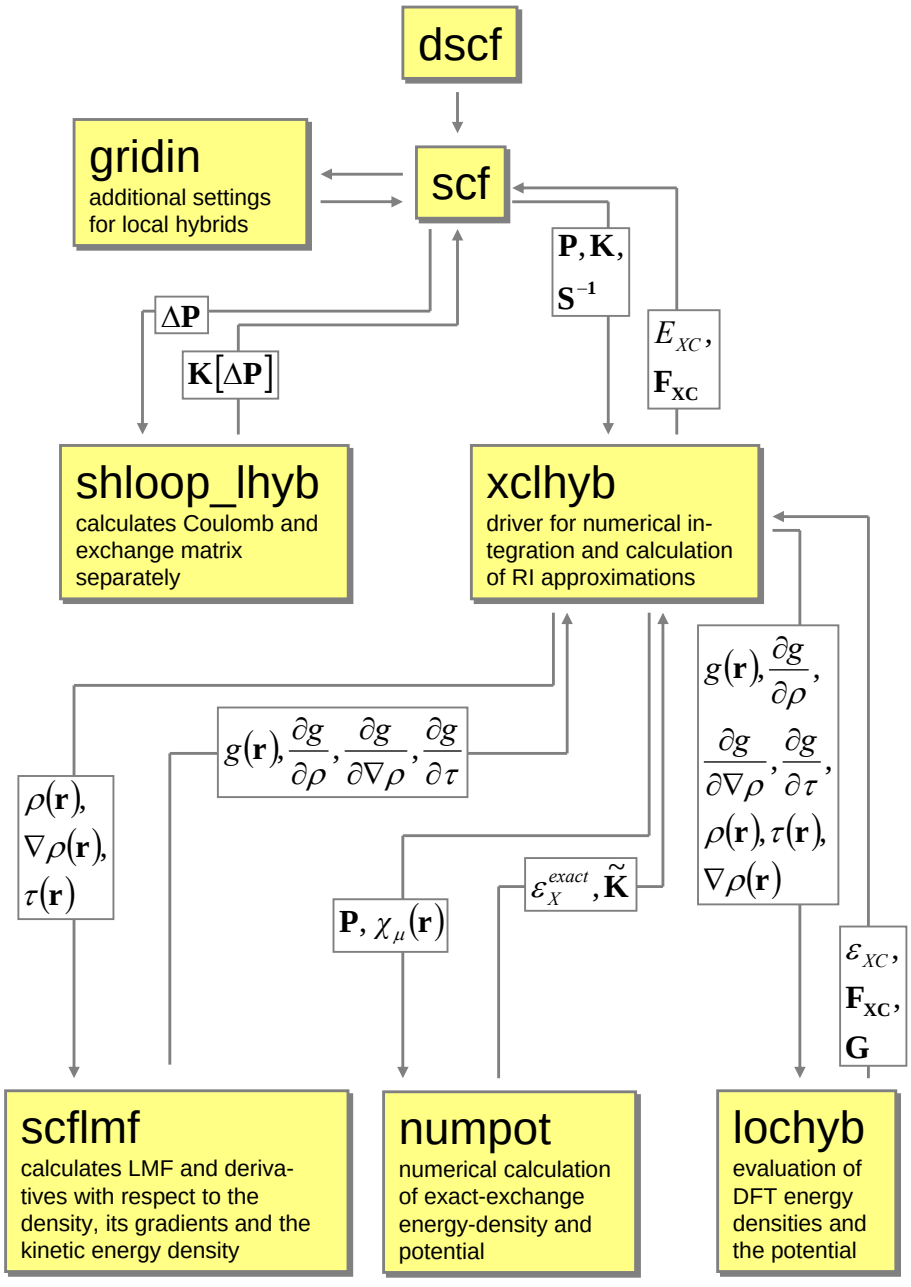

Figure 5.1: Overview over some modified and new subroutines for local hybrid calculations in the dscf module of our local version of Turbomole 5.10.

5.2.2 Numerical local hybrid potential

For the numerical exact solution to the exact-exchange energy-density and numerical integration of the LMF weighted exact-exchange potential (rhs of Eq. (2.59)), the one-electron Coulomb integrals

$$V_{\mu\nu}(\mathbf{r}_1) = \int \chi_\mu(\mathbf{r}_2)\chi_\nu(\mathbf{r}_2) r_{12}^{-1} d\mathbf{r}_2 \; . \tag{5.5}$$

have to to be evaluated on each grid point. This is conventionally done following a Rys scheme that allows for the exact solution based on a Gauss quadrature. [129] The corresponding driver subroutine *numpot* has been derived from the one that computes the numerical Slater potential in the framework of the localized Hartree Fock method. [78]

As the evaluation of $V_{\mu\nu}(\mathbf{r})$ is very time-consuming, each matrix element is calculated just once and used simultaneously for the exact-exchange energy density and the integrals $\tilde{K}_{\mu\nu}$.

5.2.3 Timings

From the matrix expression for the RI approximation to the local hybrid potential follows that the overall scaling is equal to global hybrid calculations in the same basis. Depending on the auxiliary basis, a larger prefactor may occur for local hybrid functionals. Since a local hybrid run uses additional subroutines to the ones for global hybrid calculations the prefactor is slightly larger. This is confirmed by the CPU time per iteration which is given in Table 5.1 for the molecules in the AE6/BH6 set. Timings with a local hybrid with Slater exchange, VWN correlation and a *t*-LMF are compared to TPSS hybrid calculations since both functionals require kinetic energy densities and the density gradient. Independent of the system size, the local hybrid calcu-

lation is slower by a factor of only 1.14 per iteration on average confirming the identical scaling behavior. Given that the emphasis of the implementation was not efficiency the prefactor can be further reduced by optimizing system calls, matrix manipulations and reducing I/O operations for a given local hybrid functional. This clearly contradicts former statements that local hybrid functionals are significantly more expensive than global hybrid calculations. [130] It should be noted, however, that so far large uncontracted basis sets are required with the RI option for the potential thus rendering local hybrid functionals rendering more expensive in practice.

5.2.4 Summary of the options with local hybrid functionals

If the total energy only of a local hybrid functionals is requested, a customized LMF with the variables r, s and t can be used. Due to the system call and especially I/O operations the gain in flexibility is accompagnied by a loss of efficiency. Therefore, several LMFs were hard-coded as well. Those available LMFs in post-SCF runs include the two-parameter spin polarized t-LMF and s-LMF (cf Eqs. 4.7 and 4.9) and a two-parameter mixed LMF of the form

$$g(\mathbf{r}) = at(\mathbf{r}) + (1-a)erf(\lambda s) \; . \tag{5.6}$$

For efficiency the LMF cannot be customized in self-consistent calculations and only three types of LMFs are currently available: the simple one-parameter t- and s-LMFs and the above mentioned mixed LMF. Besides specifying the LMF parameters, one can choose between the numerically exact potential or the more efficient RI approximation.

Based on the general form of a local hybrid functional

$$E_{XC}^{Lh} = \int g\left(\mathbf{r}\right) \varepsilon_X^{exact}\left(\mathbf{r}\right) d\mathbf{r} \tag{5.7}$$

$$+ \int \left(1 - g\left(\mathbf{r}\right)\right) \left(\varepsilon_X^{Slater}\left(\mathbf{r}\right) + b\Delta\varepsilon_X^{(meta-)GGA}\left(\mathbf{r}\right)\right) d\mathbf{r} \tag{5.8}$$

$$+ E_C^{VWN} + c\Delta E_C^{(meta-)GGA}\,, \tag{5.9}$$

additionally to the LMF, the amount of gradient correction to density functional exchange (b) and correlation (c) may be varied.

Molecule	t/iteration (iterations)		$\frac{t(\text{Local Hybrid})}{t(\text{TPSSh})}$
	Local hybrid	TPSSh	
S	1.82 (6)	1.61 (6)	1.13
C	1.17 (6)	1.04 (6)	1.13
SH	7.23 (6)	6.11 (6)	1.18
OH	5.01 (7)	4.36 (6)	1.15
H_2	0.19 (5)	0.18 (5)	1.07
H	0.34 (5)	0.35 (5)	0.98
HSHHts	17.65 (7)	15.88 (6)	1.11
Si	1.81 (6)	1.59 (6)	1.14
C_3H_4 (propyne)	94.89 (8)	89.13 (8)	1.06
H_2S	3.39 (7)	3.09 (6)	1.09
HOHts	11.52 (7)	9.72 (8)	1.19
C_4H_8 (cyclobutane)	540.64 (8)	466.28 (8)	1.16
CH_3HOHts	107.60 (8)	95.49 (8)	1.13
CH_3	5.28 (6)	4.72 (6)	1.12
CH_4	2.14 (6)	2.00 (6)	1.07
O	1.12 (6)	1.01 (6)	1.11
S_2	4.86 (7)	4.60 (6)	1.06
$C_2H_2O_2$ (glyoxal)	38.76 (7)	35.26 (7)	1.10
SiO	4.75 (6)	4.39 (7)	1.08
H_2O	2.48 (7)	2.12 (8)	1.17
SiH_4	7.20 (6)	6.26 (6)	1.14
Σ	859.84	755.19	1.14

Table 5.1: CPU time t in seconds per iteration for self-consistent energy calculations of the molecules in the AE6/BH6 test set. The local hybrid functional is based on Slater exchange and VWN correlation with the LMF $g(\mathbf{r}) = 0.48t(\mathbf{r})$.

CHAPTER 6

COMPUTATIONAL DETAILS

If not stated otherwise all energy as well as the self-consistent calculations have been carried out using a local version of the Turbomole program package [124, 125] (version 5.10). Open-shell species have been calculated at spin-unrestricted Kohn-Sham level. Non self-consistent energy calculations are based on previously obtained B3LYP [4, 13, 65] orbitals for which the convergency threshold has been set to 6 in order to ensure well relaxed orbitals. For consistency the same threshold was applied for self-consistent local hybrid calculations.

For the large G3 set (including subsets G2-1 and G2) of atomization energies, MP2/6-31G structures were taken from Refs. [87, 88, 131, 132] and supplementary materials therein. Their experimental atomization energies were calculated by subtracting HF/6-31G thermal corrections and zero-point energies from experimental enthalpies of formation.

For the barrier heights QCISD/MG3 structures were used [9, 94, 95] and our theoretical values were compared to best estimates from Refs. [9, 94] for the HTBH38 hydrogen-transfer barrier set and from Ref. [95] for the NHTBH38 heavy-atom transfer reaction set. QCISD/MG3 molecular structures for barrier heights and additional structures for the molecules in the AE6 set were downloaded from the Minnesota Database Collection [133]. A large grid (size 6) was used for thermochemistry and reaction barriers.

Isotropic hyperfine coupling constants were calculated using the contracted and decontracted IGLO-II, IGLO-III and IGLO-IV basis sets [134]. For all other properties and generation of the orbitals the QZVP [135] basis

set was employed. Because the exact-exchange energy density is computed based on a resolution of the identity, the QZVP basis has been decontracted beforehand. In order to avoid linear dependencies, one s-function with the exponent 32.9926 had to be removed from the silicon QZVP basis set.

Dissociation curves of the 2-center 3-electron systems have been obtained by computing the energies non-self-consistently (see above, based on B3LYP orbitals using the uncontracted QZVP basis). Following previously suggested procedures, [24] the structures of the fragments taken from Ref. [136] were kept constant varying only the inter-fragment distance. The equilibrium distance was then determined by a least-squares-fit of a polynomial to at least six points on the dissociation curves. Corresponding dissociation energies were subsequently calculated for the optimized equilibrium structure in each case relative to separated cation and neutral fragments. They refer thus to the correct asymptote.

The isotropic hyperfine coupling constants were calculated with experimental structures taken from Ref. [110]. While the orbitals were obtained using the Turbomole package with a grid of size 5, the MAG-ReSpect [137] suite of programs has been employed the computation of magnetic properties.

The *s*-*d* transfer energies have been calculated following a procedure suggested in Ref. [105]. That is, atomic orbitals were obtained in O_h symmetry in order to suppress mixing of s and d orbitals. If this results in fractional occupation numbers, as e.g. in case of the d^6s^2 state of Fe a subsequent transformation to C_1 symmetry and non-self consistent calculation for the two possible states are performed.

Some post-SCF local hybrid results that were obtained with an implementation in the ReSpect program package will be marked specifically. In these cases the cc-pVQZ basis (omitting g-functions) has been used, and the

orbitals have been obtained from a global hybrid with Slater exchange, VWN correlation and 10% exact exchange.

For each test set a python script is provided which, starting from a B3LYP calculation replaces the functional in the control file by a given local hybrid and launches a dscf run. From the resulting total energies, the properties (e.g. atomization energies, barrier heights, equilibrium distances for TM dimers or hydrides etc.) are computed with the help of one or several other Python scripts. Usually, the same program also evaluates deviations from benchmark values as well as mean errors. To simplify discussions for whole sets of n_{mols} molecules the mean signed error (MSE)

$$MSE = \frac{1}{n_{mols}} \sum_{i}^{n_{mols}} E_i^{calc} - E_i^{benchmark} \tag{6.1}$$

and the mean absolute error (MAE)

$$MAE = \frac{1}{n_{mols}} \sum_{i}^{n_{mols}} \left| E_i^{calc} - E_i^{benchmark} \right| \tag{6.2}$$

are calculated according to their definitions.

CHAPTER 7

ASSESSMENT

In this chapter several local hybrid functionals with at least one semi-empirical parameter fitted to empirical data will be presented and their performance for thermochemical and kinetic properties will be evaluated. As a preface to a more detailed discussion of the fit results and the assessment, the development of the first competitive local hybrid functional shall be summarized briefly.

Most of the successful and the first thermochemically competitive local hybrid functionals presented in this work are based on Slater exchange and VWN correlation. One reason for starting from the LSDA rather than from a GGA functional can be traced back to error cancellation. Considering atomization energies, the limiting cases of pure LSDA (S-VWN) and of 100% exact exchange combined with LSDA correlation (EXX-VWN) lead - not unexpectedly - to dramatic over- and underbinding respectively, resulting in similarly large MAEs of around 30 kcal/mol. Note also the mean signed deviations in Table 7.1 that express better under-/overbinding tendencies.

Functional	G2-1	
	MAE	MSE
S-VWN	35.92	35.83
EXX-VWN	28.47	-24.58
S-EXX-VWN with $a_0 = 0.5$	9.87	3.43

Table 7.1: Errors in (kcal/mol) obtained with ReSpect and the corresponding procedure described in chapter 6. At the same level, the MAE for B3LYP is 3.17 (kcal/mol) and for B3PW91 it is 3.27 (kcal/mol)

.

One expects an appreciable improvement already for a global hybrid of the underlying components, which is indeed the case: The best overall performance is obtained with exactly 50% exact exchange (cf. Fig. 7.1, leading to a reduction of the overall MAE by a factor of 3 to less than 10 kcal/mol. This corresponds actually to the very first hybrid functional published by Becke, [39] "the half-and-half" functional that mixes 50% LSDA exchange with 50% exact exchange. Turning now to local hybrids with the simple LMF $g = at(\mathbf{r})$ (see plots in Fig. 7.1), we see a remarkable improvement of the MAE over the best global hybrid by another factor of almost 3 when the parameter a approaches values around 0.5 (the best value found is $a = 0.48$). Obviously, the dependence on the scaling parameter is more pronounced for local than for global hybrids.

The MAE of 3.73 kcal/mol for the G2-1 set of atomization energies with $a = 0.48$ is in the range of the best state-of-the-art global hybrid functionals and this is obtained only by position-dependent admixture of exact exchange to local exchange, without any GGA involved! Notably, this functional with scaled LMF and thus one semi-empirical parameter improves performance dramatically over the unscaled t-LMF by dropping the requirement of 100% exact-exchange admixture in one-electron regions. Now one-electron regions exhibit 48% exact exchange. This appears reasonable when considering the H_2 molecule: Here $t(\mathbf{r})$ would yield 100% exact exchange everywhere in space, independent of, e.g., a stretching of the H-H bond. This does clearly not account for the necessary nondynamical correlation contributions in this case and in related situations, e.g., for bonds between hydrogen and other atoms. [76] The LMF plots along the bond axes in chapter 4 in Figs. (4.1, 4.2, 4.4) show that this scaled LMF yields 48% exact exchange around the nuclei and in asymptotic regions and exclusively local exchange in homogeneous

regions as should be the case. Obviously, this position dependence of exact-exchange admixture has a strikingly favorable effect on the thermochemical performance of the functional. On the other hand, it is clear that performance for a one-electron system like $H_2{}^+$ will be worse than with the unscaled t-LMF as the resulting hybrid with 48% exact-exchange admixture will not eliminate self interaction completely but, of course, better than typical global hybrids with a global factor between 0.2 and 0.25.

We may obtain an average exact-exchange admixture $\overline{g}$ for a local hybrid functional by density averaging [76]

$$\overline{g}_\sigma = \frac{1}{N_\sigma} \int \rho_\sigma(\mathbf{r}) g_\sigma(\mathbf{r}) d\mathbf{r} \ . \tag{7.1}$$

For open shell systems, a spin-averaged admixture a is calculated from

$$\overline{g} = \frac{N_\alpha \overline{g}_\alpha + N_\beta \overline{g}_\beta}{N_\alpha + N_\beta} \ , \tag{7.2}$$

where N_σ is the number of electrons with σ spin. For the SVWN local hybrid with SVWN and $g(\mathbf{r}) = 0.48t(\mathbf{r})$, this procedure followed by averaging the $\overline{g}$ values over the G2-1 set provides a=0.293, i.e., a value that is considerably lower than the best constant exact-exchange admixture of $a_0 = 0.5$.In conclusion, the position-dependent exact-exchange admixture with only local exchange and correlation gives a simple local hybrid functional with no GGA component that provides thermochemical accuracy competitive with the best state-of-the-art functionals

7.1 Fit results and dependency on the training set

It has been argued in the literature that some failures of B3LYP could be attributed to the limited size of the fitting set. [138] However, we have used

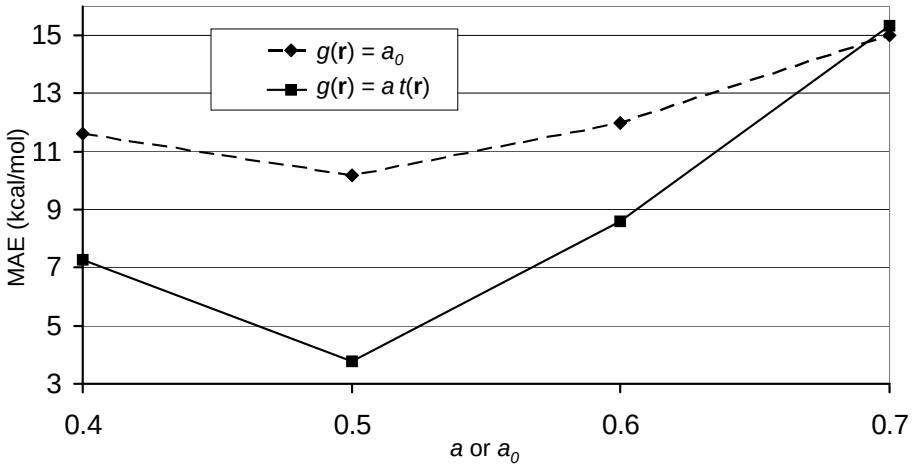

Figure 7.1: MAE for the 55 atomization energies of the G2-1 set with a SVWN global and local hybrid functional as a function of the mixing parameters a_0 (constant) and a (scaling parameter inside the t-LMF).

the same, namely the small G2-1 set of atomization energies. Fig. 7.2 shows that the optimal parameter for the scaled t-LMF (cf. Eq. (4.2)) obtained from the small G2-1 set corresponds overall also to the best parameter of the G3 set. Considering the molecule types, (cf. Fig. 7.2) only the non-hydrogen systems would be improved significantly with a smaller scaling parameter. Obviously the optimal value depends much more on the property under investigation which can be seen from Fig. 7.3 where the MAEs for barrier heights are plotted as a function of the scaling parameter a: a larger value of a leads to an only slightly better description of hydrogen transfer barriers. A more pronounced improvement for non-hydrogen transfer barriers is observed and possible reasons will be discussed below.

In Table 7.2 the local hybrid functionals including between one and three optimized parameters are summarized, and a name is assigned to each functional, in order to facilitate the following discussion. Mainly the G2-1 and the AE6/BH6 set have been employed as training sets in this work. The

AE6/BH6 set includes only 6 atomization energies (as compared to 55 in the G2-1 set) and additionally barriers. But, at least in case of the one-parameter *t*- and *s*-LMFs, the fit results are equivalent for the two training sets. Actually, the one-parameter functionals *tLMF*-SVWN and *sLMF*-SVWN originate from a previous fit to the G2-1 set using the ReSpect program and corresponding settings (cc-pVQZ basis, for details see chapter 6). Optimization with the current settings (Turbomole implementation and decontracted QZVP basis set) yields slightly increased scaling parameters of 0.49 and 0.23 for the *t*- and *s*-LMF, respectively. However, for consistency, we will usually refer to the former LMFs as the "best" *t*- and *s*-LMF for Slater exchange and VWN correlation and use the corresponding local hybrid functionals for the assessment. This is all the more justifiable considering that (with the current settings) they perform better for the complete G3 set of atomization energies than their updated versions (see Table 7.2). Even the discrepancies in the G2-1 MAE due to a re-optimization of the scaling parameters are marginal, especially as compared to deviations in the MAEs due to different types of functionals. One other local hybrid functional, sLMF1-SLYP, that has been previously optimized by A. et al. is included as well. It uses full LYP gradient correction in the correlation functional, LSDA exchange and a Padé mapping of the reduced density gradient as a local mixing function (cf. Eq. (4.5)).

Based on these results and for efficiency, LMFs with a non-linear dependency on the parameter are optimized for the smaller fit set only. If possible, as e.g. for the *t*-LMF and its spin-polarized counterpart also the larger G3 set is used as a reference. As expected, the optimized spin-polarized *t*-LMFs differ only slightly depending on the fit set: In the *SPt1*-SVWN functional, that was fitted to the G3 set, the first parameter a (see definition of parameters in Eq. (4.7)) turns out to be larger by roughly 0.01 as compared to the optimal

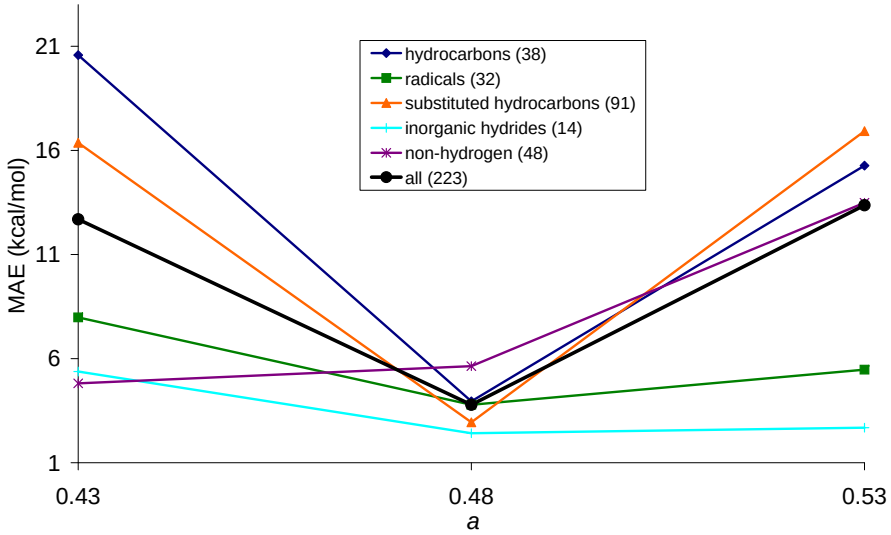

Figure 7.2: MAE broken down for atomization energies of molecule types in the G3 set as function of the scaling parameter in the local mixing function $g(\mathbf{r}) = a\,t(\mathbf{r})$ of a SVWN local hybrid functional. Numbers of molecules in parenthesis.

value for the AE6/BH6 set in the *SPt2*-SVWN functional. The situation is reversed for the second parameter in the LMF, probably balancing out the amount of exact exchange between the two local hybrid functionals. Corresponding to the above-discussed results for the optimized one-parameter LMFs, the two functionals *SPt1*-SVWN and *SPt2*-SVWN yield MAEs that differ only marginally for any of the test sets in Table 7.2.

7.2 Local hybrids with gradient-corrected functionals

The first local hybrid functional presented by Jaramillo et al. had gradient-corrected DFT exchange and correlation included and performed rather poorly for thermochemistry. It has been explained above why a local hybrid without gradient-correction is expected to yield better atomization energies. Still, our first tests also included fitting more complex LMFs to gradient corrected

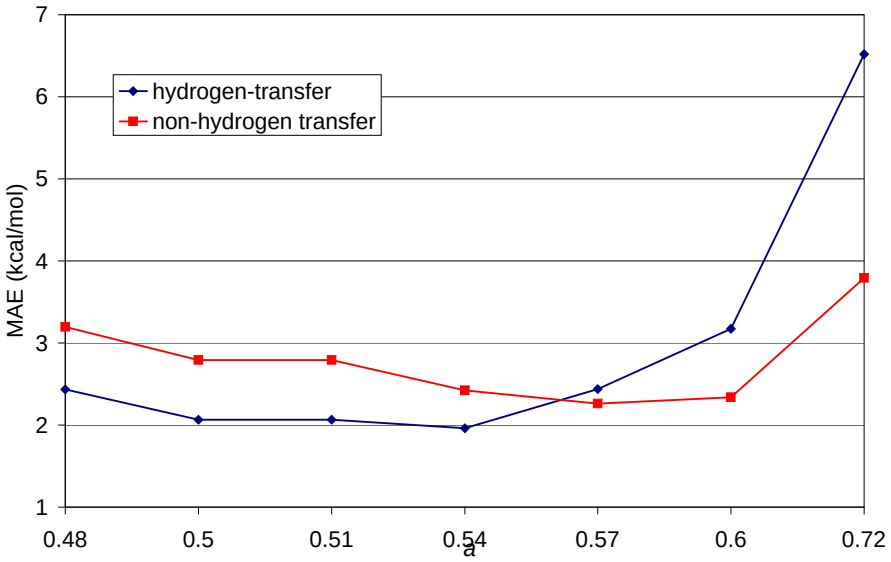

Figure 7.3: MAE of 38 hydrogen-transfer and 38 non-hydrogen transfer barrier heights as a function of the scaling parameter in the local mixing function $g(\mathbf{r}) = a\,t(\mathbf{r})$ of a SVWN local hybrid functional

density functionals. But the resulting τ-dependent LMF that was optimized to Becke exchange and PW91 correlation (cf. Fig. 7.4) exhibits a rather unphysical or counterintuitive behavior: At long range this local hybrid goes to 100% GGA exchange, which is not desirable, given the large self-interaction error of GGA exchange. The LMF also drops to zero at the nuclei and adds a considerable amount of exact exchange along the bond axes. As compared to the best LMF for SVWN (which is essentially the scaled t-LMF), the density averaged LMF is reduced by a factor of two, suggesting an overall low exact-exchange admixture. Consequently it does not provide any improvement over standard global hybrid functionals for atomization energies and barriers. [139]

Instead of allowing for higher exponents of t and thus a more flexible LMF while keeping full gradient correction, a possible parametrization, similar to the B3-scheme, would be to adjust the scaling factor in the simple t-LMF

Exchange-Correlation	LMF	MAE (kcal/mol) G2-1	G3	AE6/BH6	BH	Functional
B3LYP	-	2.53	6.17	4.36	4.7	-
S-VWN[a]	$0.48\,t(\mathbf{r})$	3.73	3.84	3.12	2.5	*tLMF*-SVWN
S-VWN[b,c]	$0.49\,t(\mathbf{r})$	3.68	4.09	3.31	-	-
TPSS-TPSS[d] $nlx = 0.00$ $nlc = 0.17$	$0.50\,t(\mathbf{r})$	3.65	3.63	3.24	2.5	*tLMF*-STPSS
B-LYP[d] $nlx = 0.25$ $nlc = 0.49$	$0.45\,t(\mathbf{r})$	2.38	2.68	2.71	3.5	*tLMF*-BLYP
S-VWN[a]	$\mathrm{erf}\,[0.22\,s(\mathbf{r})]$	4.90	5.28	4.41	3.9	*sLMF*-SVWN
S-VWN[b,c]	$\mathrm{erf}\,[0.23\,s(\mathbf{r})]$	4.79	5.83	4.40	-	-
S-LYP[c]	$\mathrm{erf}\,[0.2383\,s(\mathbf{r})]$	2.94	3.45	4.17	5.3	*sLMF2*-SLYP
S-LYP[c] $nlc = 0.77$	$(\frac{s(\mathbf{r})}{0.73+s(\mathbf{r})})^2$	2.58	6.08	4.83	5.8	*sLMF1*-SLYP
S-VWN[d]	$(0.455 \pm \zeta 0.0423)t_\sigma$	2.77	2.84	2.54	2.7	*SPt1*-SVWN
S-VWN[c]	$(0.446 \pm \zeta 0.0531)t_\sigma$	2.66	2.96	2.40	2.8	*SPt2*-SVWN
S-VWN[c]	$\mathrm{erf}\,[(0.197 + \zeta 0.0423)\,s_\sigma)]$	3.30	3.15	3.58	4.4	*SPs*-SVWN

Table 7.2: MAEs for different test sets with local hybrid functionals. Parameters in the LMFs and for gradient corrections are fitted to the [a]G2-1 set with ReSpect and cc-pVQZ, the [b]G2-1 set, the [c]AE6/BH6 set or the [d]G3 set. The G2-1 and the full G3 set include 55 and 223 atomization energies, respectively. In the first column the functional is given in the format *Exchange-Correlation* functional.

(cf. Eq. (4.3)) together with the amount of gradient correction within the DFT exchange and correlation part (cf. Eq. (5.9)). Table 7.2 includes two accordingly obtained three-parameter local hybrids based on the *t*-LMF and *s*-LMF, respectively.

The scaling parameters a as well as the amount of gradient-correction to Becke or TPSS exchange (nlx)and LYP or TPSS correlation (nlc) respectively are fitted to the G3 set. Especially a local hybrid functional with meta-GGA would be of great interest since the corresponding pure density

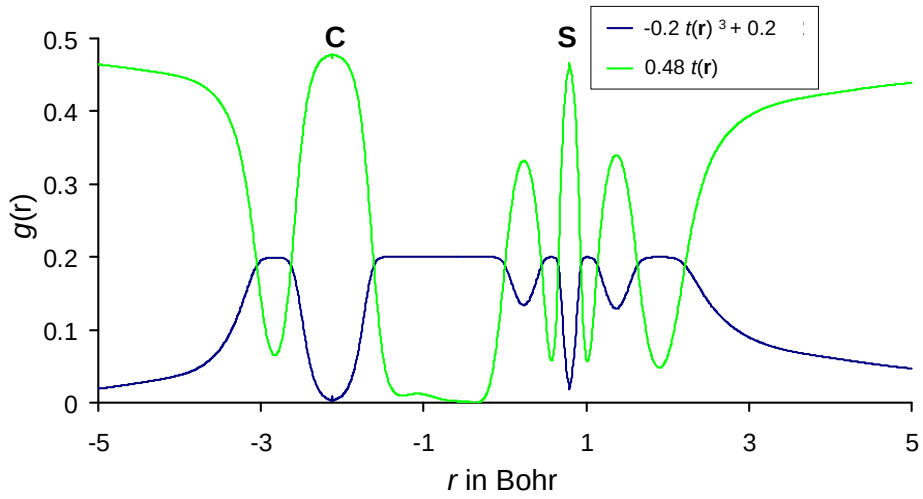

Figure 7.4: Local mixing function plotted along the bond axis in the CS molecule

functionals fulfill more exact constraints such as the one-electron limit. However, the fit results shows that in combination with a scaled t-LMF only a small amount ($nlc = 0.17$) of TPSS correlation is used and no correction at all to local exchange is applied. The corresponding functional is referred to as *tLMF*-STPSS. Fitting the amount of meta-gradient correction within TPSS correlation together with the scaling parameter in the s-LMF using Slater exchange simply reduces to the functional *sLMF*-SVWN. The improvement with *tLMF*-STPSS for atomization energies over the best S-VWN local hybrid with $g(\mathbf{r}) = 0.48t(\mathbf{r})$ is marginal. A larger improvement of more than 1 kcal/mol in the MAE of the G2-1 and the G3 set is provided by the *tLMF*-BLYP local hybrid. It exhibits a slightly smaller scaling factor of $a = 0.45$ inside the LMF than *tLMF*-SVWN. With a factor of 0.25 for gradient-correction to exchange and 0.49 to correlation, respectively, this functional is so far the best local hybrid GGA functional presented in this work and yields overall the best results for atomization energies.

7.3 Thermochemistry

Shortly after the introduction of global hybrid functional in 1993, the nowadays very popular B3LYP functional has been assessed to perform remarkably well thermochemical properties such as the atomization energies in the G2 set. [87] Since then, numerous studies have revealed that B3LYP leads to increasing errors in the atomization energies upon enlargening the test set. [88] This behavior is illustrated in Fig. 7.5 that depicts the MAE in the atomization energies as a function if test-set size. For B3LYP an overall increase in the MAE from below 3 kcal/mol to more than 6 kcal/mol with a clear tendency towards underbinding (see mean deviations in Table 7.3) can be observed.

The G3 subset contains a majority of large organic molecules and on one hand the above described tendency could be attributed to an accumulation of systematic errors. Similar errors have been identified indeed, in particular, for many chemical reactions and isomerizations in organic chemistry. [140,141] However, such a systematic error is not as well defined as, e.g., in wave function methods and it is important to consider that DFT largely benefits from error cancellation. [142] Deterioration of atomization energies upon going to larger molecules (which appears to hold for all standard GGA or global hybrid functionals) has been explained on the other hand by an incorrect description of medium-range interpair correlation effects. [143] On this basis semi-empirical dispersion corrections have been introduced which are also expected to cure the increasing errors in atomization energies for larger systems. Following an approach suggested by Grimme et al. [144] a dispersion correction has been fitted to several local hybrid functionals that are also discussed here. [145] For most of the resulting functionals the MAE of the full G3 set even deteriorates. A positive exception is the spin-polarized

t-LMF with dispersion correction that shows slightly improved atomization energies, especially for the G3 subset. We aim thus for local hybrid functionals that yield accurate atomization energies regardless of the system size. It is furthermore assumed that a consistent performance for all molecules in the G3 set also reflects a physically reasonable common ground for the local hybrid functionals presented in this work.

For the one-parameter local hybrid functionals *tLMF*-SVWN and *sLMF*-SVWN, the MAE of the G2-1 set is slightly larger as compared to the B3LYP results. When the additional molecules of the G2 subset are included the MAE increases only slightly. Adding the G3 subset even lowers the MAE marginally for these two simple local hybrid functionals. Note that the corresponding parameters were fitted to the small G2-1 test set only. For the *SP1*-SVWN functional and the *tLMF*-BLYP that have been optimized for the complete G3 set, the MAE increases slightly with test set size, although by less than 0.5 kcal/mol. Only the *SPs*-SVWN functional shows the opposite tendency of a decreasing MAE upon including more molecules in the test set. With the MAEs not varying by more than 0.5 kcal/mol for any of our functionals as compared to more than 3 kcal/mol for B3LYP, the local hybrids do not appear to suffer from a systematic error buildup for larger molecules in contrast to B3LYP which they all clearly outperform for the full G3/99 set. So far our best MAE of 2.68 kcal/mol for the whole set of atomization energies is obtained with the gradient-corrected local hybrid functional *tLMF*-BLYP.

The almost constant MAE in the atomization energies is also related to a more statistical error distribution as can be seen from the signed errors in Tables 7.3 and 7.4. In this context, it should also be noted that the maximum deviation is not necessarily reduced with local hybrid functionals

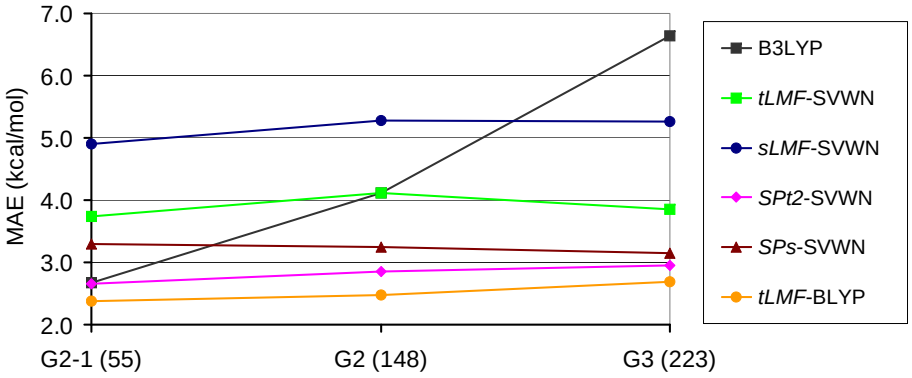

Figure 7.5: MAE for atomization energies as a function of the test set size. For details on the functionals see Table 7.2

as compared to B3LYP and with the sLMF2-SLYP functional even takes larger values (see results for the G2 subset in Table 7.3). The MSE in the atomization energies indicate a tendency towards overbinding for most of the subclasses with local hybrids in contrast to the B3LYP functional that usually underestimates enthalpies of formation. One exception is the sLMF2-SLYP functional that yields negative MSEs or smaller positive MSEs for parts of the G2-1 set. This can be attributed to the correlation functional since the LMF does not differ much from the *s*-LMF that was optimized for VWN correlation, and both local hybrids use only local exchange.

Also the non-hydrogen compounds seem to be tricky: they tend to be underbound for the one-parameter local hybrids based on LSDA exchange and correlation while the other functionals yield a more balanced description (a MSE closer to zero) or rather overbind (i.e. the sLMF2-SLYP functional). Since the local hybrid functionals under investigation in this work allow for more flexibility in the exchange functional only, the large correlation effects that occur in some of these molecules such as F_2, SF_6 or O_3 still remain a challenge and probably specifically designed correlation functionals will be required at some point.

In general atomization energies are better with local hybrid functionals based on a τ-dependent LMF as compared to local hybrids with *s*-LMFs. Comparing the two simplest functionals *tLMF*-SVWN and *sLMF*-SVWN, the latter yields about 1 kcal/mol larger MAEs. For the spin-polarized LMFs that yield improved results for thermochemistry as compared to their simpler one-parameter counterparts, the same effect is observed on a smaller scale.

Concentrating on different subclasses of molecules within the different subsets, no particularly large variation of MAEs is found. In the G3 subset the, especially for B3LYP problematic hydrocarbons, are usually well described except for the one-parameter *sLMF*-SVWN functional. For the two functionals that were fitted to the AE6/BH6 training set (*SPt1*-SVWN and *SPs*-SVWN respectively) the additional radicals in the G3 subset stand out with a larger absolute deviation of more than 6 kcal/mol.

Starting from simple *t*- and *s*-LMFs, inclusion of spin polarization, as in the *SPs*-, *SPt1*- and *SPt2*-SVWN functionals further improves thermochemistry significantly which is illustrated in Fig. 7.5 and Table 7.2. The improvement is particularly notable for the *s*-LMF, where the mean absolute error for the full G3 set drops by 40%. However, even for the *t*-LMF, the MAE is reduced by about 1 kcal/mol. Given their very simple structure with only LSDA exchange and correlation and exact exchange and only two adjustable parameters, all three local hybrids based on spin-polarized LMFs provide G3 set atomization energies that are a remarkable improvement over standard functionals like B3LYP. To our knowledge, the obtained mean absolute errors around 3.0 kcal/mol (given the MP2-optimized structures; cf. chapter 6) are competitive those of known occupied-orbital-dependent functional (and close to "double hybrids" like B2PLYP, [17] which incorporate electron correlation via inclusion of the virtual orbital space in a MP2- like

correlation term). The ζ-dependence makes an effect exclusively for open-shell systems. While the small G2-1 test set includes 18 open-shell species out of 55 molecules, this number drops to 12 for the additional molecules of the G2 set (totally 93 molecules) and becomes very small (only 2) for the subset of 75 species constituting the rest of the full G3 set. Yet, the improvement of the atomization energies by inclusion of the ζ-dependence is notable for all of the subsets. This points to an improvement predominantly of the reference valence atomic energies (13 of 14 atoms involved in the G3 test set are open shell species). Note that here we specifically do not refer to the quality of the total energies as these are appreciably affected by the LMF in the core region, which we have not attempted to optimize so far. [81]

Functional	B3LYP	*tLMF*-SVWN	*tLMF*-STPSS	*tLMF*-BLYP	*SPt2*-SVWN	*SPt1*-SVWN
G2-1						
Hydrocarbons	0.98 (-0.41)	3.94 (3.60)	3.64 (2.31)	2.05 (0.87)	2.21 (0.69)	2.46 (1.04)
Radicals	2.56 (2.16)	3.88 (2.14)	3.67 (1.38)	3.09 (1.97)	3.23 (1.73)	3.27 (1.69)
Substituted hydrocarbons	1.48 (-1.48)	4.12 (1.89)	3.94 (0.72)	1.96 (0.44)	2.53 (0.41)	2.67 (0.43)
Inorganic hydrides	2.09 (0.38)	2.99 (2.93)	2.23 (1.67)	1.00 (0.87)	1.13 (0.67)	1.36 (0.99)
Non-hydrogen	3.84 (-3.84)	4.00 (-3.64)	4.83 (-4.46)	3.02 (-2.51)	3.57 (-2.44)	3.58 (-2.86)
MAE(55 molecules)	2.53	3.73	3.65	2.38	2.66	2.77
MSE(55 molecules)	-0.35	0.97	-0.01	0.33	0.20	0.19
max. deviation	-10.01 (SO_2)	-12.86 (N_2)	-15.18 (N_2)	-9.22 (N_2)	-11.87 (N_2)	-12.31 (N_2)
G2						
Hydrocarbons	4.62 (-4.52)	5.18 (5.18)	4.21 (4.21)	1.66 (1.53)	2.36 (2.32)	2.25 (2.24)
Radicals	1.75 (0.65)	4.76 (3.69)	4.08 (2.59)	2.76 (2.20)	2.68 (2.15)	2.70 (2.10)
Substituted hydrocarbons	3.78 (-3.62)	4.04 (1.46)	3.63 (0.11)	2.39 (0.39)	2.88 (0.71)	2.70 (0.30)
Inorganic hydrides	1.13 (1.13)	5.27 (5.27)	4.37 (4.37)	1.95 (1.95)	2.30 (2.30)	2.91 (2.91)
Non-hydrogen	8.07 (-7.68)	4.00 (-2.69)	4.35 (-3.08)	3.38 (-0.12)	3.85 (1.68)	3.58 (0.36)
MAE(93 molecules)	4.61	4.35	3.96	2.52	2.97	2.82
MSE(93 molecules)	-4.10	1.53	0.51	0.73	1.43	0.93
max. deviation	-20.73 ($SiCl_4$)	-15.83 (NCCN)	-18.71 (NCCN)	-14.20 ($(CH_3)_2SO$)	-12.95 ($(CH_3)_2SO$)	-13.44 ($(CH_3)_2SO$)
G3						
Hydrocarbons	11.51 (-11.51)	3.92 (2.14)	2.91 (0.94)	2.71 (-2.12)	2.51 (-1.24)	2.18 (-1.72)
Radicals	3.03 (-3.03)	2.42 (2.42)	2.29 (2.29)	4.32 (4.32)	6.18 (6.18)	4.71 (4.71)
Substituted hydrocarbons	10.16 (-10.11)	2.91 (-0.36)	3.08 (-1.76)	3.27 (-2.15)	3.30 (-1.49)	3.20 (-2.26)
Non-hydrogen	13.06 (-13.06)	4.06 (-2.51)	4.19 (-1.70)	2.80 (-0.19)	3.06 (2.29)	2.63 (0.84)
MAE(75 molecules)	10.76	3.31	3.21	3.10	3.16	2.92
MSE(75 molecules)	-10.73	-0.12	-1.07	-1.63	-0.58	-1.42
max. deviation	-21.87 (PCl_5)	-19.70 ($C_2H_6SO_2$)	-21.58 ($C_2H_6SO_2$)	-21.20 ($C_2H_6SO_2$)	-18.80 ($C_2H_6SO_2$)	-19.88 ($C_2H_6SO_2$)
MAE (223 molecules)	6.17	3.84	3.63	2.68	2.96	2.84
MSE (223 molecules)	-5.41	0.83	-0.15	-0.16	0.45	-0.04

Table 7.3: Mean absolut errors and mean signed errors in paranthesis in kcal/mol for molecule types in the G2-1, G2 and G3 set for local hybrid functionals with *t*-LMFs and their spin-polarized counterparts.

	Functional	*sLMF*-SVWN	*sLMF2*-SLYP	*SPs*-SVWN
G2-1	Hydrocarbons	5.43 (4.05)	2.37 (-1.73)	2.63 (0.20)
	Radicals	4.75 (2.89)	3.43 (1.68)	3.80 (2.30)
	Substituted hydrocarbons	5.59 (2.61)	3.05 (-0.42)	3.37 (0.64)
	Inorganic hydrides	4.94 (4.94)	1.43 (0.68)	2.01 (1.79)
	Non-hydrogen	4.62 (-4.19)	3.87 (-2.50)	4.07 (-2.54)
	MAE(55 molecules)	4.90	2.94	3.30
	MSE(55 molecules)	1.65	-0.12	0.60
	max. deviation	15.21 (si2h6)	-12.05 (n2)	-12.36 (n2)
G2	Hydrocarbons	5.78 (5.61)	1.88 (0.81)	1.84 (1.46)
	Radicals	6.11 (5.00)	2.78 (1.73)	3.57 (2.73)
	Substituted hydrocarbons	5.32 (3.06)	3.53 (1.95)	3.26 (1.75)
	Inorganic hydrides	5.68 (5.68)	0.32 (-0.32)	1.95 (1.95)
	Non-hydrogen	5.29 (-4.39)	5.40 (3.35)	4.05 (1.37)
	MAE(93 molecules)	5.50	3.52	3.20
	MSE(93 molecules)	2.12	2.00	1.74
	max. deviation	21.90 (ch3cocl)	25.74 (ch3cocl)	21.13 (ch3cocl)
G3	Hydrocarbons	7.08 (2.69)	2.25 (-1.38)	3.00 (-2.72)
	Radicals	1.19 (-0.38)	6.36 (6.36)	4.34 (4.34)
	Substituted hydrocarbons	4.43 (0.26)	2.96 (-0.16)	2.76 (-1.89)
	Non-hydrogen	6.19 (-4.13)	7.76 (7.34)	3.43 (2.01)
	MAE(75 molecules)	5.22	3.73	2.97
	MSE(75 molecules)	0.00	1.05	-1.23
	max. deviation	-17.04 (c4h4n2)	16.79 (cl2s2)	-14.56 (c4h4n2)
MAE (223 molecules)		5.26	3.45	3.15
MSE (223 molecules)		1.29	1.16	0.46

Table 7.4: Mean absolute errors and mean signed errors in parenthesis in kcal/mol for molecule types in the G2-1, G2 and G3 set for local hybrid functionals with *s*-LMFs and their spin-polarized counterparts.

To allow for comparison with exact-exchange admixtures of global hybrids, the density-averaged LMFs for a *t*-LMF, *s*-LMF and their spin-polarized versions are provided in Table 7.5. Since, the same orbitals are used for all post-SCF results discussed here, only one representative of each class of LMF (namely, *t*-LMF, *s*-LMF and a spin-polarized version for each) is depicted. Higher average values can be deduced from larger scaling parameters and vice versa. The average values for subclasses of molecules in the G3/99 set and the whole set respectively as compared to the average over atoms give some idea about how much exact exchange has been included overall.

Considering the LMF plots in chapter 4 differences between subsets as for example the larger average for hydrocarbons as compared to non-hydrogen compounds are most like to be dominated by the inner-core region given that the latter subset contains more second-row elements. Note that for all LMFs the average exact-exchange admixture is significantly larger in atoms than in molecules. Given that more nondynamical correlation as represented through DFT exchange occurs in molecules this effect is desirable and supports the good thermochemical performance of our local hybrid functionals. Interestingly, the difference is most pronounced for the *t*-LMF, which also provides the best atomization energies.

Comparison between different types of LMF reveals an overall larger exact-exchange admixture in *t*-LMFs which is most likely due to the strong weighting of the core region were the *s*-LMFs exhibit a dip and *t*-LMFs a maximum (cf. Figs. 4.1, , 4.2, 4.3,4.4 and 4.5). The *t*-LMF optimized for Slater exchange and TPSS correlation consequently provides the largest amount of exact exchange due to the higher scaling parameter. Variation of the average values between different subclasses of molecules are very moderate. A significant outlier on the large side is the value for the inorganic hydrides of the G2 subset represented only by the H_2 molecule. Although the effect can be observed for all LMFs, it is less pronounced for functions based on the reduced density gradient. Actually, for this molecule the *t*-LMF degenerates into a global hybrid with a constant exact-exchange admixture equal to the scaling parameter. From Fig. 4.3 can be seen that the *t*-LMF takes large values around the hydrogen atom in other molecules as well. The lowest average exact-exchange admixtures are therefore seen for non-hydrogen molecules, in particular for ones in the G3 extension set.

	Functional	*tLMF*-SVWN	*sLMF*-SVWN	*SPt2*-SVWN	*SPs*-SVWN
G2-1	Hydrocarbons	0.314	0.253	0.292	0.229
	Radicals	0.300	0.247	0.280	0.225
	Substituted hydrocarbons	0.282	0.235	0.262	0.212
	Inorganic hydrides	0.291	0.241	0.271	0.218
	Non-hydrogen	0.282	0.238	0.262	0.215
	All (55 molecules)	0.293	0.243	0.272	0.220
G2	Hydrocarbons	0.289	0.235	0.268	0.212
	Radicals	0.289	0.238	0.269	0.216
	Substituted hydrocarbons	0.278	0.231	0.258	0.208
	Inorganic hydrides	0.480	0.342	0.446	0.312
	Non-hydrogen	0.260	0.223	0.242	0.201
	All(93 molecules)	0.280	0.232	0.260	0.209
G3	Hydrocarbons	0.283	0.231	0.263	0.208
	Radicals	0.276	0.230	0.256	0.208
	Substituted hydrocarbons	0.277	0.228	0.257	0.206
	Non-hydrogen	0.244	0.212	0.227	0.191
	All(75 molecules)	0.273	0.226	0.253	0.204
Mean Average (223 molecules)		0.281	0.233	0.261	0.210
Mean Average (14 Atoms)		0.330	0.268	0.314	0.251

Table 7.5: Density-weighted average local mixing functions further averaged over type of molecules and subsets of the G3 set.

An important feature of spin-polarized LMFs is the difference between averaged α- and β- LMFs

$$\Delta\overline{g} = \overline{g}_\beta - \overline{g}_\alpha \,. \tag{7.3}$$

The calculated values for the quantity $\Delta\overline{g}$ are given in Table 7.6 and as already mentioned in chapter 4 for almost all open-shell systems studied the beta LMF takes larger values on average. Considering the definition for spin-polarized LMFs (cf. Eqs. 4.7 and 4.9) one might expect that the difference will be reduced upon inclusion of the explicit dependence on spin polarization. This is indeed the case as can be seen from the third and fifth column in Table 7.6. Apparently, the decrease of $\Delta\overline{g}$ is significantly larger than one would expect from the reduction of the same-spin scaling factor a (cf. definitions in Eqs. 4.7 and 4.9). For spin-polarized s-LMFs, the difference between β and α average is reduced by more than a factor of 2 while the effect is less pronounced for t-LMFs. This adjustment of different spin-averaged LMFs correlates with the observed improved thermochemical performance although reasons for this remain to be studied in more detail.

7.4 Reaction barriers

Table 7.7 lists MAEs and MSEs for the two classical barrier height test sets. For comparison, results obtained with B3LYP and Becke's half and half functional that combines 50% exact exchange with Slater exchange and local correlation are given as well. As pointed out before, GGA functionals underestimate barriers significantly and systematically. While exact-exchange admixture in global hybrids increases and thus overall improves barriers it has been demonstrated before, that the relatively small mixing parameters

atom/radical, multiplicity	*tLMF*-SVWN	*SPt2*-SVWN	*sLMF*-SVWN	*SPs*-SVWN
Li, 2	0.0579	0.0307	0.0235	-0.0046
C, 3	0.0964	0.0665	0.0630	0.0262
N, 4	0.1356	0.0986	0.0885	0.0417
O, 3	0.0929	0.0718	0.0570	0.0295
F, 2	0.0392	0.0303	0.0259	0.0138
Si, 3	0.0138	0.0030	0.0143	-0.0012
P, 4	0.0282	0.0140	0.0254	0.0048
S, 3	0.0274	0.0181	0.0206	0.0072
Cl, 2	0.0141	0.0098	0.0109	0.0045
BeH, 2	0.0405	0.0218	0.0276	0.0070
CH, 2	0.0581	0.0445	0.0312	0.0148
CH2, 3	0.1126	0.0896	0.0583	0.0304
CH3, 2	0.0595	0.0488	0.0299	0.0167
ClO, 2	0.0071	0.0044	0.0058	0.0020
CN, 2	0.0103	0.0050	0.0112	0.0033
HCO, 2	0.0103	0.0051	0.0082	0.0013
NH, 3	0.1004	0.0786	0.0576	0.0300
NH2, 2	0.0470	0.0374	0.0277	0.0152
NO, 2	0.0134	0.0085	0.0098	0.0033
O2, 3	0.0240	0.0155	0.0197	0.0080
OH, 2	0.0418	0.0327	0.0266	0.0144
PH2, 2	0.0186	0.0137	0.0119	0.0051
S2, 3	0.0083	0.0041	0.0084	0.0021
Si2, 3	0.0157	0.0148	0.0130	0.0062
SiH2, 3	0.0268	0.0166	0.0177	0.0040
SiH3, 2	0.0169	0.0115	0.0101	0.0032
SO, 3	0.0121	0.0064	0.0113	0.0031
Average	0.0418	0.0297	0.0265	0.0108

Table 7.6: Difference between averaged α- and β- LMFs for SVWN local hybrid functionals with one-parameter *t*- and *s*-LMFs as well as their spin-polarized counterparts.

in thermochemically optimized global hybrids such as B3LYP or PBE0 is not sufficient to cure the tendency of underestimation. The LSDA-based global hybrid with 50% exact-exchange improves barrier heights as compared to B3LYP, but performs poorly for thermochemistry (see above). It has already be discussed that the thermochemically optimized parameter in the simplest LSDA-based local hybrid *tLMF*-SVWN is not far from the optimal values for barriers either or that, at least no large improvement can be obtained upon variation of the scaling parameter in the tLMF. With a MAE of 2.5 kcal/mol for both test sets the *tLMF*-SVWN functional is superior to B3LYP although it was optimized for thermochestry. The mean signed errors indicate a similar systematic underestimation of barriers though. For the same database, the BMK functional with 42% exact-exchange and the M06-2X functional including 54% exact exchange attain MAEs of 1.3 kcal/mol and 1.1 kcal/mol, respectively. [15] As compared to the simple one-parameter local hybrid functional *tLMF*-SVWN, these global hybrid functionals are, however, highly parameterized and include a larger amount of exact exchange. The long-range corrected PBE hybrid functional yields a MAE of 1.3 kcal/mol for hydrogen-transfer barriers and 2.4 kcal/mol for non-hydrogen transfer reactions. The performance of our local hybrid is thus not far from the best-performing functionals for reaction barriers. Incorporation of GGA or even meta-GGA correction into a local hybrid functional based on a *t*-LMF does unfortunately not improve the barrier heights: The *tLMF*-STPSS performs similarly to *tLMF*-SVWN. The *tLMF*-BLYP yields MAEs of 3.6 kcal/mol and 3.3 kcal/mol for the hydrogen-transfer and the non-hydrogen-transfer barrier heights, respectively and thus inferior to the *tLMF*-SVWN functional discussed above. This is most likely due to the smaller exact-exchange admixture in the GGA-based local hybrid functional.

Local hybrid functionals with *s*-LMFs yield larger deviations from experimental barrier heights than *t*-LMFs. Especially the MAEs with the simplest representative of this family, the *sLMF*-SVWN functional, are 1 (HTBH) and 1.3 (NHTBH) kcal/mol larger than the MAEs of *tLMF*-SVWN and represent only a small improvement over B3LYP. Again, combination with GGA correction rather worsens the MAEs of more than 5 kcal/mol.

The superiority of *t*-LMFs over *s*-LMFs for barrier heights can be explained by their larger sensitivity in the bond region as discussed in chapter 4. It has already been pointed out that the *t*-LMF exhibits more pronounced local maxima at an intermediate position along the bond-dissociation pathway than the *s*-LMF. Such an electronic structure is according to Grüning et al. [90] a sign of occupation of antibindung orbitals and corresponds to weaker nondynamical correlation as compared to a normal two-center two electron bond. This is also the reason why GGA functionals overstabilize transition states and thus underestimate barrier heights. Since in our local hybrid model the LMF establishes the balance between nondynamical correlation in the exchange density functional and exact exchange, at the transition state structure more exact exchange is traded in for Slater exchange. Thereby, the tLMF corrects the overstabilization of the transition state. For normal two-center two-electron bond situations where nondynamical correlation is stronger, no such corrections are introduced with our LMFs and the net computed barrier is thus increased and typically improved.

Although explicitly fit to barrier heights within the AE6/BH6 set, the ζ-dependent local hybrids *SPt2*-SVWN and *SPs*-SVWN moderately deteriorate barriers as compared to the simpler *s*- and *t*-LMFs. While the mean absolute errors for non-hydrogen transfer barriers remain essentially unmodified upon inclusion of spin polarization, results are clearly worsened by up to

Functional	Hydrogen-transfer		Non-hydrogen transfer	
	MAE	MSE	MAE	MSE
B3LYP	4.3	-4.3	5.0	-4.8
S-HandH-VWN[a]	2.5	-2.1	2.8	0.0
tLMF-SVWN	2.5	-2.1	2.5	-1.5
tLMF-STPSS	2.5	-2.2	2.4	-1.3
tLMF-BLYP	3.6	-3.5	3.3	-2.8
sLMF-SVWN	3.5	-3.4	4.3	-3.7
sLMF2-SLYP	5.2	-5.2	5.3	-5.0
SPt1-SVWN	2.9	-2.6	2.5	-1.8
SPt2-SVWN	3.0	-2.9	2.6	-1.9
SPs-SVWN	4.3	-4.3	4.4	-4.4

Table 7.7: Mean absolute and mean signed errors in kcal/mol for 38 hydrogen-transfer and 38 non-hydrogen transfer reaction barriers. [a] SCF calculation with a global hybrid functional that mixes 50% exact exchange with Slater exchange and VWN correlation (Becke's half-and-half functional).
.

0.8 kcal/mol for the hydrogen transfer barriers. This observation reflects the overall lower exact-exchange admixture as discussed in the previous section. In this context, it was also concluded that the improved thermochemistry could be traced back to a better description of atoms relative to the molecules which does not affect reaction barriers.

7.5 Dissociation of symmetric radical cations

So far, it is shown that some of the local hybrids investigated in this work perform rather accurately for both thermochemistry and reaction barriers due to a more balanced description of nondynamical correlation and cancellation of self-interaction. The latter is also the predominant problem in symmetrical

two-center three-electron dimer systems, while nondynamical correlation is essentially absent. In order to further test the flexibility of local hybrid functionals, bond lengths and dissociation energies for the seven radical cations introduced in chapter 3 have been calculated. Table 7.8 shows computational results with local hybrids, B3LYP and the S-HandH-VWN functional. For comparison, CCSD(T) benchmark values are given as well.

Overall, the results bond lengths and dissociation energies are improved with local hybrid functionals as compared to B3LYP. The latter is, however, known to yield poor results for these properties. Better results are generally obtained with S-HandH-VWN, a global hybrid including 50% exact exchange (with the dissociation energy of $He_2{}^+$ being a peculiar outlier). Yet, all functionals substantially overestimate bond lengths as well as dissociation energies. The differences of 1.5 to 3 kcal/mol between dissociation energies with different local hybrid functionals are rather small as compared to more than 10 kcal/mol deviation from the benchmark values for most of the systems. $H_2{}^+$ is an exception since most of the existing functionals are quite close to the CCSD(T) energy (within 3.5 kcal/mol), and it is a one-electron system with no correlation whatsoever. Comparing the two different families of LMFs, functionals based on τ-dependent LMFs usually perform better than local hybrids with local mixing functions of the reduced density gradient. Among the *t*-LMF-based local hybrids including ζ-dependent LMFs, the *tLMF*-STPSS functionals yields the lowest and thus best dissociation energies which can be ascribed to the largest scaling factor in the t-LFM yielding a slightly larger exact-exchange admixture. Surprisingly the *s*-dependent one-parameter functional *sLMF*-SVWN performs similarly except for the $H_2{}^+$ and $He_2{}^+$ dissociation energies. Interestingly, for the cations $Ne_2{}^+$, $Ar_2{}^+$, $(HF)_2{}^+$, $(H_2O)_2{}^+$, $(NH_3)^+$ the best equilibrium distances are ob-

tained with sLMF2-SLYP which is neither optimal for thermochemistry nor for barriers. Bond lengths of the lighter H_2^+ and He_2^+ are less sensitive in general and usually better described with *t*-LMF based local hybrid functionals. The spin-polarized LMFs give essentially the same distances as their unpolarized counterparts and marginally larger binding energies (likely due to the overall somewhat lower exact exchange, given the slightly lower scaling parameter a).

These results suggest that the flexibility of the present local hybrid functionals with one- and two-parameter LMFs is not sufficient to extend the good performance for general thermochemical and barrier data to these systems with rather special bonding situations. Other variables than kinetic energy densities and the reduced density gradient and more parameters will probably be required in order to provide the higher amount of exact exchange that is clearly needed in this case.

Functional	H_2^+		He_2^+		Ne_2^+		Ar_2^+		$(HF)_2^+$		$(H_2O)_2^+$		$(NH_3)_2^+$	
	D_e	r_e	D_e	r_e	D_e	r_e	D_e	r_e	D_e	r_e	D_e	r_e	D_e	r_e
B3LYP	67.8	2.10	77.6	2.16	59.0	3.42	43.2	4.78	58.1	3.65	52.7	3.96	51.5	4.25
S-HandH-VWN[a]	65.7	2.06	71.6	2.07	42.5	3.23	37.8	4.57	47.7	3.47	45.9	3.75	48.3	4.09
tLMF-SVWN	65.6	2.06	68.1	2.11	55.4	3.45	41.7	4.74	55.0	3.66	50.2	3.96	49.0	4.26
tLMF-STPSS	65.5	2.06	67.2	2.10	54.4	3.44	41.5	4.72	54.4	3.65	49.7	3.95	48.8	4.25
tLMF-BLYP	65.8	2.07	68.8	2.11	57.5	3.44	43.1	4.74	57.0	3.65	51.9	3.95	50.6	4.25
sLMF-SVWN	66.5	2.10	73.6	2.13	54.8	3.45	41.7	4.73	54.4	3.65	49.6	3.95	48.8	4.23
sLMF2-SLYP	65.9	2.11	71.7	2.12	55.8	3.41	43.2	4.68	56.0	3.61	51.3	3.91	50.6	4.19
SPt1-SVWN	65.6	2.06	68.8	2.11	56.7	3.45	42.5	4.74	56.2	3.65	51.1	3.96	49.8	4.26
SPt2-SVWN	65.6	2.06	68.2	2.11	57.2	3.45	42.7	4.74	56.6	3.65	51.5	3.96	50.1	4.26
SPs-SVWN	66.4	2.09	73.0	2.15	57.5	3.46	43.0	4.72	56.7	3.65	51.5	3.95	50.2	4.23
CCSD(t)[a]	64.3	2.00	56.0	2.04	30.8	3.23	29.3	4.57	40.2	3.50	40.8	3.84	36.3	4.10

Table 7.8: Calculated dissociation energies D_e (in kcal/mol) and equilibrium bond lengths (in Bohr) for optimized local hybrid functionals. If not stated otherwise CCSD(T) equilibrium bond lengths and dissociation energies were taken from Ref. [102]. [a]CCSD(T) single point calculation at MP2 structures from Ref. [99]

7.6 Transition metal compounds

When going down the periodic table, the reliability of density functionals becomes even more problematic. Although transition metal complexes can be calculated fairly accurately with B3LYP, transition metal dimers, hydrides and *s*-*d* interconfigurational energies remain challenging. Results for these three properties reflect different particular shortcomings of existing density functionals. The inferiority of hybrid functionals as compared to GGAs and meta-GGAs for predicting binding energies of covalently bonded transition metal dimers has been attributed to the importance of nondynamical correlation. Underestimation of *s*-*d* transfer energies on the other hand has been related to self-interaction errors. The purpose of these preliminary tests for transition metal is thus not a thorough assessment but rather to get an idea of the applicability range and possible limits of local hybrid functionals that are designed to balance nondynamical correlation and self-interaction correction in real-space.

7.6.1 Atomic *s*-*d* Transfer energies

Table 7.9 displays the calculated *s*-*d* transfer energies for all local hybrid functionals and B3LYP together with benchmark values. A severe underestimation tendency can be seen from the mean signed error for all density functionals. Only B3LYP yields slightly too large 4*s*-3*d* interconfigurational energies for the atoms Ni and Cu. Wrong ground states are predicted for the Co atom with any functional in Table 7.9 and for the Fe atom with the *sLMF*-VWN and *SPs*-SVWN functional. Among the local hybrids, two functionals with LYP correlation but different LMFs perform best with MAEs of 0.42 and 0.52 eV for sLMF1-SLYP and *tLMF*-BLYP respectively. Considering that the local hybrid based on the *t*-LMF yields impressively accurate

enthalpies of formation this result is quite surprising although B3LYP with an MAE of 0.33 eV remains superior. The other local hybrid functionals yield MAEs almost twice as large. Comparing LSDA-based local hybrid functionals suggests that the *s*-LMFs are inferior to *t*-LMFs. Introduction of spin polarization into local hybrid functionals has a small negative effect on the *s*-*d* transfer energies. In contrast to barrier heights and thermochemistry where *t*-LMFs usually performed better, it can not be deduced whether a *t*- or a *s*-LMF is to be preferred for the calculation of *s*-*d* transfer energies.

It can be concluded that further studies of *s*-*d* transfer energies with local hybrid functionals are mandatory. In particular the basis set dependence should be investigated considering the underlying resolution of identity in our calculations. In other studies, it was discussed that underestimation of *s*-*d* interconfigurational energies with pure GGA functionals is probably due to a lack of long-range exchange interaction between $4s$ and $3d$ electrons. [106] Subsequently, a long-range corrected GGA was specifically optimized to yield energies close to experiment exceeding the performance of B3LYP, although the overall amount of exact exchange is similar. [74] Based on the results with long-range corrected hybrid functionals, comparison of average exact-exchange admixture with the local hybrid functionals would be worthwhile. LMFs that are specifically optimized to transition metals and interconfigurational energies might give further insight into the requirements on more flexible local hybrid functionals. Finally, self-consistent calculation may be more appropriate for this sensitive property. It becomes evident that none of the local hybrid functionals fitted to thermochemical and kinetic data are an improvement over B3LYP for $4s$-$3d$ interconfiguration energies in $3d$ transition metal atoms. However, keeping in mind that the second best local hybrid functional for *s*-*d* transfer energies yields an average absolute error be-

low most of the established GGA and meta-GGA functionals (such as PBE, TPSS or TPSSh) also happens to be outstanding for thermochemistry and further development of local hybrid functionals seems promising.

Atom	Excitation	Exp.	B3LYP	*s-d* transfer energy (eV)							
				tLMF -SVWN	*tLMF* -STPSS	*tLMF* -BLYP	*SPt2* -SVWN	*sLMF1* -SLYP	*sLMF* -SVWN	*sLMF2* -SLYP	*SPs* -SVWN
Ca	$d^0s^2(^1S) \rightarrow d^1s^1(^3D)$	2.44[a]	1.88	1.80	1.80	1.84	1.79	1.88	1.62	1.72	1.61
Sc	$d^1s^2(^2D) \rightarrow d^2s^1(^4F)$	1.33	0.68	0.49	0.48	0.56	0.49	0.66	0.36	0.49	0.35
Ti	$d^2s^2(^3F) \rightarrow d^3s^1(^5F)$	0.69	0.22	-0.16	-0.19	-0.06	-0.17	0.11	-0.26	-0.11	-0.29
V	$d^3s^2(^4F) \rightarrow d^4s^1(^6D)$	0.11	-0.15	-0.73	-0.78	-0.58	-0.74	-0.34	-0.79	-0.60	-0.83
Cr	$d^4s^2(^5D) \rightarrow d^5s^1(^7S)$	-1.17	-1.44	-2.07	-2.12	-1.89	-2.07	-1.66	-2.14	-1.92	-2.16
Mn	$d^5s^2(^6S) \rightarrow d^6s^1(^6D)$	1.97	1.48	1.44	1.46	1.46	1.42	1.60	1.19	1.38	1.16
Fe	$d^6s^2(^5D) \rightarrow d^7s^1(^5F)$	0.65	0.18	0.07	0.09	0.10	0.06	0.22	-0.18	0.01	-0.19
Co	$d^7s^2(^4F) \rightarrow d^8s^1(^4F)$	0.17	-0.09	-0.36	-0.34	-0.31	-0.38	-0.24	-0.61	-0.44	-0.63
Ni	$d^8s^2(^3F) \rightarrow d^9s^1(^3D)$	-0.33	-0.31	-0.72	-0.71	-0.65	-0.75	-0.59	-0.92	-0.78	-0.95
Ni	$d^9s^1(^3D) \rightarrow d^{10}(^1S)$	1.57	1.73	1.52	1.55	1.51	1.48	1.54	1.37	1.45	1.33
Cu	$d^9s^2(^2D) \rightarrow d^{10}s^1(^2S)$	-1.85	-1.85	-2.26	-2.25	-2.19	-2.29	-2.17	-2.47	-2.34	-2.49
	MSE	-	-0.29	-0.60	-0.60	-0.52	-0.61	-0.42	-0.76	-0.61	-0.79
	MAE	-	0.33	0.60	0.60	0.52	0.61	0.42	0.76	0.61	0.79

Table 7.9: Atomic *s-d* transfer energies in eV. Experimental values including relativistic effects are taken from Ref. [105]. [a]Experimental value for Ca from Ref. [146].

7.6.2 $3d$ transition metal dimers and monohydrides

Since a more detailed discussion of the performance of local hybrid functionals will be presented in another context, [147] only average errors for the 11 dissociation energies and 9 respectively 8 equilibrium distances of transition metal dimers and monohydrides are given in Table 7.10. For the same reason and as mentioned above, a reduced number of local hybrid functionals is considered. Turning to the atomization energies of $3d$ metal dimers, it can be seen that the τ-dependent one-parameter functional *tLMF*-SVWN gives only slightly worse results than B3LYP while both local hybrids based on *s*-LMFs yield considerably larger mean absolute errors. The MSE reveals strong underbinding of the dimers with all functionals in Table 7.10. Although the small and positive MSE for equilibrium bond length points towards a more random error distribution, the order in the performance of local hybrid functionals is the same as for dissociation energies. Apparently too much nondynamical correlation is lost with the present local hybrid functionals in regions that are crucial for a better description of $3d$ transition metal dimers.

For $3d$ transition metal monohydrides hybrid functionals such as B3LYP were observed to perform best. This has been related to the partly canceled self-interaction error. [105] Even better results for the same systems are obtained with local hybrid functionals. The MAE for dissociation energies is reduced by more than 1 kcal/mol with the sLMF1-SLYP functional as compared to B3LYP. The local hybrid functional without gradient correction based on a *t*-LMF gives results only slightly better than B3LYP and the corresponding functional based on a *s*-LMF performs worse. Again, the same holds for the equilibrium distances.

Keeping in mind that not all density functionals predict the correct ground state for some of the dimers, self-consistent calculations with local hybrids

might be helpful in order to consider the symmetry of the ground state in a more quantitative and detailed discussion of these results.

Functional	M_2		MH	
	D_e	r_e	D_e	r_e
B3LYP	12.4	0.094	8.3	0.015
	(-10.7)	(0.043)	(8.1)	(0.005)
tLMF-SVWN	13.8	0.095	7.9	0.015
	(-12.3)	(0.030)	(7.9)	(-0.003)
sLMF-SVWN	18.1	0.104	10.6	0.044
	(-16.4)	(0.0038)	(10.6)	(-0.038)
sLMF1-SLYP	17.4	0.099	7.1	0.012
	(-17.4)	(0.031)	(6.5)	(-0.004)

Table 7.10: Mean absolute errors for 11 dissociation energies D_e (in kcal/mol) and 9 equilibrium distances r_e (in Bohr) of $3d$ transition metal dimers and monohydrides. Mean signed errors are given in brackets. The molecules and benchmark data are given in Table 3.4.

7.7 Conclusion

In a thorough assessment of semi-empirical local hybrid functionals for atomization energies and barrier heights, it is shown that quite accurate results close or better than those of the best state-of-the-art density functionals are obtained for both properties. This is even more interesting given that some functionals were fit to atomization energies exclusively. Fit results were nearly independent from the size of the underlying training set. Thus rather simple one- or two-parameter local hybrid functionals which are pre-

dominantly based on LSDA exchange and correlation are able to compete with the best state-of-the-art functionals for thermochemistry and barriers. This result is even more impressive considering the large amount of empirical parameters in other successful global hybrids such as B98 and BMK, for example. Concerning the different types of LMFs, it has been shown that t-LMFs are superior for thermochemistry and reaction barriers of main group compounds. No such statement can be made for transition metals. Further investigation for the latter is necessary in order to discuss performance of local hybrids for dissociation energies and equilibrium bond length of transition metal dimers and monohydrides more quantitatively.

Parallel to this work, another local hybrid functional (PSTS) has been introduced by Perdew et al. [27] It is based on TPSS exchange and correlation and contains five empirical parameters that are fitted to enthalpies of formation and barrier heights. The corresponding local mixing function itself depends on the LSDA exchange energy density and the TPSS correlation energy density in the high density limit. The LMF uses 100% exact exchange in one-electron regions, rapidly varying density regions and for non-uniform high densities. In the PSTS functional, the spin polarization is employed to distingish between the stretched $H_2{}^+$ and the stretched neutral H_2 which require full exact exchange and density functional exchange, respectively. For the atomization energies of the full G3 set a MAE of 4.9 kcal/mol was obtained with this local hybrid functional. It performed similarly to B3LYP for barrier heights. [84] The PSTS contains thus more parameters but performs less well than the local hybrid functionals presented in this work. Since it fulfills a more exact constraints, it may be considered physically more meaningful.

CHAPTER 8

THE LOCAL HYBRID POTENTIAL

In this chapter, the self-consistent implementation of local hybrid functionals into the Turbomole package is validated. Following previous work, the FDO potential has been implemented using an RI approximation, for efficiency. However, no rigorous tests are available that allow estimation of the error introduced by such an approximation. Hence, as explained in chapter 5 the numerically exact potential has been implemented as well. In order to assess the accuracy of the RI potential, orbital energies, total energies and isotropic hyperfine coupling constants obtained with the *tLMF*-SVWN local hybrid functional will be compared for different basis sets.

8.1 Total energies

According to the variational principle, the total energy obtained from a trial density that differs from the true ground state density for a given energy functional has to be larger than the energy from a self-consistent calculation. Thus by comparing total energies obtained from post-SCF calculations with the SCF energy for a given functional, the implementation of the corresponding potential can be validated. As an example energies from local hybrid functionals based on Slater exchange and VWN correlation with the optimized *t*- and *s*-LMF are listed in Table 8.1. The total energy is lowered by 10 to 100 meV during a self-consistent calculation. The energy difference is slightly larger for the *t*-LMF as compared to the *s*-LMF. A possible reason for this could be that the B3LYP orbitals (that are used for post-SCF calculations) are closer to the orbitals obtained with the *s*-LMF-based functional.

The *s*-LMF post-SCF energies could also be fortuitously closer to the SCF energies since the value $E_{post-SCF} - E_{SCF}^{numerical}$ also contains errors in the total post-SCF energies due to the RI approximation to the exact-exchange energy density.

In order to get more insight into the accuracy of the RI approximation to the potential and the exact-exchange energy density, the difference between SCF energies from the RI potential and SCF energies from the numerical potential are given in the third and fourth columns of Table 8.1. The differences go up to ca. 11 meV but are typically much smaller. Strikingly, the RI energies are with one exception lower than the numerically exact one indicating that an auxiliary basis cannot be optimized variationally but has to be fitted explicitly to the numerical potential. Overall, the error in the total energy due to the RI approximation is larger for the *s*-LMF. This finding suggests that an erroneous energy lowering occurs as well in post-SCF calculations leading to the above discussed smaller differences between post-SCF and SCF energies with the *s*-LMF. Furthermore, the largest deviations are observed for the carbon atom, the oxygen atom and the OH radical despite their smaller (absolute) total energies as compared to e.g. the heavier sulfur atom and sulfur containing molecules. While the difference between post-SCF and SCF energies depends clearly on the total energy, the error in total SCF energies due to the RI approximations appears thus to be more random. It might be related somehow to the amount of exact exchange since the density-weighted averaged LMFs are smaller in heavier atoms which are therefore probably less affected by small discrepancies in the corresponding terms of the potential.

If highly accurate energies are sought such unsystematic errors might become problematic and moreover lead to a stronger basis set dependence of

Molecule	$E_{post-SCF} - E_{SCF}^{numerical}$		$E_{SCF}^{RI} - E_{SCF}^{numerical}$ (meV)	
	s-LMF[a]	t-LMF[b]	s-LMF[a]	t-LMF[b]
C	14.7	28.7	-7.68	-4.00
CH_3	30.1	48.5	-3.83	-2.98
CH_4	38.4	57.6	-1.33	-1.42
H_2	4.6	10.1	0.03	0.00
H_2O	30.5	46.5	-2.29	-1.95
H_2S	42.7	63.9	-2.27	-0.96
H	2.7	4.6	0.06	0.00
O	13.4	31.4	-11.22	-6.53
OH	19.0	37.5	-9.32	-5.33
S_2	69.1	92.4	-3.69	-2.96
S	33.9	48.8	-0.37	0.78
SH	37.6	55.8	-1.47	-0.18
Si	36.3	45.3	0.21	-0.73
SiH_4	44.6	79.1	-3.94	-4.24
SiO	58.0	78.2	-3.45	-2.74

Table 8.1: Differences in total energies for some molecules ofthe AE6/BH6 set. $E_{post-SCF}$ denotes the non-SCF total energy obtained with B3LYP orbitals. $E_{SCF}^{numerical}$ and E_{SCF}^{RI} are self-consistent total energies from the numerically exact potential and the RI approximation respectively. The local hybrid functionals employed are based on Slater exchange and VWN correlation . [a] $g = erf(0.22s)$. [b] $g = 0.48 * t$

.

calculations with local hybrids than with density functionals that do not rely on a RI approximation. The *t*-LMF reduces to a constant value throughout the hydrogen molecule and the hydrogen atom which explains why the RI approximation is highly accurate for this particular molecule. Given the small dimension of energy differences the RI approximation seems to be quite accurate. It should be kept in mind, however, that these values have been obtained with the rather large decontracted QZVP basis set. The respective configurations are 15s8p3d2f1g and 20s14p4d2f1g for first row elements B through F and second row elements Al through Cl. Parts of the quite unsystematic errors might by compensated by empirical parameters fitted with a given basis. Attention should therefore be paid when other basis sets are employed or the overall basis set size is reduced.

8.2 Isotropic hyperfine coupling constants

Since the focus of this chapter is rather validation of the RI approximation than assessment of local hybrids for isotropic hyperfine coupling constants, the following discussion concentrates mostly on the sensitivity of RI results towards basis set size and contraction. However, Fig. 8.1 illustrates a regression analysis for the calculation of isotropic HFCCs with our two simplest local hybrid functionals *tLMF*-SVWN and *sLMF*-SVWN (using the numerically correct potential) in comparison to B3LYP. The *tLMF*-SVWN functional yields results only slightly inferior to B3LYP: While the MAE of ca. 33 MHz is increased by less than 4 MHz with the local hybrid functionals and the slope deteriorates by 0.02, the (positive) inception drops by 1 MHz. According to other studies including GGA, meta-GGA and hybrid functionals, B3LYP is the most suitable functionals for isotropic HFCCs of main group compounds. [110, 112] It can thus be concluded that the one-parameter local

hybrid that has been optimized for thermochemistry is competitive not only for thermochemical properties and barrier heights but also close to the best functionals for the calculation of isotropic hyperfine coupling constants of small radicals. Keeping in mind its simplicity there seems to be room for improvement through inclusion of other variables and additional adjustable parameters. Results for the *tLMF*-BLYP are not shown but similar. With the local hybrid functional based on a local mixing function of the reduced density gradient the deviations from experimental values are considerably larger which can be seen both from the regression analysis and the MAE of over 40 MHz. This could be related to the negative cusp of *s*-LMFs at the position of the nuclei leading to small exact-exchange admixtures in this region.

8.2.1 Validation of the RI approximation

In order to avoid additional errors or even error cancellation due to the resolution of the identity for the exact-exchange parts in the local hybrid potential, the results discussed above were obtained with the numerical potential. Turning to the validation of the RI approximation, the mean deviations of calculated isotropic HFCCs between the RI and the numerical results in percent are shown in Figs. 8.2 to 8.4 for the IGLO-II, IGLO-III and IGLO-VI basis set respectively. The average over all atomic values has been calculated for each molecules ,and the corresponding values for the decontracted are shown as well for comparison. These values were obtained with the *tLMF*-SVWN functional and will be considered representative for all local hybrid functionals investigated in this work.

With the medium-sized IGLO-II basis, the percentage deviation in the isotropic hyperfine coupling constants for individual molecules amounts to

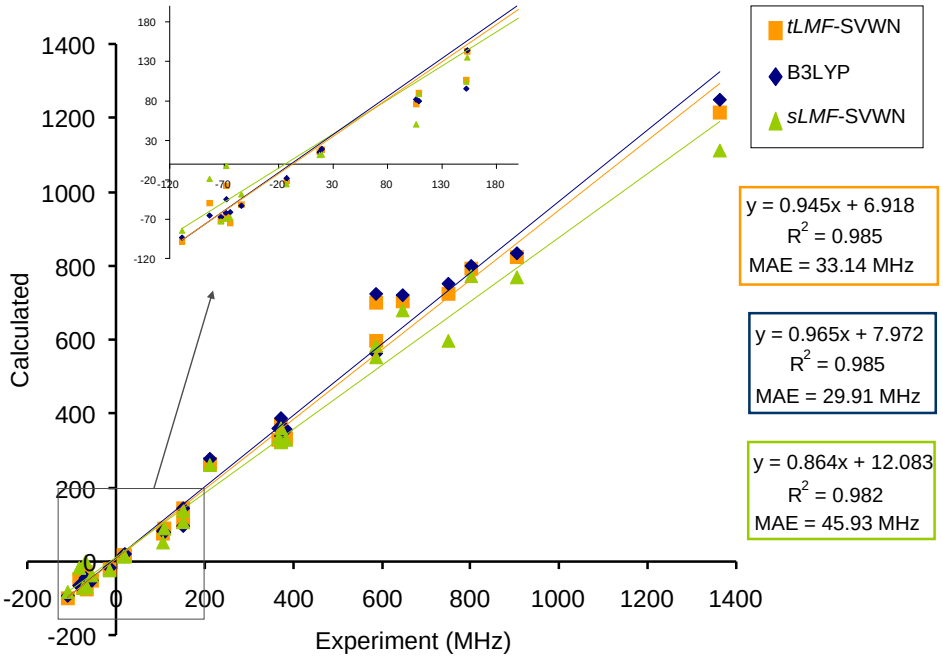

Figure 8.1: Linear regression analysis for 26 isotropic hyperfine coupling constants. Calculations were performed with the IGLO-IV basis set and numerical local hybrid potentials.

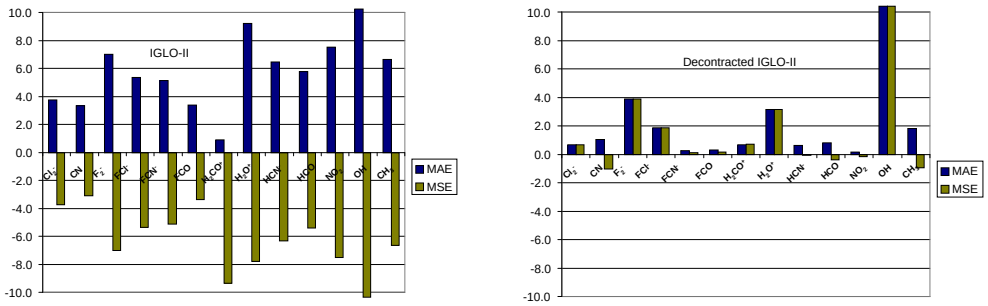

Figure 8.2: Percent errors for isotropic hyperfine coupling constants with the local hybrid RI potential as compared to the numerical potential. The *tLMF*-SVWN functional has been employed together with IGLO-II basis set.

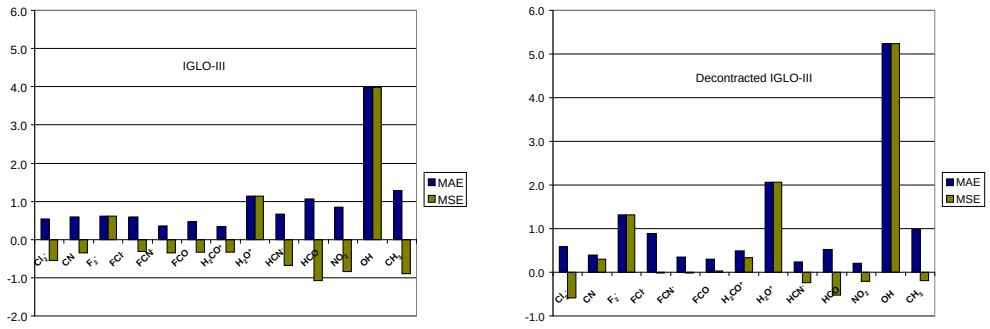

Figure 8.3: Percent errors for isotropic hyperfine coupling constants with the local hybrid RI potential as compared to the numerical potential. The *tLMF*-SVWN functional has been employed together with IGLO-III basis set.

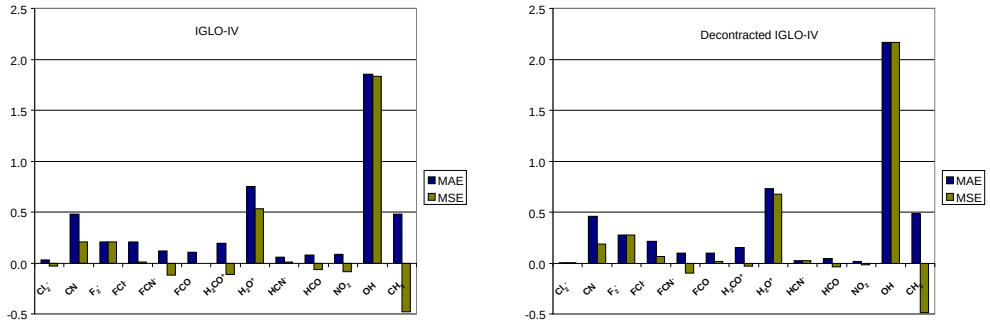

Figure 8.4: Percent errors for isotropic hyperfine coupling constants with the local hybrid RI potential as compared to the numerical potential. The *tLMF*-SVWN functional has been employed together with IGLO-IV basis set.

over 20%. The error range is decreased significantly to 4% with the IGLO-III and further down to 2% with the large IGLO-IV basis set. The accuracy of the RI results with respect to the numerical values is thus improved substantially by an increasing number of contracted basis functions. With some exceptions the deviation from numerical results with the RI approximation are reduced as well upon decontraction of the basis, to a much smaller extent though. The improvement is most pronounced for the IGLO-II and barely visibly for the larger IGLO-IV basis set. This is not too surprising considering that all IGLO basis sets employed in this work are only loosely contracted and the ratio between decontracted basis functions and contracted one is simply the largest for IGLO-II. For all basis sets, the OH and the H_2O^+ molecule seem to suffer most from errors in the RI approximation and, with IGLO-III and IGLO-IV the deviation from the numerically exact solution is even increased upon decontraction of the basis. Possibly, the percent errors appear to be large in these two cases because the corresponding isotropic HFCCs are comparatively small. Following from the MSE bars, there is no systematic under- or overestimation of the isotropic hyperfine coupling constants due to the RI approximation which contrasts with the observation for total energies that were systematically underestimated.

Potential	Contracted			Decontracted		
	IGLO-II	IGLO-III	IGLO-IV	IGLO-II	IGLO-III	IGLO-IV
Numerical	44.87	32.82	33.14	43.16	33.60	33.51
RI	44.49	32.36	33.01	42.19	32.93	33.34

Table 8.2: MAE in isotropic 26 HFCCs. The molecules and benchmark values are given in Table 3.5. Results from SCF calulations with the numerically exact and the RI potential are given for each basis set.

.

Since fitting procedures and assessments are generally performed for test

set averaged errors, the mean absolut error over all 26 isotropic HFCCs with the RI potential are compared to numerical results in Table 8.2. For a given basis, the RI and the numerical MAEs differ by less than 1 MHz. The largest deviation of 0.93 MHz occurs with the decontracted IGLO-II basis. As compared to the isotropic HFCCs of a single molecule, the average error is thus less sensitive to inaccuracies in the RI potential due to an incomplete basis. The RI MAE is generally smaller than the numerical MAE indicating that fortuitously more accurate results may be obtained due to an incomplete basis set when the RI approximation is used in the local hybrid potential.

Fig. 8.5 illustrates the difference between RI and numerical energies for the α orbitals of the CN molecule. Based on the previous observation that decontraction of a given basis has considerably smaller effects on the results than augmenting the number of contracted basis functions, only the contracted IGLO basis sets are considered in this context. The energy differences for individual orbitals due to the RI approximation are of the same magnitude or slightly smaller than total energy differences (see discussion above). With the contracted IGLO-IV basis set all occupied orbital energies and the first eight virtual orbital energies are reproduced within 10 meV accuracy. Considering the magnitude of total orbital energies, the error introduced by the RI approximation seems to be negligible. However, supporting the results for isotropic hyperfine coupling constant no clear tendency in the orbital energy differences can be observed. The HOMO energy for instance is overestimated by almost 3 meV using the IGLO-II basis set and underestimated by 7 meV with the larger IGLO-III basis.

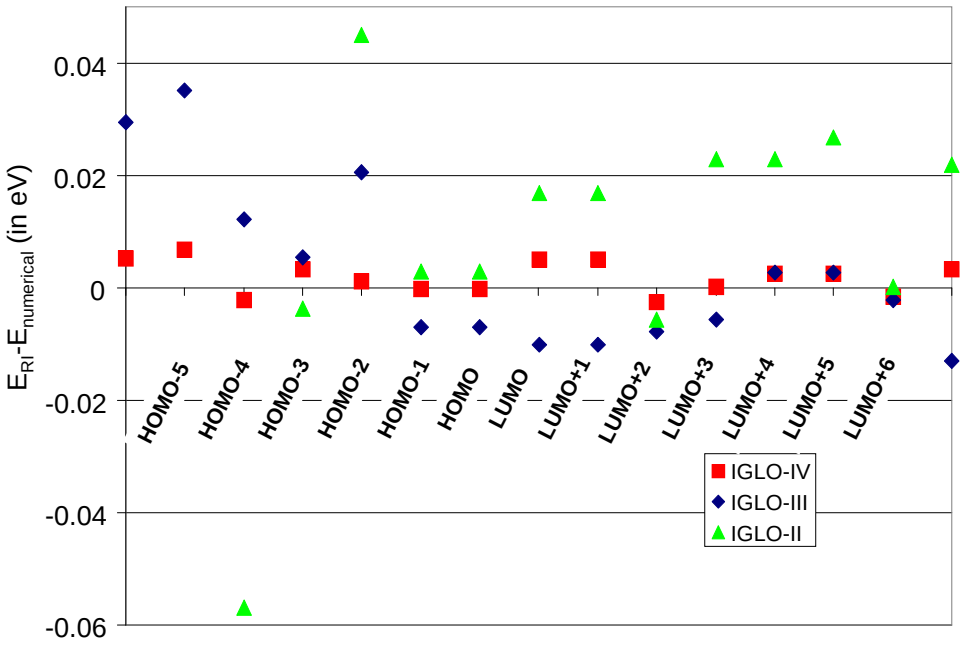

Figure 8.5: Differences between RI and numerical orbital energies of the CN molecule calculated with different IGLO basis sets.

8.3 Conclusion

For mean average errors of whole test sets the RI error seems to be negligible, even if medium-sized basis sets are employed. Individual molecular properties on the other hand may be subject to a stronger basis set dependence. Especially too small basis sets for the RI approximation may lead to fortuitously more accurate results. In the assessment of new local hybrid functionals large and unconctracted basis sets should therefore be used.

In a parallel work, local hybrid functionals have been assessed among other properties for the total energies of the first 18 elements. With all local hybrid functionals tested in that work, the mean absolute error in the total energies of the first 18 elements is by more than two orders of magnitude larger than the above-discussed RI error in total energies. The inaccuracies in total energies due to the RI approximation are thus minor as compared to the attainable deviations from experimental values.

Finally, the introduction of an auxiliary basis set for the RI approximation to exact-exchange terms in the local hybrid potential is recommended in order to avoid decontraction of the atomic basis set and to reduce the visibly stronger basis set dependence of calculations with local hybrid functionals.

CHAPTER 9

CONCLUSION AND OUTLOOK

In this work, the implementation, development and assessment of new density functionals with a position-dependent admixture of exact exchange has been disussed. The presented local hybrid functionals contain up to three empirical parameters fitted to atomization and barrier heights. It has been verified that the optimized values for the parameters are mostly independent of the underlying fit set. For a spin polarized *t*-LMF two slightly different sets of parameters have been obtained. But the performance of the corresponding functionals coincides, considering the properties discussed in this work. For atomization energies and reaction barriers the local hybrid functionals perform better than or similarly to the best state-of-the art functionals, which are often highly parameterized. Local mixing functions based on the kinetic energy densities usually yield better results for both properties than local mixing functions that depend on the reduced density gradient. The best results for atomization energies have been obtained by inclusion of spin polarization in *t*-LMFs. The local hybrid functionals yield overall better results for the dissociation energies and bond lengths of 2-center-3-electron radical cations than B3LYP. Global hybrid functionals with thermochemically too large exact-exchange admixtures are still more accurate for these systems. The description of 3*d* transition metal dimers and monohydrides is comparable to B3LYP. For isotropic hyperfine coupling constants, the one-parameter local hybrid functional tLMF-SVWN performs similarly to B3LYP. This functional is thus competitive with the best state-of-the-art density functionals although it is based on LSDA exchange and correlation and contains only

one adjustable parameter. The assessment for transition metal compounds should be extended to other local hybrid functionals.

For efficiency the local hybrid potential has been implemented using the RI approximation. In order to validate the accuracy of this approximation, the numerically exact potential has been implemented as well. With the uncontracted QZVP basis set, the errors in total energies due to the RI approximation are marginal. The impact of the RI approximation on average deviations of isotropic HFCCs from experimental data is insignificant even with a medium-sized basis. A direct comparison of the isotropic HFCCs of single molecules calculated with the RI potential to those obtained from the numerical potential revealed larger percentage errors of the RI approximation. Especially the IGLO-II basis set was shown to be insufficient in this case.

Based on these results, more studies on the accuracy of the RI approximation are recommended. Properties such as atomic s-d transfer energies, ionization potentials, and electron affinities could give more insight on possible shortcomings of the RI approximation. In the context of other studies on local hybrid functionals, [145, 148] it has been revealed that most of the above-discussed functionals yield large errors in total atomic energies. The observed underestimation is typical for the LSDA and confirms the necessity for local hybrid functionals with GGA or meta-GGA exchange and correlation. Probably due to the gauge problem and the fact that only certain combinations of exchange and correlation functionals work well, we were, however, not able to optimize a local hybrid functional with a sufficiently large meta-GGA correction in the correlation functional. Further studies on the different gauges of the exchange energy densities might thus be worthwile. A specifically designed correlation functional to be combined with a local hy-

brid exchange functional based on the LSDA could provide an alternative solution. Modifications of the current implementation to allow for auxiliary basis sets with the RI potential are recommended as well. The auxiliary basis sets that are used for RI-DFT might be sufficient. Otherwise, auxiliary basis sets have to be designed and optimized for local hybrid functionals. Other LMFs recently introduced and tested in a work parallel to this one, and spin-polarized LMFs shall be implemented self-consistently as well allowing for their assessment for orbital-dependent properties.

CHAPTER 10

SUMMARY

In order to describe complex molecular systems theoretically, an efficient and reliable solution to the underlying quantum mechanical equations of motion is required. Density functional theory (DFT) represents in most cases the best compromise between accuracy and efficiency for the treatment of electronic interactions. In Kohn-Sham DFT, the non-classical contribution to electron-electron interactions is gathered in the exchange-correlation functional, which has to be approximated in practice. While a large number of exchange-correlation functionals are of semi-empirical nature, some have been derived from physical considerations exclusively. In so-called global hybrid functionals a constant amount of the integrated DFT exchange-energy density is replaced by the exact-exchange energy from Hartree-Fock theory. The most popular functional, B3LYP, contains 20% exact exchange and several empirical parameters. It has been discovered that the optimal amount of exact exchange depends to a large extent on the molecular property to be computed. A possible solution to this problem is to use local hybrid functionals. Therein, the admixture of exact exchange is controlled by a position-dependent local mixing function (LMF), leading to molecule-specific amounts of exact exchange.

In this work a semi-empirical approach is pursued for the development of new local hybrid functionals. Parameterized LMFs are introduced in the exchange-energy density integrals, for which the DFT contributions are taken from established approximations to the exchange-correlation functional. The LMFs developed here contain at least one empirical parameter and a variable

that depends on the ratio of the von-Weizsäcker single-particle kinetic energy density to the correlated kinetic-energy density (the so-called *t*-LMFs), or on the reduced density gradient (referred to as *s*-LMF). Additional LMFs are obtained by inclusion of the spin polarization. All parameters are fitted to atomization energies and reaction barriers of well-established test sets. Visualization of the LMFs provides an additional tool for analyzing their physical and chemical behavior, potentially leading to further developments.

As a general trend, an increasing exact-exchange admixture is observed upon bond stretching for all LMFs, with a more pronounced effect for *t*-LMFs. This observation correlates with a better performance for reaction barriers of *t*-LMF-based local hybrid functionals. Most of the local hybrid functionals discussed in this work are based on the exchange and correlation functional from the local spin density approximation (LSDA) and contain therefore no gradient correction such as in the generalized gradient approximation (GGA). The new functionals were initially implemented non-self-consistently into a development version of the quantum chemical Turbomole program package. That is, only the total energy is calculated for a given set of molecular orbitals or electron density, respectively. This is a reliable approximation that allows for significant time savings especially during parameter optimizations.

In order to calculate orbital-dependent molecular properties, the local hybrid potential corresponding to the local hybrid energy is required as well. It is obtained as a functional derivative of the exchange-correlation energy with respect to the orbitals. Some of the resulting integrals contain the LMF-weighted non-local exact-exchange potential. These terms as well as the exact-exchange energy density itself cannot be calculated analytically. Following a well-established approach, they have been approximated using a basis set expansion of the exact-exchange potential. For simplicity, the

underlying atomic basis set is employed in this resolution of the identity (RI) approximation. For comparison and in view of the optimization of auxiliary basis sets, the optional calculation of the potential by numerical integration has also been implemented in this work. The computational cost of local hybrid calculations for a given basis set, using the RI approximation is comparable to the one of gobal hybrid functionals: a slightly larger prefactor applies to a calculation with a local hybrid functional as compared to a meta-GGA global hybrid, while the scaling of computational effort as a function of system size is the same.

Several molecular test sets including atomization energies, barrier heights, dissociation energies and equilibrium distances have been considered for the assessment. Some of them represent particular challenges for current density functional approximations. All of the discussed local hybrid functionals yield significantly better results for the 223 atomization energies of the G3 test set than the B3LYP functional. Especially local hybrid functionals with spin-polarized t-LMFs gives impressively small mean absolute errors for the G3 set. Most of our functionals are in addition significantly superior to B3LYP for the calculation of barrier heights. Some other global hybrid functionals perform even better than our functionals for barriers, but their intrinsic amount of exact exchange is inappropriately high for thermochemical property calculations. For the first time, LSDA-based local hybrid functional have thus been presented that gives accurate results for thermochemistry and reaction barriers simultaneously. The dissociation behavior of symmetric radical cations remains a challenge for the local hybrid functionals presented here. Dissociation energies are significantly overestimated, and the equilibrium distances are too short. The results are overall only slightly better than those obtained using the B3LYP functional. A larger amount of exact exchange is

most likely needed for these systems to reduce self-interaction errors.

Additionally, the performance of local hybrid functionals for 3d transition metal dimers and monohydrides has been studied. An accurate description of dynamical and nondynamical correlation is essential for the former. The poor performance of most exchange-correlation functionals for transition metal monohydrides can be attributed to self-interaction errors. Our local hybrid functionals perform similarly to B3LYP for the dimers and marginally better for the monohydrides. They do not provide any improvement for the atomic *s*-*d* transfer energies of 3d metals. The most suitable local hybrid functional for this particular property uses a *s*-LMF in the exchange functional and the LYP correlation functional. It yields, however, only average-quality results for thermochemistry and kinetics. Satisfactory results similar to B3LYP are obtained for the isotropic hyperfine coupling constants (HFCCs) of small main group compounds with a *t*-LMF-based local hybrid functional.

The RI approximation to the local hybrid potential has been validated by comparing it to the numerically exact potential for the calculation of total energies, isotropic HFCCs and orbital energies. The error in total energies due to the RI approximation is comparatively small considering the rather large deviations from experimental values. Comparison of mean absolute errors from experimental values of the 26 isotropic HFCCs reveals only small differences between the RI and the numerically exact local hybrid potential. Further analysis shows that inaccuracies in the RI potential may have a larger impact on the isotropic HFCCs or the orbital energies of a particular molecule, especially if only small or medium-sized basis sets are employed.

Several of the local hybrid functionals are suitable for the calculation of thermochemical and kinetic properties. Different functionals yield also results similar to other commonly used functionals for isotropic HFCCs of

small main group compounds, as well as for the dissociation energies and equilibrium distances of 3d transition metal dimers and monohydrides. The local hybrid functionals studied in this work represent therefore an important step towards the development of universal approximations to the exchange-correlation functional. For a more accurate description of certain transition metal properties and the dissociation behavior of symmetric radical cations while maintaining a good performance for thermochemistry and kinetics, more complex LMFs will have to be considered. Ultimately a local hybrid functional with meta-GGA exchange and correlation energy densities that fulfills more exact constraints is desirable. Therefore further studies on the different gauges of the exchange energy densities are necessary. Another possibility would be the development of a specifically designed correlation functional to be combined with a local hybrid exchange functional based on the LSDA.

More detailed studies on the quality of the RI approximation are recommended. Possible properties for this purpose include, e.g., ionization energies and electron affinities. Auxiliary basis sets should be implemented and optimized for the expansion of the exact-exchange potential in order to avoid additional deviations due to the RI-approximation or even fortuitously good results in the assessment of local hybrid functionals with normally contracted basis sets. Since density functional methods are applied extensively for structure optimizations, the gradient of the local hybrid energy with respect to the nuclear coordinates should be implemented to enable this feature in future versions of the code.

KAPITEL 11

ZUSAMMENFASSUNG

Für die Lösung der quantenmechanischen Bewegungsgleichungen, die komplexe, molekulare Systeme beschreiben, sind effiziente und verlässliche Näherungsverfahren erforderlich. Die Dichtefunktionaltheorie (DFT) stellt für die Behandlung der Elektronenwechselwirkung in vielen Fällen den besten Kompromiss zwischen Effizienz und Genauigkeit dar. Im Rahmen der DFT wird die gesamte nicht-klassische Elektron-Elektron-Wechselwirkung im so genannten Austausch-Korrelationsfunktional angenähert. Viele solcher Näherungen sind semi-empirischer Natur, andere wurden ausschließlich von physikalischen Überlegungen abgeleitet. In globalen Hybridfunktionale wird ein konstanter Anteil der integrierten DFT-Austauschenergiedichte durch exakten Austausch aus der Hartree-Fock Näherung ersetzt. Das populärste Funktional B3LYP enthält 20% exakten Austausch und mehrere empirische Parameter. Der optimale Prozentsatz hängt allerdings sehr stark von den zu berechnenden Systemen und molekularen Eigenschaften ab. Eine Lösung dieses Problems sollten lokale Hybridfunktionale liefern, in denen die Beimischung der exakten Austauschenergiedichte über eine lokale Mischfunktion (LMF) gesteuert wird und daher positions- und molekülabhängig ist.

In dieser Arbeit wird ein semi-empirischer Ansatz für die Entwicklung neuer lokaler Hybridfunktionale verfolgt: während die Energiedichten unverändert aus etablierten Näherungen zum Austauschkorrelationsfunktional übernommen werden, stehen parametrisierte LMFs im Zentrum der Untersuchungen. Die verschiedenen LMFs beinhalten neben mindestens einem empirischen Parameter eine Variable die vom Quotienten der von-Weizsäcker

kinetischen Energiedichte und der korrelierten kinetischen Energiedichte (sogenannte *t*-LMFs) bzw. dem reduzierten Dichtegradienten (bezeichnet als *s*-LMFs) abhängt. Weitere LMFs werden durch zusätzliche Berücksichtigung der Spinpolarisation erhalten. Alle Parameter werden an Atomisierungsenergien bzw. Reaktionsbarrieren bekannter molekularer Testsätze gefittet. Durch Visualisierung der LMFs können zusätzlich Einblicke in den physikalischen Hintergrund und in Möglichkeiten der Weiterentwicklung gewonnen werden. Es wurde beispielsweise beobachtet, dass entlang einer gedehnten Bindung höhere Werte der LMF und damit größere Beimischungen exakter Austauschenergie in Übergangszuständen einhergehen. Dieser Effekt ist für *t*-LMFs am ausgeprägtesten und korreliert mit besseren Ergebnissen für Reaktionsbarrieren mit lokalen Hybridfunktionalen, die auf einer *t*-LMF basieren. Bis auf wenige Ausnahmen leiten sich die lokalen Hybridfunktionale in dieser Arbeit aus dem Austausch- und Korrelationsfunktional der lokalen Dichtenäherung (LSDA) ab und enthalten keine Gradientenkorrektur im Sinne der GGA (*generalized gradient approximation*).

Die neuen Funktionale wurden zunächst nicht-selbstkonsistent in eine Entwicklerversion des quantenchemischen Programmpaketes Turbomole implementiert. Das bedeutet, für gegebene Molekülorbitale bzw. eine gegeben Elektronendichte kann lediglich die Gesamtenergie berechnet werden. Dies ist eine anerkannte Näherung, die vor allem für die Optimierung der Parameter eine große Zeitersparnis darstellt.

Um letztlich orbitalabhängige, molekulare Eigenschaften berechnen zu können wird neben der Gesamtenergie auch noch das zugehörige lokale Hybridpotential benötigt. Für die Implementierung wird die funktionale Ableitung der Austauschkorrelationsenergie nach den Orbitalen bestimmt. Daraus resultierend müssen neben den üblichen lokalen Austauschkorrelationspoten-

tialtermen auch Integrale berechnet werden, die das mit der LMF gewichtete nicht-lokale exakte Austauschpotential enthalten. Die entsprechenden Terme kann man, genauso wie die exakte Austauschenergiedichte an sich, nicht analytisch berechnen. Früheren Ansätzen folgend wurden sie in der vorliegenden Arbeit in einer Basissatzentwicklung angenähert, wobei der Einfachheit halber die atomaren Basisfunktionen verwendet wurden. Um die Genauigkeit dieser sogenannten RI (*resolution of the identity*)-Näherung validieren zu können und auch schon im Hinblick auf die Anpassung einer Hilfsbasis, wurde darüber hinaus die numerische Berechnung aller Integrale, die das exakte Austauschpotential und die entsprechende Energiedichte enthalten, implementiert. Unter Verwendung der RI-Näherung ist der Rechenaufwand lokaler Hybride vergleichbar mit dem globaler Hybridfunktionale: Während die formale Skalierung in Abhängigkeit der Systemgröße gleich ist, ergab sich ein etwas höherer Vorfaktor für die lokalen Hybride.

Verschiedene Literatur-bekannte Testsätze mit Atomisierungsenergien, Reaktionsbarrieren, Dissoziationsenergien oder Gleichgewichtsabständen, die teilweise einige Schwächen bisheriger Dichtefunktionalnäherungen aufdecken, wurden berücksichtigt. Für die 223 Atomisierungsenergien des G3 Testsatzes stellen alle unsere Funktionale eine signifikante Verbesserung gegenüber B3LYP dar. Atomisierungsenergien sind insofern ein sensibler Test, da alle Bindungen gebrochen werden und Fehlerkompensation eine untergeordnete Rolle spielt. Vor allem lokale Hybridfunktionale, deren LMFs neben der kinetischen Energiedichte explizit von der Spinpolarisation abhängen, lieferten hervorragende Resultate. Obwohl im Vergleich zu Atomisierungsenergien für die korrekte Berechnung von Reaktionsbarrieren im Allgemeinen mehr exakter Austausch benötigt wird, sind unsere Funktionale auch für zwei Testsätze mit jeweils 38 Reaktionsbarrieren besser als B3LYP. Zwar kann mit einem

globalen Hybrid mit 50% exaktem Austausch eine geringere Abweichung von den Richtwerten erzielt werden, aber ein solches Funktional ist für thermochemische Daten unzureichend. Hier wurde erstmals gezeigt, dass lokale Hybridfunktionale ohne Gradientenkorrektur sowohl für Thermochemie als auch für Kinetik zufrieden stellende Ergebnisse liefern können. Das Dissoziationsverhalten symmetrischer Radikalkationen stellt für die hier diskutierten Dichtefunktionale nach wie vor eine Herausforderung dar: Die Dissoziationsenergien von sieben Modellsystemen werden mit unseren Funktionalen stark überschätzt und Gleichgewichtsabstände unterschätzt. Insgesamt sind die Werte nur marginal besser als mit B3LYP. Neben Eigenschaften von Hauptgruppenverbindungen wurden zudem Übergangsmetalldimere und -monohydride untersucht. Für erstere ist eine gute Beschreibung dynamischer sowie statischer Elektronenkorrelation ausschlaggebend. In den Hydriden andererseits dominiert mit gängigen Dichtefunktionalen die unphysikalische Selbstwechselwirkung eines Elektrons mit sich selbst. Für die $3d$-Übergangsmetalldimere sind die getesteten Funktionale genauso gut wie B3LYP und für die Hydride etwas besser. Atomare s-d Transferenergien von $3d$ Übergangsmetallen verbleiben auch für unsere lokalen Hybridfunktionale, die insgesamt schlechtere Ergebnisse erzielen als B3LYP, noch problematisch. Das hierfür geeignetste lokale Hybridfunktional basiert auf einer s-LMF und beinhaltet LYP Korrelation. Für die isotropen Hyperfeinkopplungskonstanten (HFCCs) kleiner Hauptgruppenverbindungen wurden zufriedenstellende Ergebnisse (ähnlich wie B3LYP) mit einem t-LMF basierten lokalen Hybrid erzielt.

Die RI Näherung zum lokalen Hybridpotential wurde dem numerisch exakten Potential für die Berechnung von Gesamtenergien, isotrope HFCCs und Orbitalenergien für verschiedene Basissätze gegenübergestellt. Wie erwartet ist der Fehler für Gesamtenergien mit der RI-Näherungen vergleichs-

weise gering, vor allem relativ zu den verbleibenden Abweichungen von experimentellen Energien. Der Vergleich der mittleren absoluten Abweichung von experimentellen Werten für 26 isotrope HFCCs zeigt sogar für mittelgroße und kontrahierte IGLO Basissätze nur geringe Unterschiede zwischen dem RI-Potential und dem numerisch exakten lokalen Hybridpotential. Die Analyse der HFCCs einzelner Moleküle und der Orbitalenergien des CN Moleküls offenbart allerdings, dass Ungenauigkeiten aufgrund der RI-Näherung hier eine größere Rolle spielen, vor allem wenn zu kleine atomare Basissätze verwendet werden.

Von den untersuchten lokalen Hybriden stellen sich einige als hervorragende Kandidaten für die Berechnung thermochemischer und kinetischer Eigenschaften heraus. Jeweils unterschiedliche Funktionale erzielen darüber hinaus mit den besten bekannten Funktionalen vergleichbare Ergebnisse für isotrope Hyperfeinkopplungskonstanten und ausgewählte Eigenschaften kleiner Übergangsmetallverbindungen. Die in dieser Arbeit präsentierten lokalen Hybridfunktionale stellen daher einen wichtigen Schritt in der Entwicklung universeller Näherungen zum Austauschkorrelationsfunktional dar. Zur akkuraten Beschreibung molekularer Eigenschaften von Übergangsmetallkomplexen und dem Dissoziationsverhalten von Radikal-Kation-Dimeren neben Thermochemie und Kinetik, werden in Zukunft wohl komplexere LMFs benötigt. Um konkurrenzfähige lokale Hybride mit gradientenkorrigierter Austausch- und Korrelationsenergiedichte zu entwickeln, müssen darüber hinaus weitere Studien zum Einfluss des abweichenden Eichursprungs der miteinander kombinierten Austauschenergiedichten durchgeführt werden. Eine andere Möglichkeit ist die Entwicklung speziell abgestimmter Korrelationsfunktionale für lokale Hybride. Außerdem sollte die Qualität der RI-Näherung zum lokalen Hybridpotential detaillierter untersucht werden. Hierfür könnten zum Bei-

spiel Ionisierungsenergien und Elektronenaffinitäten herangezogen werden. Um zusätzliche Abweichungen oder sogar fälschlicherweise ßu guteËrgebnisse bei Validierungsrechnungen zu vermeiden, sollten Hilfsbasen für die Entwicklung des nicht-lokalen exakten Austauschpotentials implementiert und optimiert werden. Einer der nächsten Implementierungsschritte sollte auch Gradienten bezüglich der Kernkoordinaten beinhalten, um die Validierung der neuen lokalen Hybridfunktionale auf Strukturoptimierungen auszuweiten.

BIBLIOGRAPHY

[1] W. Kohn, *Electronic Structure of Matter - Wave Functions and Density Functionals*, World Scientific Publishing Co., Singapore, 2003.

[2] W. Kohn and L. J. Sham, *Phys. Rev.* **140**, 1133 (1965).

[3] A. D. Becke, *Phys. Rev. A* **38**, 3098 (1988).

[4] C. Lee, W. Yang, and R. Parr, *Phys. Rev. B* **37**, 785 (1988).

[5] J. P. Perdew, J. A. Chevary, S. H. Vosko, K. A. Jackson, M. R. Pederson, D. J. Singh, and C. Fiolhais, *Phys. Rev. B* **46**, 6671 (1992).

[6] J. P. Perdew, K. Burke, and M. Ernzerhof, *Phys. Rev. Lett.* **77**, 3865 (1996).

[7] J. Tao, J. P. Perdew, V. N. Staroverov, and G. E. Scuseria, *Phys. Rev. Lett.* **91**, 146401 (2003).

[8] J. P. Perdew, M. Ernzerhof, and K. Burke, *J. Chem. Phys.* **105**, 9982 (1996).

[9] Y. Zhao, N. González-García, and D. G. Truhlar, *J. Phys. Chem. A* **109**, 2012 (2005).

[10] L. A. Curtiss, P. C. Redfern, and K. Raghavachari, *J. Chem. Phys.* **123**, 124107 (2005).

[11] A. Nakata, Y. Imamura, T. Otsuka, and H. Nakai, *J. Chem. Phys.* **124**, 094105 (2006).

[12] A. Arbuznikov and M. Kaupp, *Chem. Phys. Lett.* **386**, 8 (2004).

[13] B. Miehlich, A. Savin, H. Stoll, and H. Preuss, *Chem. Phys. Lett.* **157**, 200 (1989).

[14] A. D. Becke, *J. Chem. Phys.* **107**, 8554 (1997).

[15] Y. Zhao and D. G. Truhlar, *Theor. Chem. Acc.* **120**, 215 (2008).

[16] H. L. Schmider and A. D. Becke, *J. Chem. Phys.* **108**, 9624 (1998).

[17] T. Schwabe and S. Grimme, *Phys. Chem. Chem. Phys.* **8**, 4398 (2006).

[18] A. Dreuw, J. L. Weisman, and M. Head-Gordon, *J. Chem. Phys.* **119**, 2943 (2003).

[19] O. A. Vydrov, J. Hey, A. V. Krukau, and G. E. Scuseria, *J. Chem. Phys.* **125**, 074106 (2006).

[20] T. Yanai, D. Tew, and N. Handy, *Chem. Phys. Lett.* **393**, 51 (2004).

[21] C. A. Jiménez-Hoyos, B. G. Janesko, and G. E. Scuseria, *Phys. Chem. Chem. Phys.* **10**, 6621 (2008).

[22] O. A. Vydrov and G. E. Scuseria, *J. Chem. Phys.* **125**, 234109 (2006).

[23] M. J. G. Peach, T. Helgaker, P. S. ek, T. W. Keal, O. B. L. s, D. J. Tozer, and N. C. Handy, *Phys. Chem. Chem. Phys.* **8**, 558 (2006).

[24] J. Jaramillo, G. E. Scuseria, and M. Ernzerhof, *J. Chem. Phys.* **118**, 1068 (2003).

[25] A. V. Arbuznikov and M. Kaupp, *J. Chem. Phys.* **128**, 214107 (2008).

[26] B. G. Janesko and G. E. Scuseria, *J. Chem. Phys.* **127**, 164117 (2007).

[27] J. P. Perdew, V. N. Staroverov, J. Tao, and G. E. Scuseria, *Phys. Rev. A* **78**, 052513 (2008).

[28] P. Hohenberg and W. Kohn, *Phys. Rev.* **136**, 864 (1964).

[29] R. G. Parr and W. Yang, *Density-Functional Theory of Atoms and Molecules*, Oxford Science Publications, 1989.

[30] P. Mori-Sánchez, A. J. Cohen, and W. Yang, *J. Chem. Phys.* **124**, 091102 (2006).

[31] A. Ruzsinszky, J. P. Perdew, G. I. Csonka, O. A. Vydrov, and G. E. Scuseria, *J. Chem. Phys.* **126**, 104102 (2007).

[32] J. P. Perdew and A. Zunger, *Phys. Rev. B* **23**, 5048 (1981).

[33] O. A. Vydrov and G. E. Scuseria, *J. Chem. Phys.* **121**, 8187 (2004).

[34] O. A. Vydrov and G. E. Scuseria, *J. Chem. Phys.* **122**, 184107 (2005).

[35] K. Burke, M. Ernzerhof, and J. P. Perdew, *Chem. Phys. Lett.* **265**, 115 (1997).

[36] J. Harris, *Phys. Rev. A* **29**, 1648 (1984).

[37] A. Görling and M. Levy, *Phys. Rev. B* **47**, 13105 (1993).

[38] A. Görling and M. Levy, *Phys. Rev. A* **50**, 196 (1994).

[39] A. D. Becke, *J. Chem. Phys.* **98**, 1372 (1993).

[40] M. J. G. Peach, A. M. Miller, A. M. Teale, and D. J. Tozer, *J. Chem. Phys.* **129**, 064105 (2008).

[41] K. Burke, J. P. Perdew, and M. Ernzerhof, *J. Chem. Phys.* **109**, 3760 (1998).

[42] K. Burke, J. P. Perdew, and D. C. Langreth, *Phys. Rev. Lett.* **73**, 1283 (1994).

[43] A. D. Becke and M. R. Roussel, *Phys. Rev. A* **39**, 3761 (1989).

[44] J. P. Perdew and Y. Wang, *J. Chem. Phys.* **46**, 12947 (1992).

[45] M. Ernzerhof and G. E. Scuseria, *J. Chem. Phys.* **111**, 911 (1999).

[46] J. P. Perdew, A. Ruzsinszky, J. Tao, V. N. Staroverov, G. E. Scuseria, and G. I. Csonka, *J. Chem. Phys.* **123**, 062201 (2005).

[47] J. P. Perdew and Y. Wang, *Phys. Rev. B* **45**, 13244 (1992).

[48] G. L. Oliver and J. P. Perdew, *Phys. Rev. A* **20**, 397 (1979).

[49] M. Ernzerhof, K. Burke, and J. P. Perdew, Density functional theory, the exchange hole, and the molecular bond, in *Recent Developments and Applications of Modern Density Functional Theory*, edited by J. M. Seminario, Elsevier, Amsterdam, 1997.

[50] M. Ernzerhof and J. P. Perdew, *J. Chem. Phys.* **109**, 3313 (1998).

[51] J. C. Kimball, *Phys. Rev. A* **7**, 1648 (1973).

[52] W. Koch and M. C. Holthausen, *A Chemist's Guide to Density Functional Theory*, Wiley-VCH Verlag GmbH, 2001.

[53] J. P. Perdew, K. Burke, and Y. Wang, *Phys. Rev. B* **54**, 16533 (1996).

[54] M. Henderson, B. G. Janesko, and G. E. Scuseria, *J. Chem. Phys.* **128**, 194105 (2008).

[55] H. Bahmann and M. Ernzerhof, *J. Chem. Phys.* **128**, 234104 (2008).

[56] J. C. Slater, *Quantum Theory of Molecular and Solids. Vol. 4: The Self-Consistent Field for Molecular and Solids*, McGraw-Hill: New York, second edition, 1974.

[57] S. H. Vosko, L. Wilk, and M. Nusair, *Can. J. Phys.* **58**, 1200 (1980).

[58] D. C. Langreth and M. J. Mehl, *Phys. Rev. B* **28**, 1809 (1983).

[59] O. Gunnarsson and B. I. Lundqvist, *Phys. Rev. B* **13**, 4274 (1976).

[60] J. P. Perdew, *Phys. Rev. Lett.* **55**, 1665 (1985).

[61] J. P. Perdew and Y. Wang, *Phys. Rev. B* **33**, 8800 (1986).

[62] A. D. Becke, *J. Chem. Phys.* **85**, 7184 (1986).

[63] K. Burke, F. G. Cruz, and K.-C. Lam, *J. Chem. Phys.* **109**, 8161 (1998).

[64] J. P. Perdew, Unified Theory of Exchange and Correlation Beyond the Local Density Approximation, in *Electronic Structure of Solids*,

edited by P. Ziesche and H. Eschrig, Akademie Verlag, Berlin, 1991.

[65] A. D. Becke, *J. Chem. Phys.* **98**, 5648 (1993).

[66] M. Kaupp, A. V. Arbuznikov, and H. Bahmann, *Z. Phys. Chemie* **224**, 545 (2010).

[67] F. A. Hamprecht, A. J. Cohen, D. J. Tozer, and N. C. Handy, *J. Chem. Phys.* **109**, 6264 (1998).

[68] A. D. Boese and N. C. Handy, *J. Chem. Phys.* **116**, 9559 (2002).

[69] Y. Zhao, N. E. Schulz, and D. G. Truhlar, *J. Chem. Phys.* **123**, 161103 (2005).

[70] Y. Zhao, N. E. Schulz, and D. G. Truhlar, *J. Chem. Theory Comput.* **2**, 364 (2006).

[71] A. D. Boese and J. M. L. Martin, *J. Chem. Phys.* **121**, 3405 (2004).

[72] Y. Zhao, N. E. Schulz, and D. G. Truhlar, *J. Chem. Phys.* **124**, 224105 (2006).

[73] Y. Zhao and D. G. Truhlar, *Acc. Chem. Res.* **41**, 157 (2008).

[74] H. Iikura, T. Tsuneda, T. Yanai, and K. Hirao, *J. Chem. Phys.* **115**, 3540 (2001).

[75] T. M. Henderson, A. F. Izmaylov, G. E. Scuseria, and A. Savin, *J. Chem. Phys.* **127**, 221103 (2007).

[76] A. V. Arbuznikov, M. Kaupp, and H. Bahmann, *J. Chem. Phys.* **124**, 204102 (2006).

[77] J. D. Talman and W. F. Shadwick, *Phys. Rev. A* **14**, 36 (1976).

[78] F. D. Sala and A. Görling, *J. Chem. Phys.* **115**, 5718 (2001).

[79] F. D. Sala and A. Görling, *J. Chem. Phys.* **116**, 5374 (2002).

[80] A. Hesselmann, A. W. Götz, F. D. Sala, and A. Görling, *J. Chem. Phys.* **127**, 054102 (2007).

[81] A. V. Arbuznikov, H. Bahmann, and M. Kaupp, *J. Phys. Chem. A* **113**, 11898 (2009).

[82] R. Armiento and A. Mattson, *Phys. Rev. B* **66**, 165117 (2002).

[83] J. Tao, V. N. Staroverov, G. E. Scuseria, and J. P. Perdew, *Phys. Rev. A* **77**, 012509 (2008).

[84] C. A. Jiménez-Hoyos, B. G. Janesko, G. E. Scuseria, V. N. Staroverov, and J. P. Perdew, *Mol. Phys.* **107**, 1077 (2009).

[85] F. Weigend, *Phys. Chem. Chem. Phys.* **4**, 4285 (2002).

[86] A. Hesselmann and F. Manby, *J. Chem. Phys.* **123**, 164116 (2005).

[87] L. A. Curtiss, K. Raghavachari, P. C. Redfern, and J. A. Pople, *J. Chem. Phys.* **106**, 1063 (1997).

[88] L. A. Curtiss, K. Raghavachari, P. C. Redfern, and J. A. Pople, *J. Chem. Phys.* **112**, 7374 (2000).

[89] C. Adamo, M. Ernzerhof, and G. E. Scuseria, *J. Chem. Phys.* **112**, 2643 (2000).

[90] M. Grüning, O. V. Gritsenko, and E. J. Baerends, *J. Phys. Chem. A* **108**, 4459 (2004).

[91] B. Lynch, P. L. Fast, M. Harris, and D. G. Truhlar, *J. Phys. Chem. A* **104**, 4811 (2000).

[92] B. Lynch and D. G. Truhlar, *J. Phys. Chem. A* **106**, 842 (2002).

[93] Y. Zhao, B. Lynch, and D. G. Truhlar, *J. Phys. Chem. A* **108**, 2715 (2004).

[94] Y. Zhao, B. Lynch, and D. G. Truhlar, *Phys. Chem. Chem. Phys.* **7**, 43 (2007).

[95] B. Lynch and D. G. Truhlar, *J. Phys. Chem. A* **107**, 8996 (2003).

[96] B. Lynch and D. G. Truhlar, *J. Phys. Chem. A* **107**, 3898 (2003).

[97] P. L. Fast, N. E. Schultz, and D. G. Truhlar, *J. Phys. Chem. A* **105**, 4143 (2001).

[98] R. Merkle, A. Savin, and H. Preuss, *J. Chem. Phys.* **97**, 9216 (1992).

[99] B. Braïda, P. C. Hiberty, and A. Savin, *J. Phys. Chem. A* **102**, 7872 (1997).

[100] M. Sodupe, J. Bertran, L. Rodriguez-Santiago, and E. J. Baerends, *J. Phys. Chem. A* **103**, 166 (1999).

[101] M. Grüning, O. V. Gritsenko, S. J. A. Gisbergen, and E. J. Baerends, *J. Phys. Chem. A* **105**, 9211 (2001).

[102] J. Gräfenstein, E. Kraka, and D. Cremer, *Phys. Chem. Chem. Phys.* **6**, 1096 (2004).

[103] N. E. Schultz, Y. Zhao, and D. G. Truhlar, *J. Phys. Chem. A* **109**, 4388 (2005).

[104] S. Niu and M. B. Hall, *Chem. Rev.* **100**, 353 (2000).

[105] F. Furche and J. P. Perdew, *J. Chem. Phys.* **124**, 044103 (2006).

[106] S. Yanagisawa, T. Tsuneda, and K. Hirao, *J. Chem. Phys.* **112**, 545 (2000).

[107] V. N. Staroverov, G. E. Scuseria, J. Tao, and J. P. Perdew, *J. Chem. Phys.* **119**, 12129 (2003).

[108] C. J. Barden, J. C. Rienstra-Kiracofe, and H. F. SchaeferIII, *J. Chem. Phys.* **113**, 690 (2000).

[109] G. L. Gutsev and J. Charles W. Bauschlicher, *J. Phys. Chem. A* **107**, 4755 (2003).

[110] L. A. Eriksson, O. L. Malkina, V. G. Malkin, and D. R. Salahub, *J. Chem. Phys.* **100**, 5066 (1965).

[111] A. V. Arbuznikov, M. Kaupp, V. G. Malkin, R. Reviakine, and O. L. Malkina, *Phys. Chem. Chem. Phys.* **100**, 5467 (2002).

[112] L. Hermosilla, P. Calle, J. M. G. de la Vega, and C. Sieiro, *J. Phys. Chem. A* **109**, 1114 (2005).

[113] M. Kaupp, A. V. Arbuznikov, A. Hesselmann, and A. Görling, *J. Chem. Phys.* **132**, 184107 (2010).

[114] F. G. Cruz, K.-C. Lam, , and K. Burke, *J. Phys. Chem. A* **102**, 4911 (1998).

[115] H. Bahmann, A. Rodenberg, A. V. Arbuznikov, and M. Kaupp, *J. Chem. Phys.* **126**, 011103 (2007).

[116] B. G. Janesko and G. E. Scuseria, *J. Chem. Phys.* **128**, 084111 (2008).

[117] A. V. Arbuznikov and M. Kaupp, *Chem. Phys. Lett* **440**, 160 (2007).

[118] A. D. Becke, *J. Chem. Phys.* **119**, 2972 (2003).

[119] A. D. Becke, *J. Chem. Phys.* **122**, 064101 (2005).

[120] W. H. Press, S. A. Teukolsky, and W. T. Vetterling, *Numerical Recipes in FORTRAN 77. The Art of Scientific Computing: Fortran Numerical Recipes Vol 1.*, Cambridge Univerity Press, second edition, 1992.

[121] N. Metropolis, A. W. Rosenbluth, M. N. Rosenbluth, and A. H. Teller, *J. Chem. Phys.* **21**, 1087 (1953).

[122] J. Nelder and R. Mead, *Computer Journal* **7**, 308 (1965).

[123] D. N. Sparks, D. G. Clayton, R. O. I. D. Hill, R. Peto, and F. Yates, *Applied Statistics* **20**, 327 (1971).

[124] R. Ahlrichs, M. Baer, M. Haeser, H. Horn, and C. Koelmel, *Chem. Phys. Lett.* **165**, 200 (1989).

[125] O. Treutler and R. Ahlrichs, *J. Chem. Phys.* **102**, 346 (1995).

[126] K. Eichkorn, O. Treutler, H. Öhm, M. Häser, and R. Ahlrichs, *Chem. Phys. Lett.* **240**, 283 (1995).

[127] F. Weigend, *J. Comp. Chem.* **29**, 167 (2008).

[128] M. Häser and R. Ahlrichs, *J. Comp. Chem.* **10**, 104 (1989).

[129] T. Helgaker, P. Jorgensen, and J. Olsen, *Molecular Electronic Structure Theory*, Wiley, 2000.

[130] D. Rappoport, F. Furche, D. Sebastiani, and T. Fleig, *Nachr. Chem.* **57**, 305 (2009).

[131] J. A. Pople, M. Head-Gordon, D. J. Fox, K. Raghavachari, and L. A. Curtiss, *J. Chem. Phys.* **90**, 5622 (1989).

[132] L. A. Curtiss, C. Jones, G. W. Trucks, K. Raghavachari, and J. A. Pople, *J. Chem. Phys.* **93**, 2537 (1990).

[133] http://t1.chem.umn.edu/misc/database_group/database_therm_bh/.

[134] W. Kutzelnigg, U. Fleischer, and M. Schindler, *The IGLO Method: Ab Initio Calculation and Interpretation of NMR Chemical Shifts and Magnetic Susceptibilities*, volume 23, p. 165, Springer, 1990.

[135] F. Weigend and R. Ahlrichs, *Phys. Chem. Chem. Phys.* **7**, 3297 (2005).

[136] P. Gill and L. Radom, *J. Am. Chem. Soc.* **110**, 4931 (1988).

[137] V. G. Malkin, O. L. Malkina, R. Reviakine, A. V. Arbuznikov, M. Kaupp, B. Schimmelpfennig, I. Malkin, M. Repiský, S. Komorovský, P. Hrobarik, E. Malkin, T. Helgaker, and K. Ruud, ReSpect program, version 2.1; 2008.

[138] P. R. Schreiner, *Angew. Chem. Int. Ed.* **46**, 4217 (2007).

[139] M. Kaupp, H. Bahmann, and A. V. Arbuznikov, *J. Chem. Phys.* **127**, 194102 (2007).

[140] P. R. Schreiner, A. A. Fokin, J. Robert A. Pascal, and A. de Meijere, *Org. Lett.* **8**, 3635 (2006).

[141] M. D. Wodrich, C. Corminboeuf, and P. von Ragué Schleyer, *Org. Lett.* **8**, 3631 (2006).

[142] O. V. Gritsenko, P. R. T. Schipper, and E. J. Baerends, *J. Chem. Phys.* **107**, 5007 (1997).

[143] S. Grimme, *Angew. Chem. Int. Ed.* **27**, 4460 (2006).

[144] S. Grimme, *J. Comp. Chem.* **27**, 1787 (2006).

[145] K. Theilacker, Validierung neuer Dichtefunktionalmethoden, Master's thesis, Universität Würzburg, 2010.

[146] F. W. Kutzler and G. S. Painter, *Phys. Rev. B* **43**, 6865 (1991).

[147] R. Müller, to be published.

[148] R. Haunschild and G. E. Scuseria, *J. Chem. Phys.* **132**, 224106 (2010).

DANKSAGUNG

An dieser Stelle bedanke ich mich zunächst bei meinem Betreuer, Martin Kaupp, dafür, dass er mir dieses Projekt anvertraut und vor allem zugetraut hat. Ich habe die Arbeit an diesem Thema und enthusiastische Diskussionen zu lokalen Hybridfunktionalen sehr genossen und danke ihm für die verständnisvolle Unterstüzung auch in weniger produktiven Zeiten. Er hat mir darüber hinaus großzügigerweise den Besuch einiger Konferenzen bzw. Summer Schools ermöglicht.

Ein weiterer Dank geht nach Montréal an Matthias Ernzerhof für die herzliche Aufnahme in seinem Arbeitskreis während meines sechsmonatigen Forschungsaufenthaltes und die informativen Diskussionen und Ausführungen über spezielle Eigenschaften merkwürdiger Löcher.

Für Diskussionen und wertvolle Tipps bei der Implementierung bedanke ich mich bei Alexei Arbuznikov und Reinhold Fink.

Meinen Forschungspraktikanten Alexander Rodenberg, Markus Hock, Martin Hofmann, Jörg, Andreas Muzha, Adam Rekavka, Johannes Auerswald und Johannes Schäffer sowie Bartosz Zarzycki danke ich unter anderem für Rechnungen, Skripte, Ergebnisse, das Auffinden von Bugs und dass sie auch bei Fernbetreuung nicht verzagt haben.

Ich bedanke mich bei Sandra Schinzel und Kathrin Götz, den beiden anderen Mitgliedern des dominanten Frauentrios für die ausgelassende Stimmung während unzähliger kreativer Kaffee- und Mittagspausen und die vielen wertvollen Diskussionen.

Den aktuellen und früheren Mitgliedern meines Arbeitskreises im Allgemeinen und James Asher, Manuel Renz, Robert Müller, Kolja Theilacker und Johannes Schraut im Speziellen danke ich für die nette Arbeitsatmosphäre,

Blumen gießen, Poster abholen, Computerrepaturen, M&Ms und die tolle Zusammenarbeit.

Meinen Eltern danke ich dafür, dass sie immer an mich glauben und mich mit genug Optimismus und Selbstvertrauen ausgestattet haben, so ein Projekt wie dieses hier anzugehen und letztlich fertigzustellen. Die für diese Arbeit wichtigen grundlegenden Kenntnisse der Mathematik verdanke ich wahrscheinlich überwiegend meinem phantastischen großen Bruder, Helge Bahmann.

Für moralische Unterstützung und ein offenes Ohr in jeder Lage danke ich außerdem Nina Schuster, Alex Kerscht, Silvia Vogl, Dörte Reitzenstein, Nele Welter, Stefanie Sparka und Uschi Rüppel.

Für finanzielle Unterstützung bedanke ich mich beim Graduiertenkolleg 1221, dem DAAD und der Studienstiftung des deutschen Volkes.

Abschließend danke ich Jean Christophe Tremblay dafür, dass er mir in jeder Lebenslage beisteht, für Korrekturen in letzter Minute und ein für alle Mal für seine detaillierten Theorien über die Wissenschaft, die Menschen und das Leben an sich. Deine Zuneigung gibt mir täglich Kraft.